UNIVERSITY OF OSLO
Department of Geosciences
MetOs section

Validating OsloCTM2 using MIPAS IMK-IAA satellite data from 2003

Master thesis in Geosciences Meteorology and oceanography

Ole Kristian Kvissel

01.06.2007

Abstract

Oslo-CTM2 is a three dimensional global chemical transport model that uses well established methods to calculate the volume mixing ratio of different atmospheric compounds. A wide variety of species and both dynamical and chemical processes controlling the atmospheric composition are included in the model. MIPAS IMK-IAA uses satellite observations to describe the atmospheric composition. The dataset is based upon retrival of abundances using a very sophisticated satellite mounted instrument designed to scan the Earth's limb. The instrument is designed to, throught processing and interpretations of the mid-infrared radiation that is emitted from the atmosphere, calculate the abundances for different atmospheric species.

In this study seasonal means for abundances of several atmospheric components (CH_4, N_2O, $CFC-11$, NO, NO_2, N_2O_5, HNO_3, HO_2NO_2, ClO, $ClONO_2$ and O_3) have been calculated using the Oslo-CTM2 chemical transport model for the period December 2002 through November 2003. The Oslo-CTM2 meridional and geographical distributions of these species have been validated against retrived abundances provided by MIPAS IMK-IAA for the same period.

Overall, the results show that the performance of Oslo-CTM2 compared to MIPAS IMK-IAA is relatively good for most of the included components. However, there are some discrepancies.

E.g. the results show relatively small discrepancies between the fractional distribution between the members in the NO_y chemical family. Some of these discrepancies are shown to be caused by inaccuracies in the NO_y chemistry as represented in the model.

The Oslo-CTM2 version presented in this work is based on JPL/NASA publication 02-25. A recent update of Oslo-CTM2 to JPL/NASA publication 06-02 regarding chemical kinetics and photochemistry has reduced some of the discrepancies pointed out in this thesis.

Differences in the abundance for long-lived chemical species (CH_4, N_2O and $CFC-11$) in the lower stratosphere may indicate that the use of ECMWF IFSL60 data for advection in the model causes too weak vertical transport in this region influencing the stratosphere-troposphere exchange. Whereas the discrepancies in the upper stratosphere indicates a too strong regional meridional circulation.

In the stratosphere in general the Oslo-CTM2 reproduces the atmospheric composition in a satisfactory manner.

In the upper stratosphere and lower mesosphere the discrepancies between the datasets are caused by effects from SPEs that have not been included in the Oslo-CTM2 model.

Acknowledgements

First and foremost I want to thank my supervisor, Professor Frode Stordal, for supporting me during the work with this study and providing me with this opportunity to increase my knowledge. My co-supervisor, Line Gulstad, also deserves a big thank you for giving me support and encouragement both "in sickness and in health".

The working environment here at the Department of Geoscience, Section for Meteorology and Oceanography, University of Oslo is very special. This thesis would not have been the same without aid and guidance from the people working and studying here. I especially want to thank Amund Søvde for helping me to set up the model and for providing me with some well commented IDL routines to get me in the plotting rythm. He also deserves thanks for occasionally helping me to understand some of my own (not so well commented) IDL-programming. Bjørg Rognerud and Michael Gauss deserve a big "thank you" for helping to set up the model, teaching me the basics of how to use it and more importantly its output. I also owe a "thank tou" to Gunnar Wollan and Kjell Andresen for support, aid and fixing the computer trubles I have encountered during this period.

I also want to thank the Programme Board of the MSc programme Geosciences at the University of Oslo for covering my expenses when I attended a meeting in Karlsruhe for users of IMK-IAA generated MIPAS data.

Last but definitively not least, I want to thank my family, girlfriend and friends for support, encouragement and at least trying to make me think and do other things than spending time in front of this computer. I want to use this occasion to appologize for all the times your climate or meteorology related questions have resulted in some of my "meteorology and atmospheric chemistry" crash courses. But, to my own defense, it definitively is a complex scientific field that often need to be visualized (on and with whatevers available) when I try to explain these processes (NB!! I can try but probably won't stop doing this in the future either).

List of Abbreviations

AGAGE	Advanced Global Atmospheric Gases Experiment
BC/OC	Black Carbon/Organic Carbon
$BrONO_2$	Bromine nitrate
BrO_x	Active Bromine species
CFC	Chlorofluorocarbon
ClO	Chlorine oxide
$ClONO_2$	Chlorine nitrate
ClO_x	Active Chlorine species
CO	Carbon monoxide
CO_2	Carbon dioxide
COF_2	Carbonyl fluoride
CH_3	Metyl radical
CH_4	Methane
C_2H_2	Acetylene
C_2H_6	Ethane
DJF	December-January-February
DU	Dobson Unit
ECMWF	European Centre for Medium-Range Weather Forecasts
ENVISAT	ENVIronmental SATellite
ESA	European Space Agency
ESRL	Earth System Research Laboratory
GMD	Global Monitoring Division
HCFC	Hydrochlorofluorocarbon
HITRAN	HIgh-resolution TRANsmission
hPa	hectoPascal (10^{-2} Pascal) (unit of pressure)
H_2N_2	Hydrogen Peroxide
H_2O	Water molecule
HCl	Hydrogen chloride
HNO_3	Nitric acid
$HOCl$	Hypochlorous acid
HO_2NO_2	Peroxynitric acid
IAA	Instituto de Astrofísica Andalucía
IFOV	Instruments Field-Of-View
IFSL60	Integrated Forecasting System (60 levels)
IMK	Institute für Meteorologie und Klimaforschung
IR	InfraRed
JJA	June-July-August
JPL	Jet Propulsion Labaratory
LTE	Local Thermodynamic Equilibrium
MAM	March-April-May
MetOs	Section for Meteorology and Oceanography
MIPAS	Michelson Interferometer for Passive Atmospheric Sounding

NASA	National Aeronautics and Space Administration
NCEP	National Centers for Environmental Prediction
NH	Northern Hemisphere
NMVOC	Non Methane Volatile Organic Compounds
NOAA	National Oceanic & Atmospheric Administration
N_2	Nitrogen
N_2O	Nitrous oxide
N_2O_5	Dinitrogen pentoxide
NH_3	Amonia
NO	Nitrogen Oxide
NO_2	Nitrogen dioxide
NO_3	Nitrate
NO_x	Active nitrogen species
NO_y	Reservoir species for the active nitrogens
Oslo-CTM2	Oslo Chemical Transport Model version 2
OCS	Carbonyl sulfide
OH	Hydroxyl
$O(^1D)$	Oxygen atom in excited state
$O(^3P)$	Oxygen atom in ground-level triplet state
O_2	Oxygen
O_3	Ozone
POET	Precursors of Ozone and their Effects in the Troposphere
ppbv	parts per billion by volume
ppmv	parts per million by volume
pptv	parts per trillion by volume
PSC	Polar Stratospheric Cloud
QSSA	Quasi Steady-State Approximation
RETRO	REanalysis of the TROpospheric chemical composition
SH	Southern Hemisphere
SON	September-October-November
SOA	Secondary Organic Aerosol
SOM	Second Order Moment
SPE	Solar Proton Event
STE	Stratospheric-Tropospheric Exchange
SO_2	Sulfur dioxide
TOA	Top Of the Atmosphere
UCI	University of California, Irvine
UiO	University of Oslo
UTLS	Upper Troposphere Lower Stratosphere
UV	UltraViolet
VIS	VISible
VMR	Volume Mixing Ratio

Contents

Chapter 1

Introduction

During the last two centuries there has been an extreme expansion of mankind resulting in increased exploitation of the Earth's resources. Only in the the last few generations we have consumed large amounts of fossile fuels, 30-50% of the land surface has been transformed in some way or another by human activities and both power consumption and industrial production rates have increased enormously. Research of atmospheric chemistry has evolved rapidly during the second half of the 20^{th} century, mainly driven by the deteriorating environmental problems and the increasing awareness of anthropogenic influence. As a result of increased scientific effort one can now state as a fact that several important greenhouse gases, both naturally occuring and antropogenically developed, have increased substansially in the atmosphere. This increase in atmospheric components abundance leads to problems such as global warming and has a negative influence on human health, particularly in developed areas where the emissions are largest.

Atmospheric scientists use a wide range of methods to monitor the abundance of different molecules in the atmosphere. Developments in satellite retrivals, methods to interpret the pre-industrial atmospheric state and numerical modelling form much of the basis for the modern climate research and set the premises for the accuracy of future climate predictions.

Numerical models are important and powerful tools to understand the processes behind the observed features and climatological trends. Such models are developed to replicate the state of the atmosphere, its behavior and the complex processes involved as realistically as possible. These models are based on dividing the global atmosphere into a large number of grid cells and start from an initial condition at a specific time, t. Furthermore a computer solves a complex system of chemical and mathematical equations in order to obtain the state of the atmosphere at a later time, $t + \triangle t$, and in each of the grid cells.

This study was initiated to validate a chemical transport model for numerous primary and secondary chemical atmospheric components using well known

presentation methods and procedures. Recent increase in high quality observational data from satellite retrivals provides a good basis for model validation, particularly in the upper troposphere-lower stratosphere (UTLS) and stratospheric regions.

Oslo-CTM2 has been developed at the University of Oslo, Department of Geophysics, Section for Meteorology and Oceanography (MetOs), over several years. It has already been established as an important and widely used tool in numerous scientific projects, and especially data from the tropospheric version have been compared to observations in several studies and model inter-comparisons. MIPAS IMK-IAA satellite products are a result of reanalysis of the European Space Agency (ESA) dataset from a very sophisticated limb scanning instrument mounted on their satellite ENVISAT. The reanalysis has been provided by The Institute für Meteorologie und Klimaforschung (IMK) in collaboration with Instituto de Astrofísica Andalucía (IAA).

The main objective of this thesis is to present model distributions of various atmospheric components and validate them against the MIPAS IMK-IAA dataset. The comparisons will mainly be presented as meridional and geographical distributions of seasonal means. The chemical components included

Component	**Included seasons**
O_3	**1, 2, 3, 4**
CH_4	**1, 2, 3, 4**
NO	**4**
NO_2	**4**
N_2O	**1, 2, 3, 4**
N_2O_5	**1, 2, 3, 4**
HNO_3	**1, 2, 3, 4**
HO_2NO_2	**1, 2, 3, 4**
ClO	**1, 2, 3, 4**
$ClONO_2$	**1, 2, 3, 4**
$CFC-11$	**1, 2, 3, 4**
$Temperature$	**1, 2, 3, 4**

Table 1.1: The atmospheric components included in this work. 1=DJF, 2=MAM, 3=JJA and 4=SON

in this work are presented in Table 1.1, and the selection of components and seasons included in this study is based upon which components that are available from both MIPAS IMK-IAA and Oslo-CTM2 datasets from the year 2003.

This study will show that Oslo-CTM2, for the atmospheric species that are included in this thesis, reproduces the atmospheric chemical state in a satisfactory manner when compared to the dataset provided by MIPAS IMK-IAA. Obviously, there are discrepancies between the to methods to calculate chemical abundances, and the most significant ones will be identified and discussed in Chapter 4 of this thesis.

Chapter 2

Theory

2.1 Transport

Meridional and vertical transport of long-lived chemical species in the atmosphere are mainly controlled by the general circulation which per definition is the large-scale movement of airmasses caused by the differential heating of the Earth's surface area by the Sun (Figure 2.1a). The annual cycle of variations in solar heating, which at the surface is most significant near the equator and least significant in polar regions, is caused by the Earth's inclination and orbit around the Sun as shown in Figure 2.1b.
In the troposphere's tropical regions, the meteorological situation is dominated by the Hadley cell which is characterized by strong rising motion (convection) at the "thermal equator", poleward/eastward advection aloft, sinking motion in the subtropics and equatorward/westward advection along the surface. The strong convection carries warm and moist air, packed with earth-emitted molecules from the surface and up to the tropopause. The major mechanism for long-lived tracers to enter the stratosphere is when fractions of the Hadley cell's ascending air penetrates the tropopause and enters the stratosphere as shown in Figure 2.1c. The Hadley cell, together with the Coriolis force, also provide an explanation for the easterly and westerly trade winds, and it was in this context the mechanism was introduced by Georg Hadley as early as in 1735.
The Polar circulation cell (Figure 2.1a) is like the Hadley cell thermally direct, which means that the convection occurs at lower latitudes (higher surface temperatures) than the sinking motion. The convection associated with the Polar cell is normally not strong enough to penetrate the tropopause, and therfore it is of minor importance as a source for long-lived tracers in the stratosphere.
The secondary circulation cell obseved over the midlatitudes in Figure 2.1a is known as the Ferrell cell, and it is thermally indirect. A simplified way to describe the Ferrell cell is that it behaves much as an atmospheric ball bearing between the Hadley and the Polar circulation cells. It is in fact driven by the eddy circulations of the midlatitudes, but its excistence is maintained by its two neighbouring thermally direct circulation cells. The

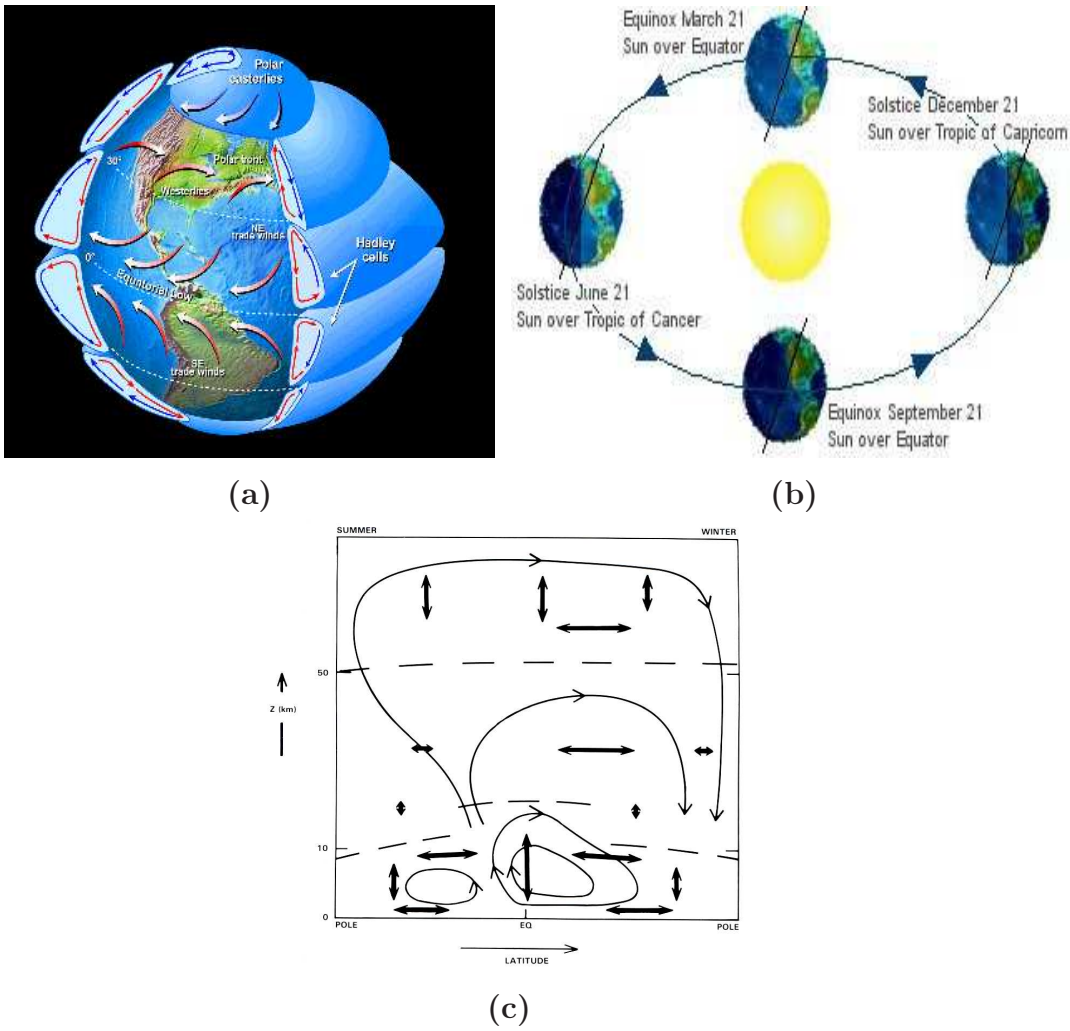

(a) **(b)**

(c)

Figure 2.1: a) The general circulation in the troposphere, b) Earth's orbit with solstices and equinoxes (Source: http://mynasadata.larc.nasa.gov/glossary.php). c) Schematic illustration of zonally-averaged transport processes up to the mesopause. Mean circulation is indicated by single arrows. Quasi-horizontal and vertical diffusion is indicated with double arrows (Source: (UNEP, 1985, page 333))

convection associated with the Ferrell cell is, as for the Polar cell, normally not strong enough to penetrate the tropopause. However, tropopause folding in association with cyclonic storms in these latitudes are on the contrary a major factor of stratospheric air intrusion to the troposphere which is a significant contributor to the downward motion observed in the stratospheric winter hemisphere as shown in Figure 2.1c.

The transport processes in the stratosphere are less dynamically complex than in the troposphere mainly because several of the processes that complicates transport in the troposphere such as phase change of water, planetary boundry layer, strong convection, are not present in this region. The strato-

sphere is as opposed to the troposphere stably stratified, implying that the temperature increases with increasing height, causing stable conditions and lesser internal mixing.
The meridional circulation in the stratosphere known as the Brewer Dobson circulation (Brewer, 1949) consists of three parts, rising motion in the tropics, horizontal poleward motions in the midlatitudes and sinking motion in the polar regions in an annual mean. Unlike the circulation in the troposphere, which is thermally driven by differential heating of the underlying surface, the circulation in the stratosphere is mainly driven by wave activities (Holton et al., 1995). As the air moves poleward from the Equator it must lose angular momentum, and in the absence of any considerable friction in the stratosphere, this loss of angular momentum can only be caused by wave breaking. Rossby waves and gravity waves that originate from the troposphere propagate vertically through the tropopause and into the stratosphere. As the air density decreases with height and the wave amplitude increases, wave breaking occures more easily. Accordingly, the waves deposit its easterly momentum and slows down the westerly wintertime polar jet. The annual variability of this two-cell structure is controlled by these features. Consequently, the cells are similar in size and strenght around equinox (sun directly over equator), whereas around solstice (sun over tropic of Cancer/Capricorn) the circulation pattern is dominated by one cell (Figure 2.1c). This cell has large scale ascent on the summer hemisphere's midlatitudes, horizontal motions towards the winter hemisphere in the upper stratosphere and subsidence in the winterhemisphere's polar regions. Due to hemispheric differences (topograpy and fraction of land/sea areas) the wave activity in the Northern Hemisphere (NH) is stronger than in the Southern Hemisphere (SH), accordingly the circulation pattern associated with NH's winter season are stonger than the SH's winter season.

2.2 Atmospheric Chemistry

In this thesis the abundance of a chemical species is presented as the dimensionless volume mixing ratios (VMR). Abundances are expressed in parts per million (ppm),parts per billion (ppb) and parts per trillion (ppt) in volume (v) corresponding to mixing ratios of 10^{-6}, 10^{-9} and 10^{-12}, respectively. The abundance of molecules in the atmosphere are essentially controlled by four types of processes:

- **Emissions**. Molecules are released into the atmosphere from Earth's surface (or in situ in the atmosphere in a few cases) by a large variety of both natural/biogenic and anthropogenic sources.

- **Chemistry**. Different forms of chemical reactions lead to both formation and removal of species in the atmosphere.

- **Transport**. Horizontal and vertical motions carrie atmospheric species away from their sources or place of origin.

- **Deposition**. Deposition takes two forms, dry and wet deposition. Dry deposition involves direct interaction between the actual component and Earth's surface while wet deposition involves scavenging by precipitation.

2.2.1 Atmospheric chemical reactions

Bimolecular reactions

A bimolecular reaction involves the collision of two reactants A and B to yield two products C and D. The collision produces an activated complex AB^* which either decomposes rapidly back to A and B or produces C and D. This reaction is commonly written as

$$A + B \rightarrow C + D \tag{2.1}$$

and its reaction rate is calculated by

$$-\frac{d}{dt}[A] = -\frac{d}{dt}[B] = \frac{d}{dt}[C] = \frac{d}{dt}[D] = k[A][B], \tag{2.2}$$

where k is the effective rate coefficient and the concentrations, in square brackets, are number densities. The rate of bimolecular reactions are dependent on the frequency of collisions and on the fate of the activated complex. The number density of an atmospheric species, x, and the mixing ratio, C_x, are related by the number density of air, n_a (molecules of air per cm^3 of air)

$$n_x = C_x n_a. \tag{2.3}$$

Three-body reactions

A three-body reaction involves reactions of two species A and B to yield one single product species AB. This reaction requires a third body M (generally N_2 and O_2 in the atmosphere) to stabilize the excited product AB^* by collision. A three-body reaction actually consists of several bimolecular reactions, but it is common practice to write the overall three-body reaction as

$$A + B + M \rightarrow AB + M \tag{2.4}$$

to emphasize the need for a third body. The reaction rate of a three-body reaction is calculated by

$$-\frac{d}{dt}[A] = -\frac{d}{dt}[B] = \frac{d}{dt}[AB] = \frac{k_3 k_5 [A][B][M]}{k_4 + k_5[M]}, \tag{2.5}$$

where k_3, k_4 and k_5 are effective rate coefficients for the different underlying bimolecular reactions.

Photolysis

Photolysis is a photochemical process by which molecules are broken down into smaller parts through the absorption of radiation. A photolysis reaction involves the breaking of a chemical bond in a molocule by a photon, and is commonly written as

$$X + h\nu \rightarrow Y + Z, \tag{2.6}$$

and its reaction rate is calculated by

$$-\frac{d}{dt}[X] = \frac{d}{dt}[Y] = \frac{d}{dt}[Z] = k[X], \tag{2.7}$$

where k is a photolysis effective rate coefficient or photolysis frequency.

Thermal decomposition reactions

Thermal decomposition is a chemical reaction where an atmospheric species breaks up spontanously into simpler compounds when it reaches a certain compound dependent temperature. Due to the relatively low temperatures in the troposphere/stratosphere this is not a very common feature, but it is significant in some regions and for some species such as HO_2NO_2, $ClOO$ and Cl_2O_2.

Heterogeneous reactions

Heterogenous chemistry refers to reactions occuring at the interface between two phases. In atmospheric chemistry, the term is often used to describe reactions ocurring inside, or at the surface, of droplets or particles. These reactions are significant for the complex chemistry in polar stratospheric clouds (PSCs) transforming reservoir species into active components responsible for the ozone-depletion that occurs especially in the Antarctic winter.

2.2.2 Atmospheric lifetime

The concept of lifetime, τ_x, is defined as the average time it takes for the abundance of a molecule, x, in the absence of production, to be redused by a factor $\frac{1}{e}$, also known as e-folding time, and it is calculated by

$$\tau_x = \frac{1}{k_x}. \tag{2.8}$$

The abundance of a molecule would, without any production, be redused according to

$$n = n_0 \exp(-kt), \tag{2.9}$$

where n_0 and n are the concentrations initially and at time t, respectively. The overall atmospheric lifetime, τ_{tot}, describes how long it takes to restore the system to equilibrium following a perturbation in the concentration of the gas in the atmosphere. Individual molecules may interact with other

reservoirs such as soil, oceans and biological systems. The net changes in concentration by all sinks determine overall atmospheric lifetime according to

$$\frac{1}{\tau_{tot}} = \frac{1}{\tau_a} + \frac{1}{\tau_b} + ..., \tag{2.10}$$

where a and b are various sinks.

2.3 Radiation

Electromagnetic radiation is energy transmitted by electromagnetic waves, and it is the most important process responsible for energy transfer in the atmosphere. All electromagnetic waves travel at the speed of light ($c \approx 3.0 * 10^8\ ms^{-1}$), and the electromagnetic spectrum consists of gamma rays, x-rays, ultraviolet light (UV), infrared radiation (IR), microwaves and visible light (VIS), which are categorized by their different wavelengths (λ), frequencies (f), or wavenumbers (ν). These are related to eachother by

$$\lambda = \frac{c}{\nu} \qquad\qquad \nu = \frac{f}{c} = \frac{1}{\lambda}. \tag{2.11}$$

The part of the electromagnetic spectrum relevant in limb scanning of the atmosphere is IR, which covers wavenumbers from 10 to 10000 (Liou, 1989).

Blackbody radiation laws

The laws of blackbody radiation are basics for understanding the absorption and emission processes for a medium under thermodynamic equilibrium. The term "blackbody" refers to an object that completely absorbs the radiation which it encounters.
At about 1900, the German physicist Max Planck stated a law for the connection between the radiation flux density of a blackbody and its temperature. To show this he assumed that oscillator energy is quantized and that atoms behave like tiny electromagnetic oscillators that do not radiate continuously, but in jumps later known as quanta. These assumptions led to Planck's function that relate the emitted monochromatic intensity to the frequency and temperature of the emitting substance.
The total radiant intensity of a blackbody can be derived by integrating the Planck function over the entire wavelenght domain from 0 to ∞. This leads to Stefan-Boltzmann law,

$$F = \sigma T^4, \tag{2.12}$$

which states that the flux density, F, emitted by a blackbody is proportional to the fourth power of its absolute temperature.
Wiens'displacement law states that the wavelenght of the maximum intensity of blackbody radiation is inversely proportional to its absolute temperature, and this wavelength, λ_m is given by

$$\lambda_m = \frac{a}{T}, \tag{2.13}$$

where $a = 2.897 \times 10^{-3}$ m deg.
An objects "blackness" or "greyness" are described by its absorptivity (A_λ) and emissivity (ε_λ), thus for a blackbody and grey bodies we have

$$A_\lambda = \varepsilon_\lambda = 1 \qquad\qquad A_\lambda = \varepsilon_\lambda < 1, \tag{2.14}$$

respectively. This is described by Kirchhoff's law which states that "At thermal equilibrium, the emissivity of a body (or surface) equals its absorptivity". Kirchhoff's laws requires the condition of thermodynamic equilibrium, so that uniform temperature and isotropic radiation are achieved. The atmosphere in its entirely is not in thermodynamic equilibrium, but below 60-70 km in a localized volume it may be considered in local thermodynamic equilibrium (LTE), and in these regions Kirchhoff's laws are applicable.

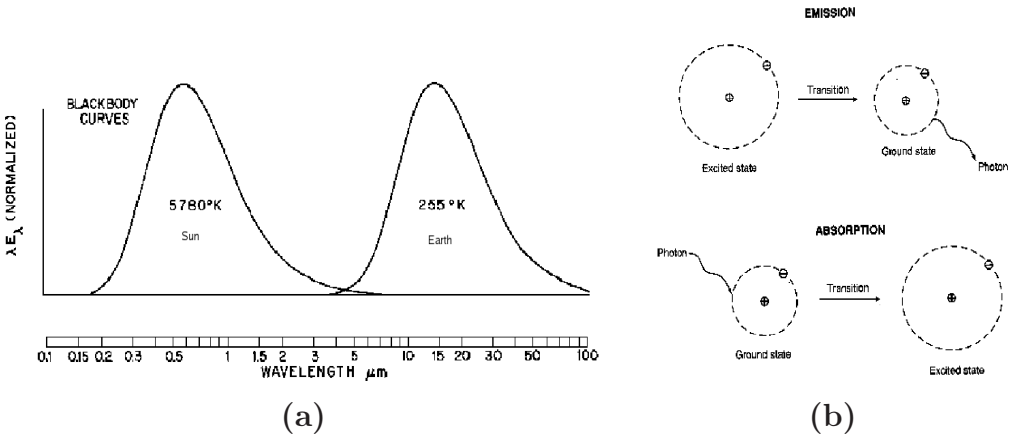

(a) **(b)**

Figure 2.2: a) Normalized blackbody curves for 5780 K and 220 K plotted so that irradiance is proportional to the areas under the curves (Source: (Wallace and Hobbs, 1977, page 332)). b) Illustrates emission and absorption for a hydrogen atom (Source: (Liou, 1989, page 15)).

Atmospheric molecules absorption and emission

MIPAS IMK-IAA retrieves the stratospheric abundances of different components from scanning the Earth's limb in the mid-IR region of the electromagnetic spectrum. This is possible since the atmosphere below 60-70 km can be considered to be in local thermodynamic equilibrium. Consequently one can assume that the molecules in this region behave like blackbodies and use the above mentioned laws to achieve their radiational characteristics. Inspection of high-resolution spectroscopy reveals that the emission spectra of certain gases are composed of a large number of individual and characteristic spectral lines. These lines are formed when an atom changes state, either due to absorption or emission of radiation, and leaves "signatures" in the electromagnetic spectrum making it possible for instruments such as spectrometers and interferometers to translate radiation to chemical abundances. Figure

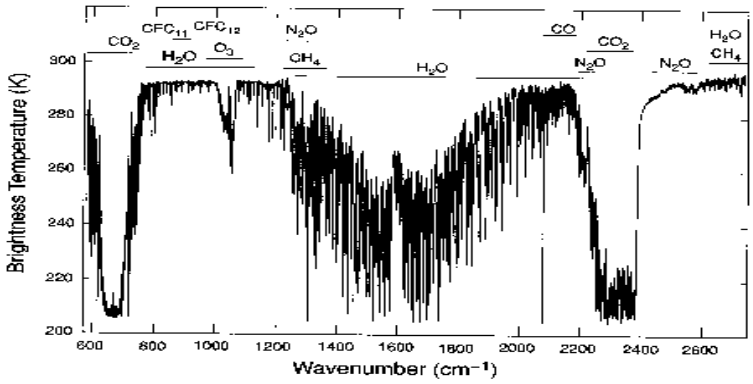

Figure 2.3: Example of an observed infrared spectrum displaying some absorbing gases and their spectral location (Source: (Liou, 1989, page 122)).

2.3 shows an example of spectral location to the absorption lines for different atmospheric components and how they influence the IR radiation emitted by Earth's atmosphere.

Chapter 3

Data and methods

3.1 Oslo-CTM2

The Oslo-CTM2 is a three dimensional global chemical transport model with several options for resolution (horizontal and vertical), meteorological data, emissions and number of chemical components and reactions.
Starting out as a tropospheric chemical transport model (Sundet, 1997; Berntsen and Isaksen, 1997), Oslo-CTM2 has evolved into a comprehensive tropospheric and stratospheric model that has separate modules that includes stratospheric chemistry (Gauss et al., 2006), sulphur chemistry (Berglen et al., 2004), sea salt (Grini et al., 2002), mineral dust (Grini et al., 2005), Black/organic carbon (BC/OC) (Berntsen et al., article in preparation), nitrate aerosols (Myhre et al., 2006), secondary organic aeroslos (SOA) (Hoyle et al., article in preparation) and updated heterogenous chemistry (Søvde, 2007). All modules are available and can be included indivudually in a model run. Recently, chemical kinetics and photochemistry have been updated by B. Rognerud (University of Oslo, MetOs section) in accordance with the Jet propulsion labaratory (JPL) of National Aeronautics and Space Administrations (NASAs) Publication No. 06-2 (Chemical Kinetics and Photochemical Data for Use in Atmospheric Studies). However, the chemical kinetics and photochemistry in the stratospheric module used in the Oslo-CTM2 version applied in this work are based on JPL/NASA Publication 02-25.

3.1.1 General description

The Oslo-CTM2 may adopt different horizontal and vertical resolutions. Horizontal resolutions available are T21(5.625^o x 5.625^o), T42(2.81^o x 2.81^o), T63(1.875^o x 1.875^o) and 1^o x 1^o, while vertical resolutions available are 19, 40 and 60 layers (Figure 3.1 and 3.2).
The European Centre for Medium-Range Weather Forecasts (ECMWF) 40 Year Re-analysis (ERA-40) or ECMWFs Integrated Forecasting System (IFS) weather forecast model can be used for the dynamical development in the periode of interest. Other weather parameters such as cloud properties, temperature, pressure and humidity are retrived from the chosen meteorological

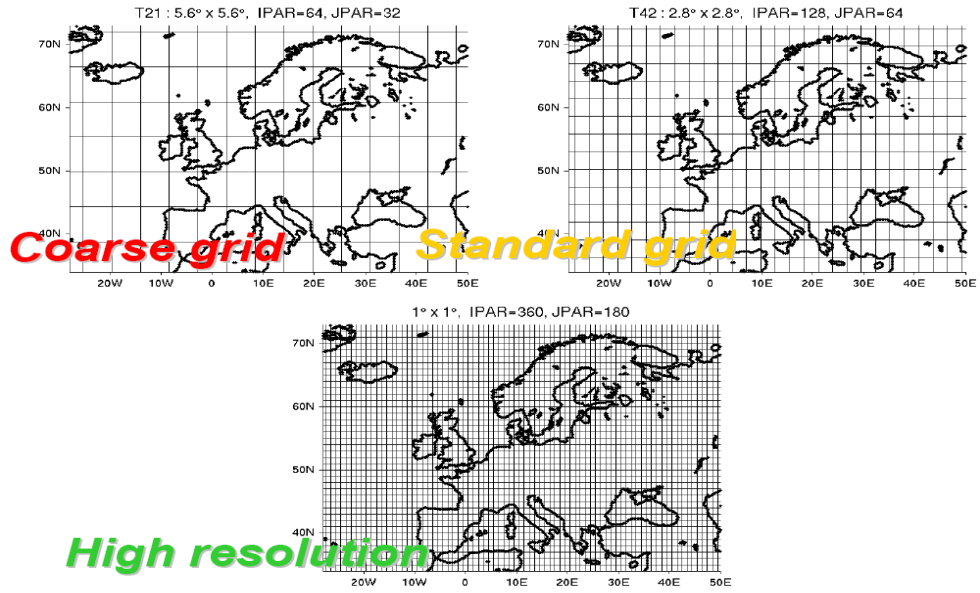

Figure 3.1: Horizontal grids available T21, T42 and 1^o x 1^o (Source: M.Gauss).

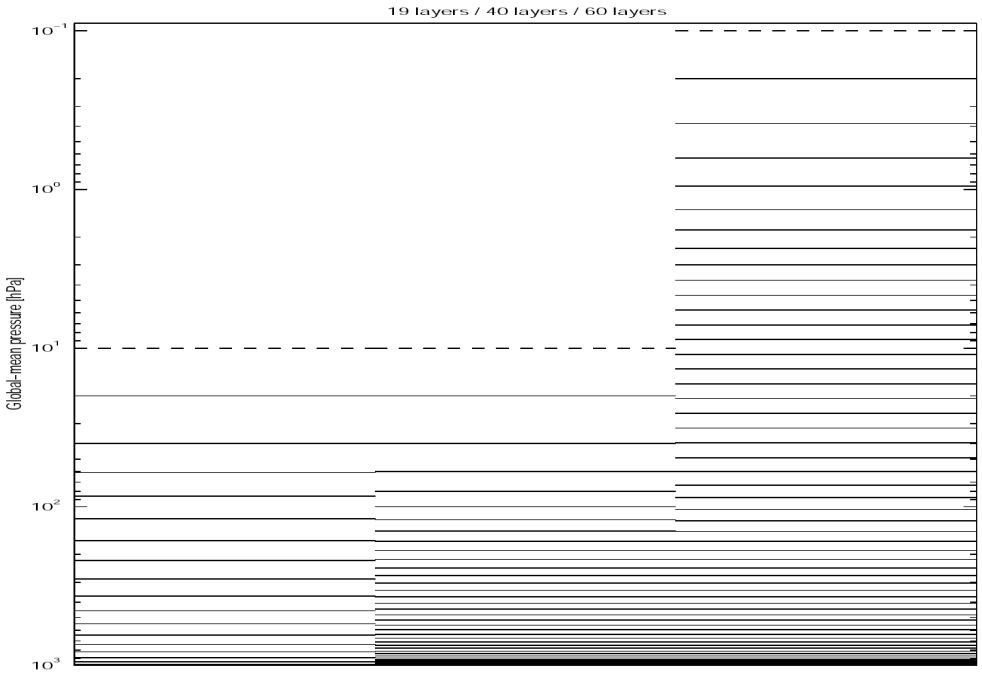

Figure 3.2: Vertical grids available 19, 40 and 60 layers (Source: M.Gauss).

dataset. Horizontal advection is solved using the Second Order Moment (SOM) method (Prather, 1986), while convection is calculated based upon vertical mass-fluxes in the respective column. Mass flux updraft, downdraft, entrainment and detrainment are provided by the chosen meteorological dataset. The planetary boundary layer (PBL) mixing is calculated using eddy

diffusion coeffisients from Holtslag et al. (1990), and the dynamical timestep of the model is one hour. Abundances of chemical tracers are solved using the Quasi steady-state approximation (QSSA) method (Hesstvedt et al., 1978), which is a mathematical way of simplifying the differential equations describing the chemical kinetic system in Oslo-CTM2. The tropospheric module contains 51 tracers, whereas 62 tracers are included in the stratospheric module. Numerous thermal and photolytic reactions are included in the model. For a complete summary of tracers and reactions see Appendix A and B adopted from Gauss (2003). The chemical timestep in the model is optional but the default value is five minutes. Whether to apply the stratospheric or tropospheric chemical module for tracer abundance calculations in a certain grid cell, is based upon The National Centers for Environmental Prediction (NCEP) tropopause data. For species important for stratospheric chemistry the upper boundary conditions are fixed by climatological mixing ratios provided by the Oslo-2D model (Stordal et al., 1985). In the near future, the basis for the emissions used in the tropospheric chemistry module may be chosen from either the EU projects RETRO (REanalysis of the TROpospheric chemical composition over the past 40 years) (Schultz et al., 2006), covering the period 1960-2000, or POET (Precursors of Ozone and their Effects in the Troposphere) (Olivier et al., 2003), covering the period 1990-2001. Currently the POET database, which includes surface emissions of active nitrogen species (NO_x), Carbon monoxide (CO), non methane volatile organic compounds ($NMVOC$s) and zonal averaged Methane emissions based on observations, is default in the model. Secondary emission inventories included in the model are lightning NO_x emissions, which are based on Price et al. (1997a,b) and Pickering et al. (1998) and aircraft emissions which again are based on a NASA inventory (Baugchum and Henderson, 1998). For dry deposition, the Rodhe and Isaksen (1980)-method is used, while for wet deposition, the model separates between large scale rainout and rainout in convective clouds (Berglen et al., 2004).

3.1.2 Oslo-CTM2 setup for this study

In this study the Oslo-CTM2 has been run with T42 horizontal resolution with 60 vertical layers covering the atmosphere from the surface up to 0.1 hPa (Figures 3.1 and 3.2). Consequently, the troposphere, stratosphere and the lower part of the mesosphere are included in the vertical model domain. Based on the main objective of this thesis, the tropospheric and stratospheric modules and the updated heterogenous chemistry are included. IFSL60 has been used for meteorological data, while POETs database for the year 2000 provided the emission inventories. Figure 3.3 shows a simplified schematic overview of the current setup and the most important vertical boundaries in the model domain.

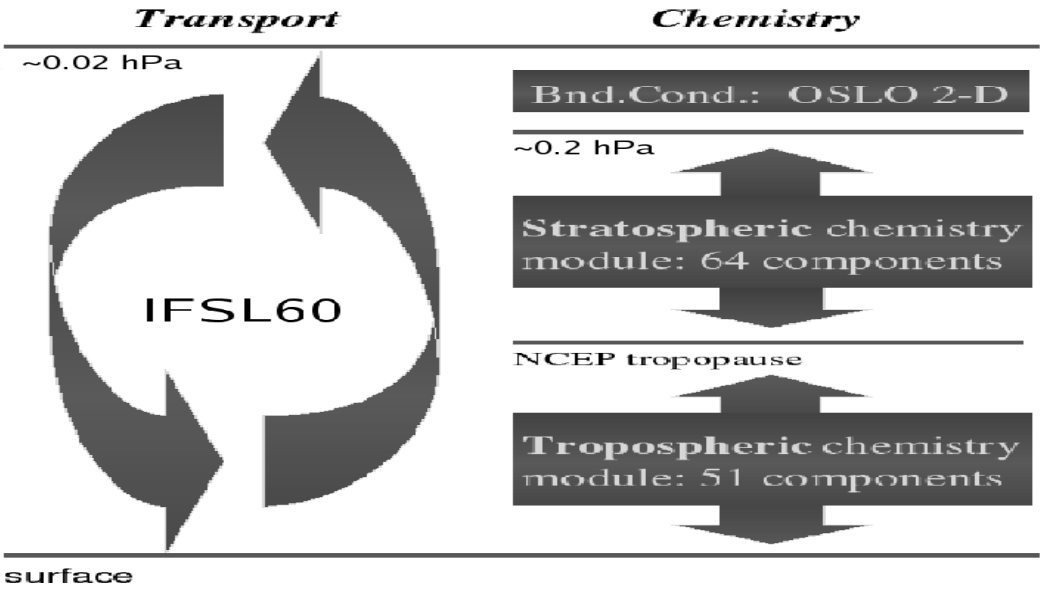

Figure 3.3: Current setup for Oslo-CTM2 (Source: M.Gauss).

The model run

The period of interest is December 2002 throught November 2003 and the model run was initiated from the 1. July 2002, ending 31. January 2004. Consequently, the spin-up time is five months, and the first day included in the model output dataset is 1. December 2002. Outputs were saved when the model reached the 1. of every month, and they consists of the previous monthly time-averaged VMRs for the chosen atmospheric components. These monthly mean files form the basis of the presented results and plots and graphics were prepared using the Interactive Data Language (IDL).

3.2 MIPAS

The Michelson Interferometer for Passive Atmospheric Sounding (MIPAS) is a Fourier transform mid-infrared limb scanning spectrometer designed for measuring atmospheric composition and temperature by means of the termal emission of the atmosphere (von Clarmann et al., 2003a). A MIPAS instrument is included as a part of the payload on the European Space Agency (ESA) Environmental Satellite (ENVISAT) that was successfully launched into its sun-synchronous orbit on 1. March 2002 (Figures 3.4 and 3.6). ENVISAT orbits the Earth once every ∼100 min, resulting in approximately 14.5 polar orbits per day.

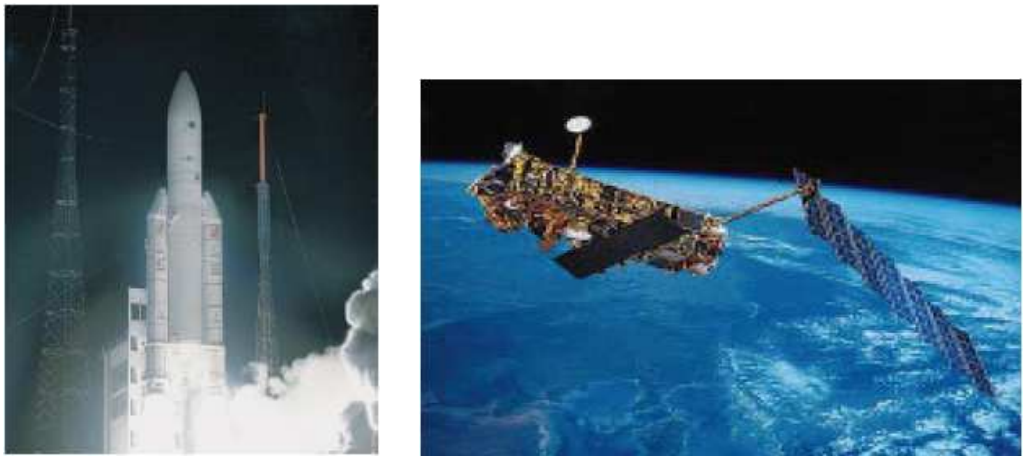

(a) **(b)**

Figure 3.4: a) Shows the successfull launch of the Ariane-V rocket that carried ENVISAT to its orbit on the 1. March 2002, while b) shows the ESA Envisat satellite in orbit (Source: ESA).

3.2.1 General description

The MIPAS instrument is specified to give near-real-time data within three hours after measurement time. This evidently implies severe operational constrains on the data products delivered directly from ESA. The spectral range of the instrument is from 685 to 2410 cm^{-1}, divided in five spectral bands: band A(685-970 cm^{-1}), band AB(1020-1170 cm^{-1}), band B(1215-1500 cm^{-1}), band C(1570-1750 cm^{-1}), and band D(1820-2410 cm^{-1}). The spectral ranges limits corresponds to 4,15 and 14.6 μm, and the spectral resolution is 0.035 cm^{-1}. Consequently MIPAS makes a high quality analysis of the mid-IR part of the electromagnetic spectrum. The pre-launch anticipated altitude range and precision are shown in Figure 3.5 adopted from Endemann et al. (2000).
In Figure 3.6a the MIPAS instruments rearward and sideway viewing ranges can be seen. The rearward view is to achieve a good global coverage, while the

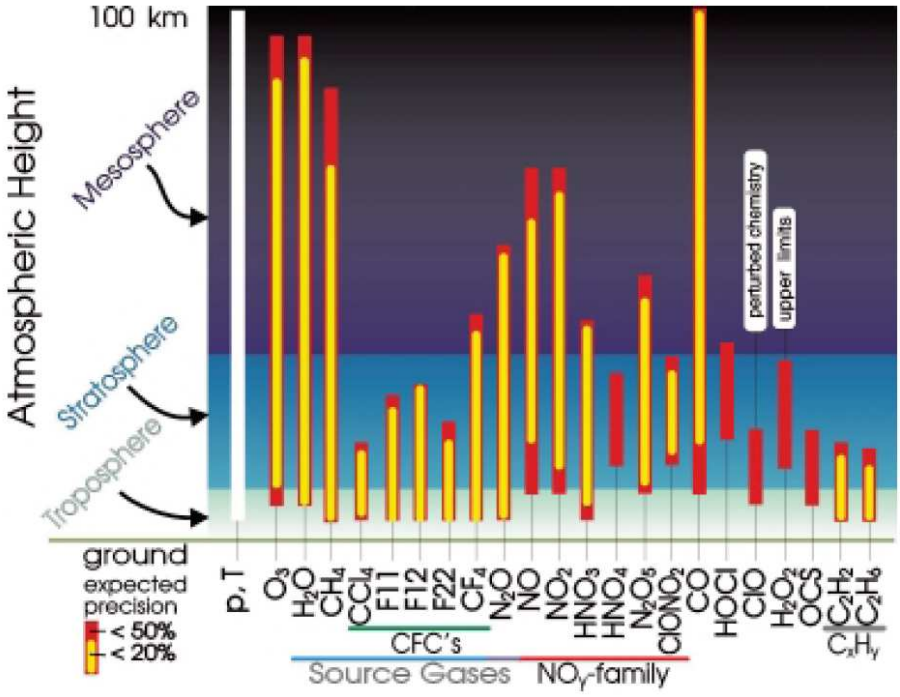

Figure 3.5: Anticipated altitude range and precisions for species that can be detected by MIPAS (Source: ESA).

sideway view is to capture special events, such as volcano eruptions, tracegas concentrations over major air-traffic routes or dusk/dawn chemistry (Endemann et al., 2000). Figure 3.6b shows the geometry of a sun-synchronous orbit where one can observe that the angle between the orbital plane and the Earth-Sun direction is almost constant troughout the year.

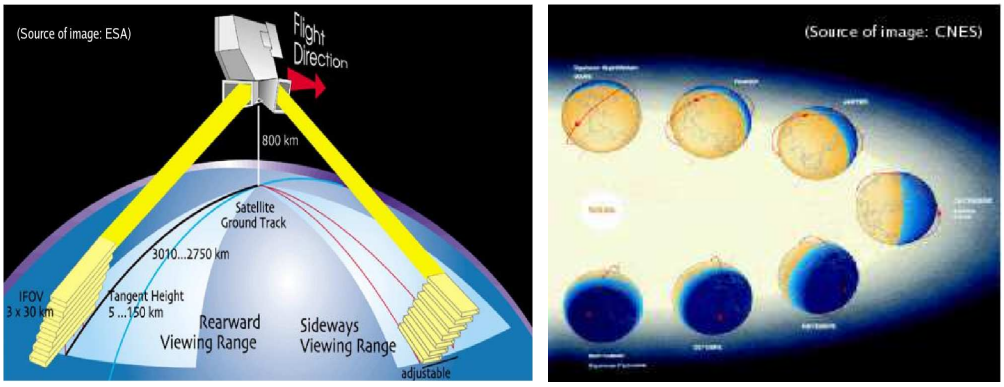

(a) **(b)**

Figure 3.6: a) MIPAS observation geometry and rearward/sideway viewing ranges, b) shows a sun-synchronous orbit.

3.2.2 The limb sounding technique

Limb sounding is the general approach for obtaining vertical profiles of atmospheric chemical species from several limb measurements (Figure 3.6a). A limb measurement is referred to as when a spectrometer, viewing horizontally, recovers radiation from the atmosphere in the instruments field-of-view (IFOV) (Liou, 1989). The IFOV of a MIPAS scan is only 3 km high (giving good vertical resolution) and about 30 km wide. The horizontal spread of the tangent points due to the satellites own movement during a sounding (Figure 3.6a) is approximately 400 km. MIPAS starts scanning from the defined top of atmosphere (TOA), and as the satellite continues in its orbit, the instrument does multiple measurements further and further down in the atmosphere until an approximately vertical sounding is achieved.

There are a number of beneficial features of limb scanning for atmospheric soundings:

- The emission orginates in the few kilometers immediately above the tangent point because of the rapid decrease in atmospheric density and pressure.
- All radiation recieved comes solely from the atmosphere.
- A large degree of opacity is involved along a horizontal path.
- The viewing direction from the satellite can be oriented in any azimuthal direction relative to the satellite motion and covers a large area.

There are also some disadvantages with the limb sounding tecnique:

- The interference of high clouds along the ray path produces considerably uncertainty in the emitted radiation.
- The horizontal stretcing of a sounding leads to problems of interpretation of large changes in the atmospheric state over this distance.

Based on the above mentioned pro and cons, the limb scanning technique has been shown to give relative accurate retrivals of atmospheric components abundances in the UTLS, stratosphere and mesosphere. While the uncertainties and source of errors increases rapidly with decreasing retrival height in the troposphere.

3.2.3 IMK-IAA processed data

IMK, situated in Karlsrühe, Germay, has in collaboration with IAA, situated in Granada, Spain, developed their own data processors, KOPRA (Karlsruhe Optimized and Precise Radiative transfer Algorithm), dedicated to reanalyse ESAs MIPAS data in view of particular scientific problems. Since no real-time processing constrains apply to these data processors, one can afford

considerably more sophisticated data analysis strategies and algorithms. The processing sequence in MIPAS IMK-IAA retrival strategy consist of four individual steps; (1) cloud detection, (2) correction of spectral shifts, (3) retrival of temperature and line of sight pointing and (4) retrival of the abundance of atmospheric species. The processing tools developed by IMK and IAA complement the official ESA level 2 MIPAS data processor (Figure 3.5) in the sense that they are designed for retrieval of additional species and to cope with more challenging retrieval applications where non-LTE, clouds or horizontal inhomogeneties have to be considered. The abundances of atmospheric constituents is represented and retrived on a relatively high resolved fixed altitude grid (4-44 km: 1 km; 44-70 km: 2 km; 70-80 km: 5 km; 80-100 km: 10 km; 100-120 km: 20 km), and the World Geodetic System 1984 (WGS84) is used as a global reference.
The main components have been individually validated and the data processor proves to be robust when applied to real MIPAS measurements data (von Clarmann et al., 2003a). In this study the spectra version V30 is used for all the included atmospheric components (Table 1.1) and temperature, and the data is downloaded from (http://www-imk.fzk.de/asf/ame/).

3.2.4 Data coverage

Due to the complexity of the processing done by IMK-IAA there are limitations to the data coverage during the year. For some species the coverage is resonably good, while for others there are relatively large periods of the year that lack data (Figure 3.7 shows some coverage examples).
The fact that MIPAS IMK-IAAs product has a relatively sparse temporal resolution is the basis for presenting results as seasonal means. The seasons are defined as December(2002)-Janury-February (DJF), March-April-May (MAM), June-July-August (JJA) and September-October-November (SON). Due to the sparse temporal data coverage provided by MIPAS IMK-IAA each defined season consists of between 10 and 25 days with full day and night coverage. DJF and SON are the seasons with best coverage, whereas MAM and JJA contain slightly less data.

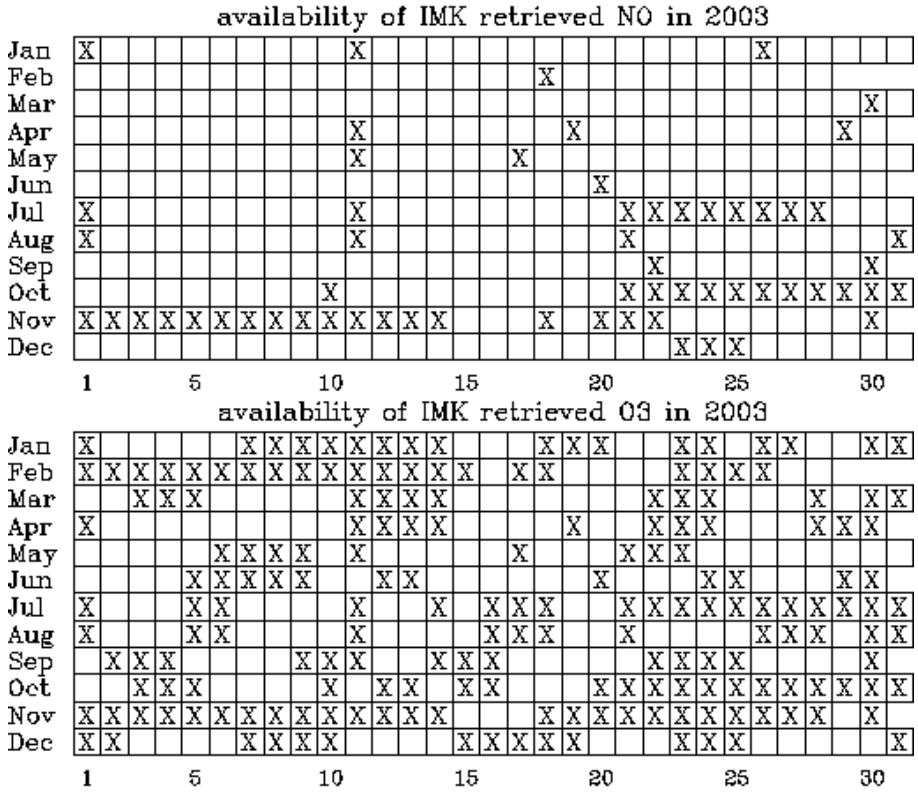

Figure 3.7: Data coverage of NO (top table) and O_3 (bottom table) provided by MIPAS IMK-IAA for the year 2003 (Source: http://www-imk.fzk.de/asf/ame/envisat-data/).

Chapter 4

Results and discussions

This chapter contains result and comparison figures between Oslo-CTM2 and MIPAS IMK-IAA for all included atmospheric species. Since the model generally performes well compared to MIPAS IMK-IAA the focus will be on the areas where the differences between the two products are largest.
The meridional distribution figures presented in this chapter are all, except Figure 4.65, presented with a vertical range from 100 hPa to 0.8 hPa. This is based on the limitations of the limb sounding technique (see Section 3.2.2) and the main objective of this study.

4.1 Methane (CH_4)

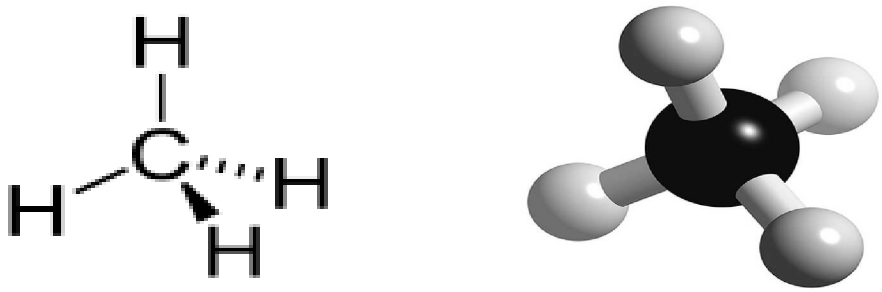

(a) **(b)**

Figure 4.1: Molecular structure of CH_4 (http://www.3Dchem.com)

CH_4 is the most abundant naturally occuring trace gas in the atmosphere and the third most abundant greenhouse gas in the troposphere after water molecule (H_2O) and carbon dioxide (CO_2). CH_4 consists of one carbon atom and four hydrogen atoms (Figure 4.1), and on a per molecule basis, CH_4 has a greater climate warming potential than CO_2. CH_4 is fairly reactive and consequently plays an important role in both tropospheric and stratospheric chemistry.

CH_4 is the end product during decomposition of organic matter in oxygen-deficient wetland habitats such as swamps, lakes, tundra and rice paddies. Approximately 35% of total CH_4 emissions are released naturally by wetlands, termites, oceans, hydrates, geological sources, wild animals and wildfires, whereas the most important anthropogenic emissions (65% of total emissions) originate from coal mining, gas/oil industry, landfills/waste treatment, ruminants, rice agriculture and biomass burning (Denman et al., 2007). The largest methane sinks are oxidation by hydroxyl (OH) and oxygen atoms in excited state ($O(^1D)$), more than 85% of the total atmospheric CH_4 is removed in this manner. Other sinks are diffusion into soils where it is consumed by bacteria and in stratospheric bimolecular reaction with chlorine producing hydrogen chloride (HCl) and the metyl radical (CH_3).
The amount of CH_4 in the atmosphere has increased dramatically since the beginning of the 19^{th} century. The most probable cause of this observed increase is the greater biogenic emissions associated with a rising human population.

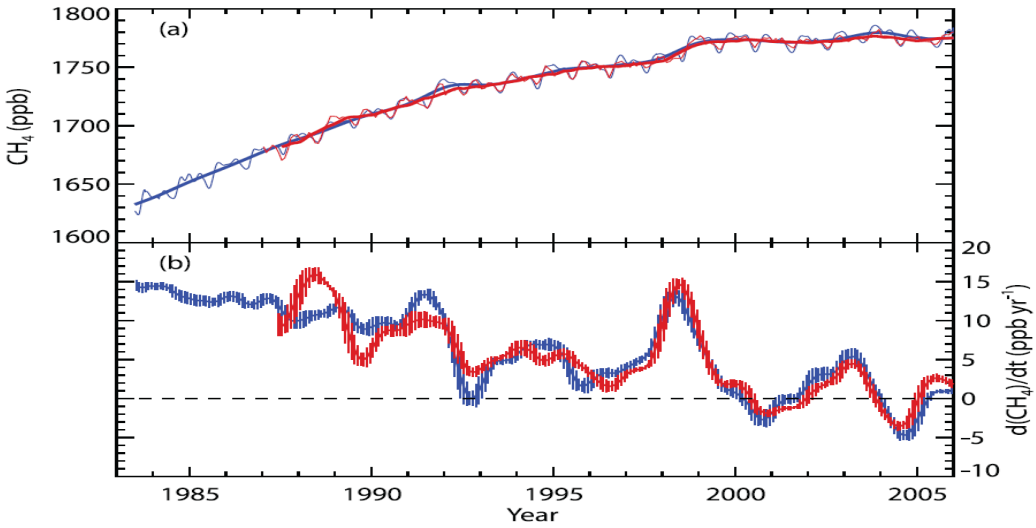

Figure 4.2: Recent CH_4 concentrations and trends. a) Time series of global CH4 abundance mole fraction (in ppb) derived from surface sites operated by NOAA/GMD (blue lines) and AGAGE (red lines). b) Annual growth rate (ppb yr^{-1}) in global atmospheric CH4 abundance from 1984 through the end of 2005 (NOAA/GMD, blue), and from 1988 to the end of 2005 (AGAGE, red) (Source: (Forster et al., 2007, page 142)).

Figure 4.2 shows the recently observed concentrations and trends for CH_4 abundances. It shows that its concentration has stabilized at approximately 1775 ppb (mole fraction) and that the annual growth rate in ppb yr^{-1} has decreased substantially in the last two decades. The reasons for the decreased atmospheric CH_4 growth rate are not fully understood, but seems to be associated with changes in the imbalances between CH_4 sources and sinks (Forster et al., 2007). CH_4 also has an important positive feedback

cycle associated with global warming. There are large quantities of methane stored in regions with permafrost that may partly, with an increase in global temperature, be released to the atmosphere and cause additional warming.
In Oslo-CTM2 methane sources are mainly emissions from the surface (POET), while its sinks are oxidation by OH, $O(^1D)$ and Cl. MIPAS IMK-IAA retrieves VMR for CH_4 and N_2O jointly, and the microwindows selected for this retrival are in the spectral region 1230-1305 cm^{-1} (Glatthor et al., 2005). Hence, the fundamental methane vibration band, ν_4, is covered. Table 4.1

Height (km)	CH_4	N_2O
10	**240 (10)**	**43 (12)**
15	**230 (11)**	**41 (12)**
20	**190 (11)**	**25 (10)**
25	**180 (12)**	**18 (10)**
30	**250 (19)**	**24 (12)**
35	**280 (24)**	**22 (23)**
40	**150 (19)**	**12 (33)**
44	**110 (19)**	**4 (30)**
50	**67 (22)**	**1 (29)**

Table 4.1: Total error for CH_4 and N_2O retrival for a scan on 26 Sep 2002 (orbit 2994) taken during daytime in SH's midlatitudes. The errors are given in absolute (ppbv) and relativ units (% in brackets). For a complete summary over the error budget for CH_4 see Glatthor et al. (2005, page 789).

shows an example of total errors from the MIPAS IMK-IAA dataset for CH_4 and N_2O. From the table one can observe that in the UTLS the relative error is approximately 10%, and that it rises with increasing height.

4.1.1 Meridional distributions

Since methane has all its major sources at the Earth's surface and its dominating sinks are in the stratosphere, the VMR abundance will decrease rapidly with increasing height in the UTLS region. Only the amount that is vertically transported across the tropopause enters the stratosphere and is influenced by this region's chemical and dynamical processes.
We find that in the meridional distributions of seasonally averaged VMR Oslo-CTM2 consistently underestimates the abundance of stratospheric CH_4, especially in the tropical region in all four seasons (Figures 4.3 to 4.6). This is most probably caused by to weak transport in Oslo-CTM2 and will be further discussed in Section 4.4. Oslo-CTM2 seems to overestimate the abundance of CH_4 inside the polar vortex, which also may be associated with a too weak stratospheric transport. Another plausible explanation for this deviation can be shortage of either $O(^1D)$, OH or Cl that are, as mentioned above, the most significant sinks for CH_4. The VMR in the meridional distributions for CH_4 are presented in ppmv for all four seasons.

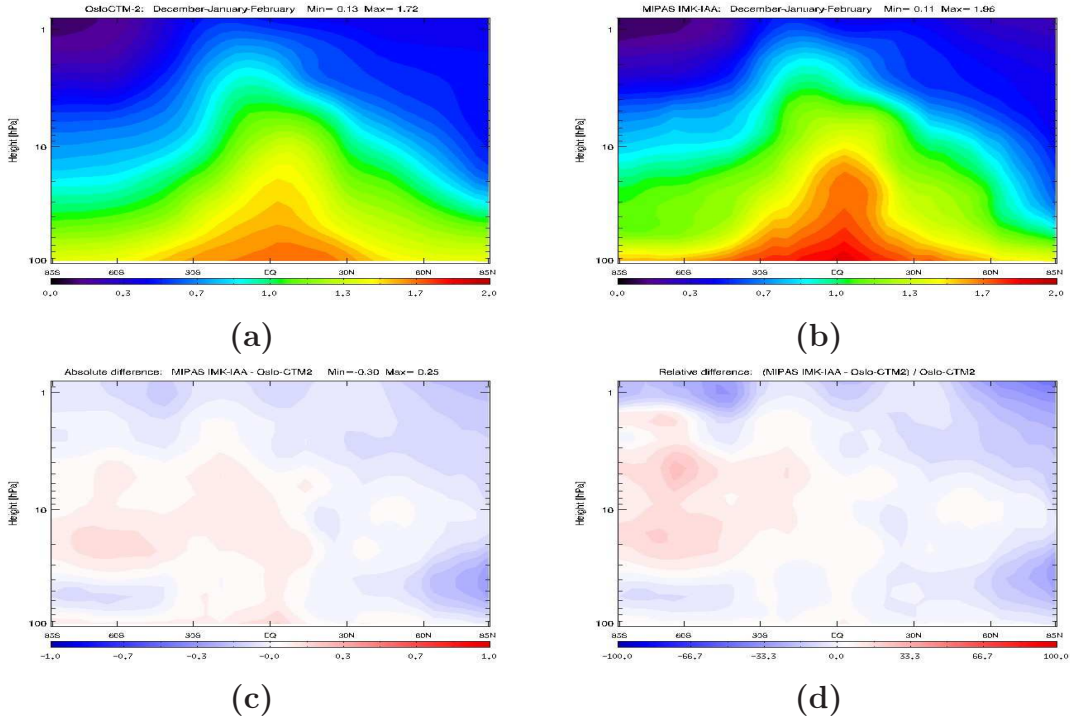

Figure 4.3: Meridional distribution of CH_4 for DJF. a) Oslo-CTM2, b) MIPAS IMK-IAA, c) absolute difference and d) relative difference.

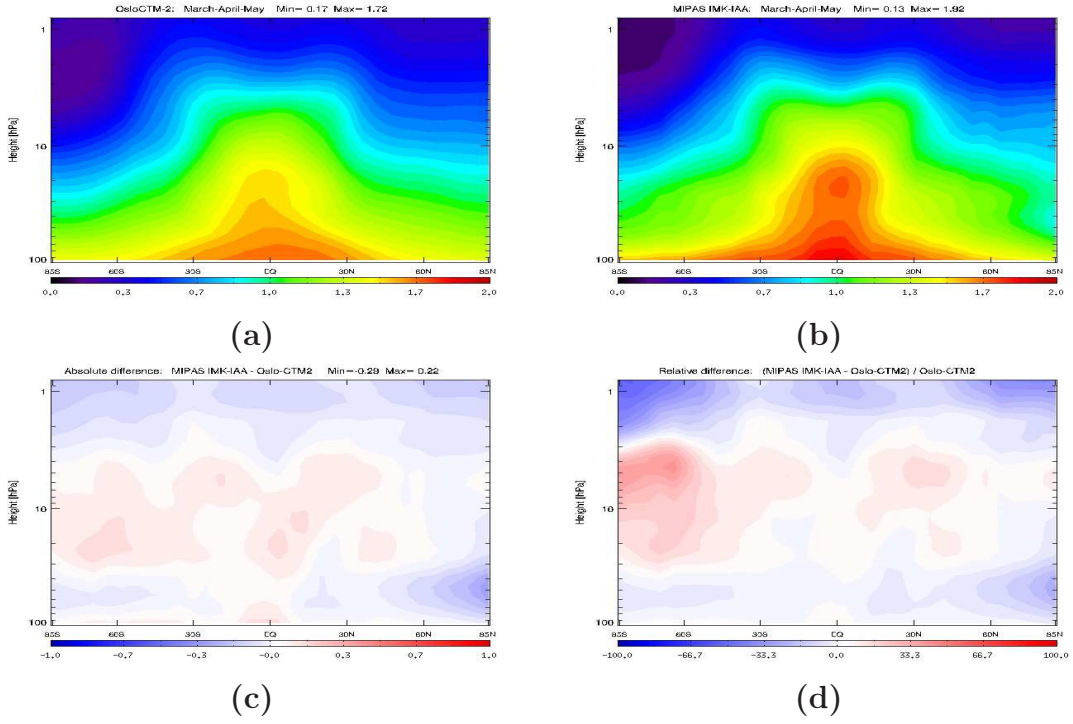

Figure 4.4: Meridional distribution of CH_4 for MAM. a) Oslo-CTM2, b) MIPAS IMK-IAA, c) absolute difference and d) relative difference.

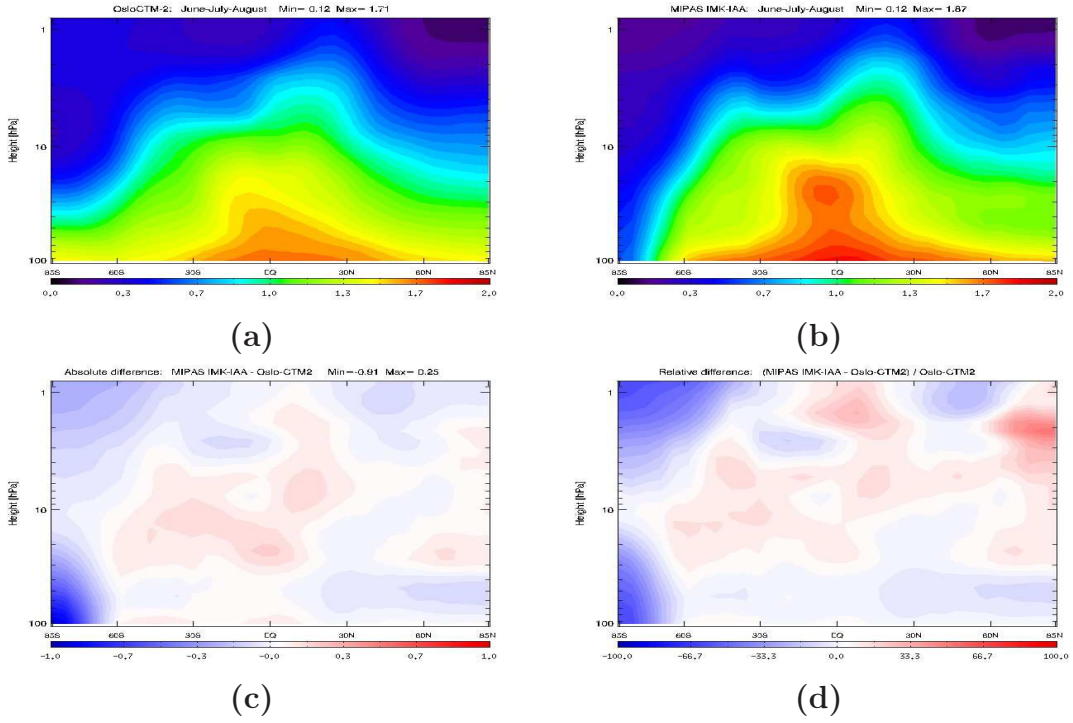

Figure 4.5: Meridional distribution of CH_4 for JJA. a) Oslo-CTM2, b) MIPAS IMK-IAA, c) absolute difference and d) relative difference.

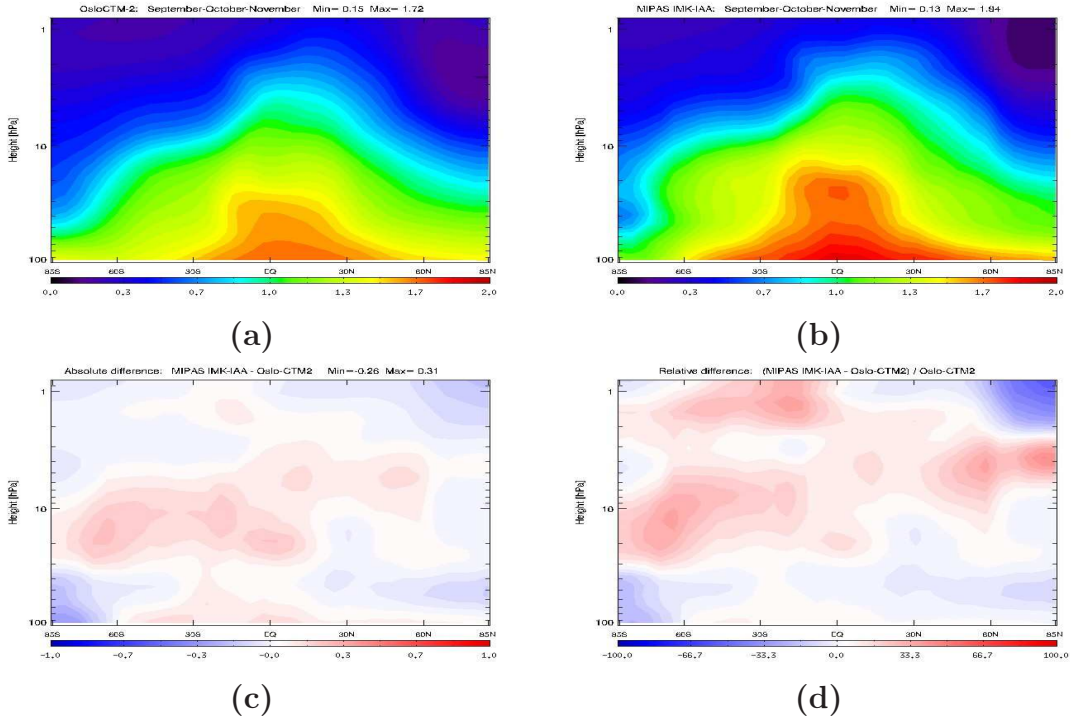

Figure 4.6: Meridional distribution of CH_4 for SON. a) Oslo-CTM2, b) MIPAS IMK-IAA, c) absolute difference and d) relative difference.

4.1.2 Vertical column for Methane

Geographical distributions

From the geographical distributions of stratospheric CH_4 columns shown in Figure 4.7, we find that Oslo-CTM2 consistently underestimates the abundance of methane in tropical regions and that it overestimates in winter hemisphere polar regions, especially in seasons containing solstices (DJF and JJA). Nevertheless it seems that besides these discrepancies, the general structures of the fields are comparable.

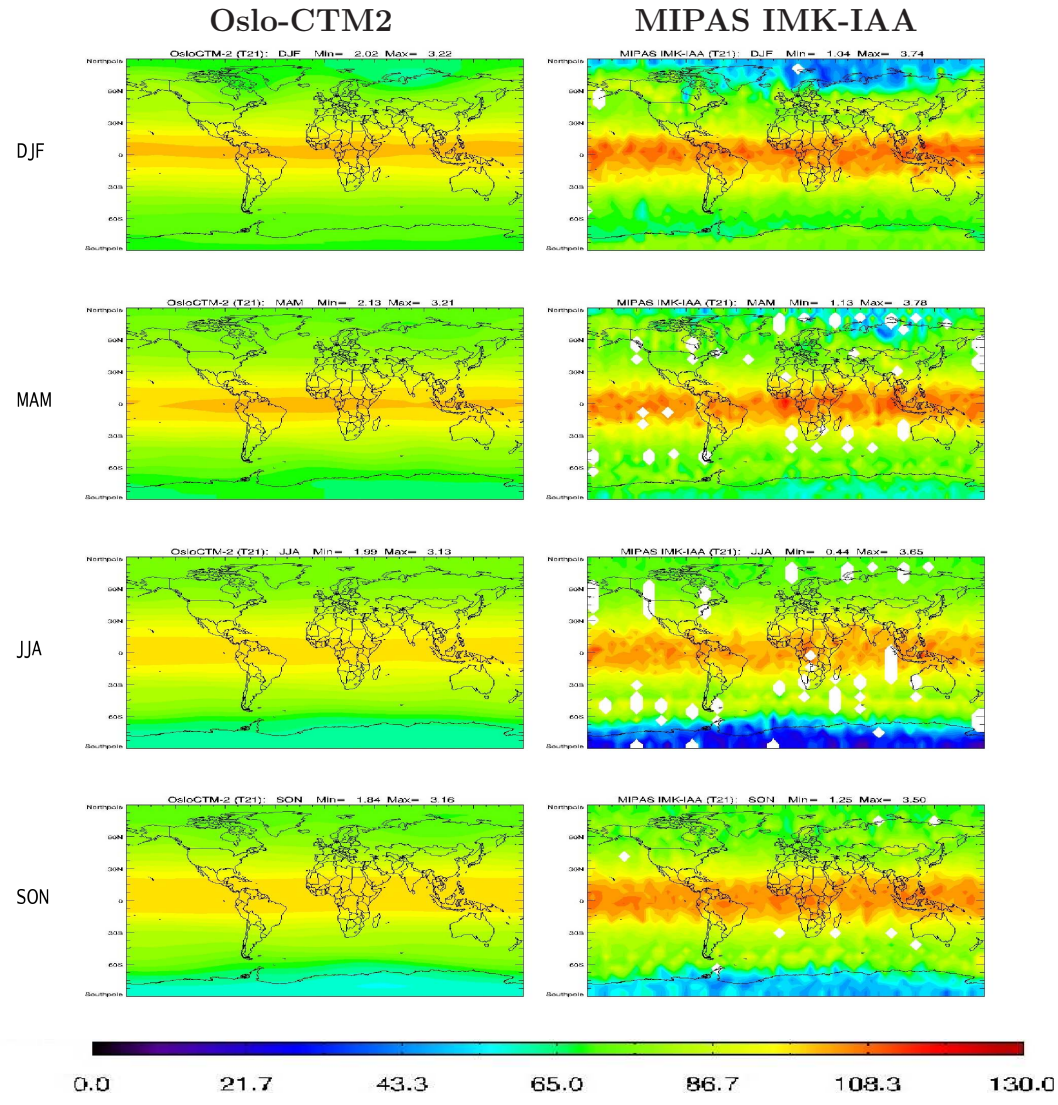

Figure 4.7: Seasonally averaged global distributions of stratospheric CH_4 columns from Oslo-CTM2 and MIPAS IMK-IAA datasets.

4.2 Nitrous oxide (N_2O)

(a) **(b)**

Figure 4.8: Molecular structure of N_2O (http://www.3Dchem.com)

Despite its relatively small concentration in the atmosphere, N_2O is the fourth most abundant greenhouse gas contributor to overall global warming, after H_2O, CO_2 and CH_4. It consists of two nitrogen and one oxygen atoms (Figure 4.8), and its radiative warming effect is substantially less than CO_2. N_2O is included in the efforts to curb greenhouse gas emissions, examplified by the Kyoto Protocol. Additionally, N_2O is a major precursor for the ozone-depleting components NO and NO_2 and is therefore routinely reviewed in the World Meteorological Organiations (WMOs) ozone assesments.
Natural emitters of N_2O are bacteria in soils and oceans. Agriculture is the main anthropogenic source of N_2O (approximately 60%). Soil cultivation, the use of nitrogen fertilizers and animal waste handling contribute to stimulate naturally occurring bacteria to produce more N_2O. Industrial sources such as chemical industry and fossile fuel combustion make up about 15% of all anthropogenic sources, whereas rivers, estuaries and coastal zones contribute with approximately 15%. Biomass burning ($<$10%) is a minor anthropogenic source to atmospheric N_2O (Jacob, 1999; Denman et al., 2007).
N_2O is a very stable molecule that has no significant sinks in the troposphere. It is therefore transported to the stratosphere where it is converted to N_2 by photolysis (90%) or encounters high consentrations of $O(^1D)$ allowing oxidation to NO (10%).
Atmospheric concentrations of N_2O have risen by $\approx$16%, from about 270 ppb during the pre-industrial era to 319 ppb in 2005 (Denman et al., 2007) (Figure 4.9). The average annual growth rate for 1999 to 2000 was 0.85 to 1.1 ppb yr^{-1}, or about 0.3% per year, and in WMOs third assesment report (TAR) its recommended atmospheric lifetime was 114 years (WMO, 2003).
In Oslo-CTM2 N_2Os source is mainly emission from the surface (POET), whereas its sinks are photolysis and oxidation by $O(^1D)$. MIPAS IMK-IAA retrieves VMR for N_2O and CH_4 jointly, and the microwindows selected for this retrival lies in the spectral region 1230-1305 cm^{-1} (Glatthor et al., 2005), which covers N_2O's ν_1 fundamental mode. Table 4.1 shows an example of

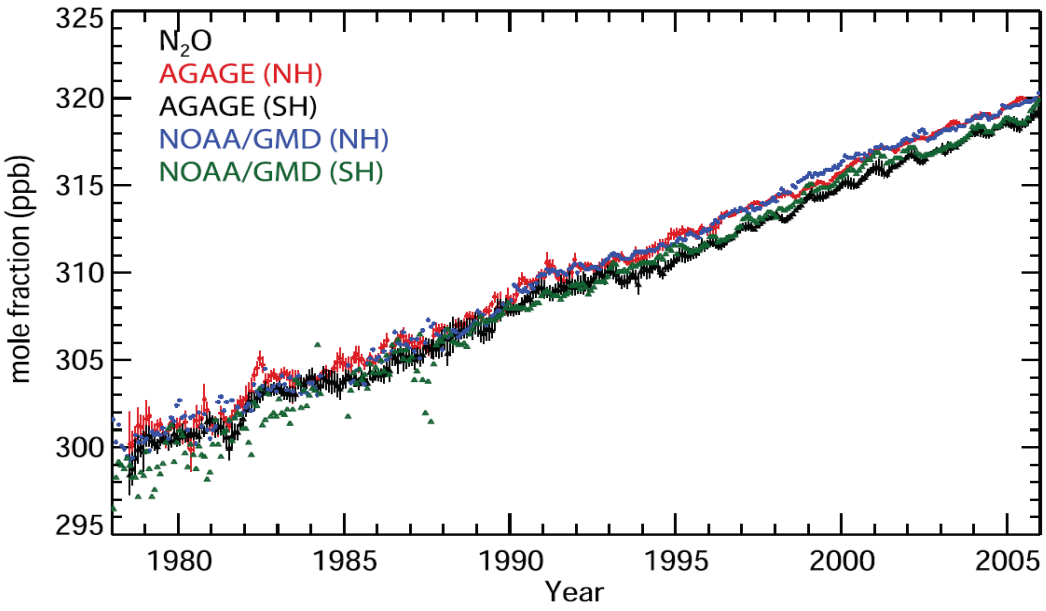

Figure 4.9: Hemispheric monthly mean N_2O concentration (ppb). The general decrease in the variability of the measurements over time is mainly due to improved instrumental precision (Source: (Forster et al., 2007, page 143)).

typical errors for retrival of CH_4 and N_2O, and as for CH_4, one can see that in the UTLS the relative errors are approximately 10% and rising with increasing stratospheric height.

4.2.1 Meridional distributions

Since atmospheric N_2O and CH_4 both originate from the surface and that they have sinks with similar distribution in the stratosphere one may assume that the structure in their meridonal distributions should be comparable. The main differences between abundance and distribution of these two gases are that there are significantly lower amounts of N_2O in the atmosphere in general. We find the same discrepancies that was found for CH_4 for N_2O, underestimation in lower stratospheric tropical regions and overestimation in lower stratospheric polar regions (Figures 4.10 to 4.13). The VMR in the meridional distributions for N_2O are presented in ppbv for all four seasons.

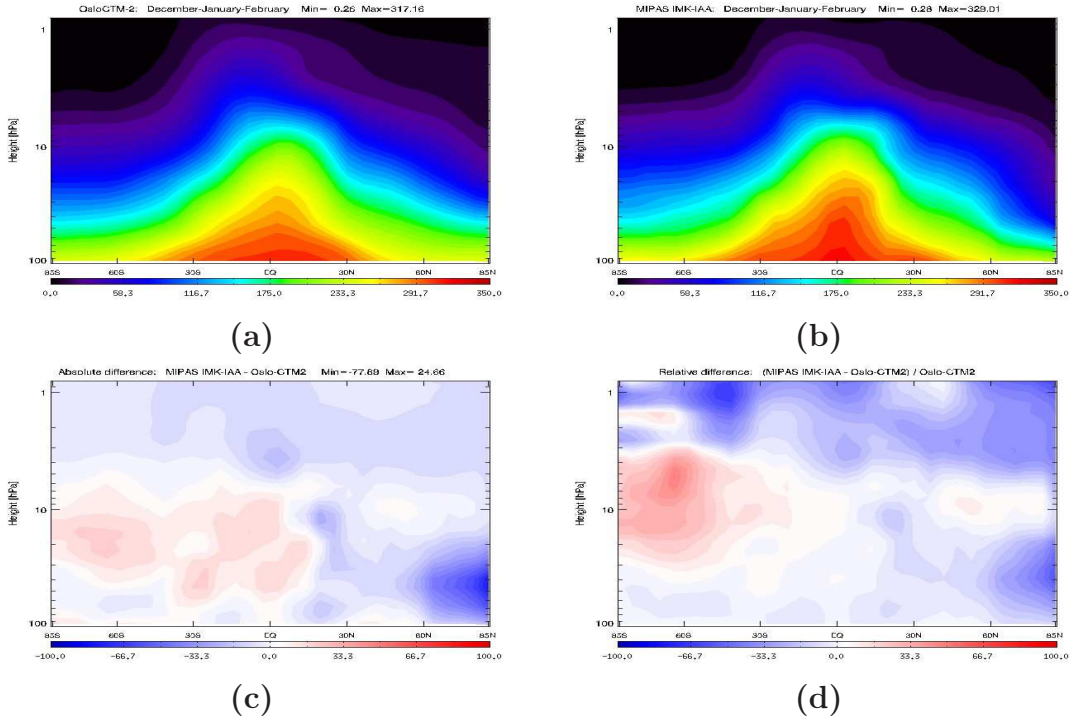

Figure 4.10: Meridional distribution of N_2O for DJF. a) Oslo-CTM2, b) MIPAS IMK-IAA, c) absolute difference and d) relative difference.

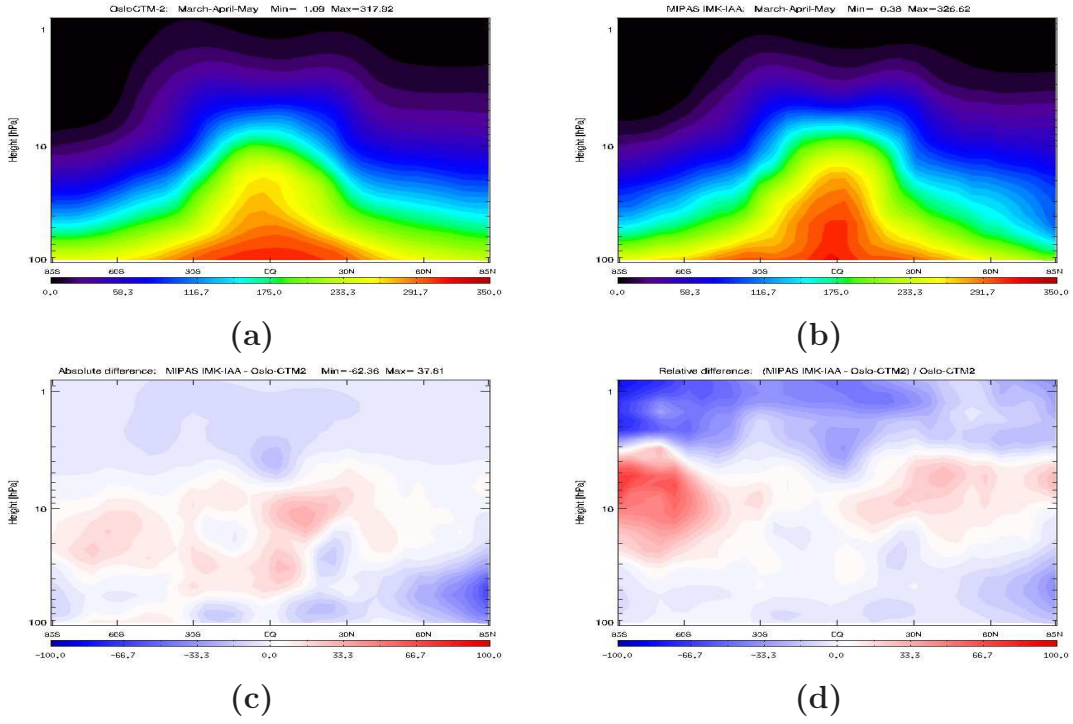

Figure 4.11: Meridional distribution of N_2O for MAM. a) Oslo-CTM2, b) MIPAS IMK-IAA, c) absolute difference and d) relative difference.

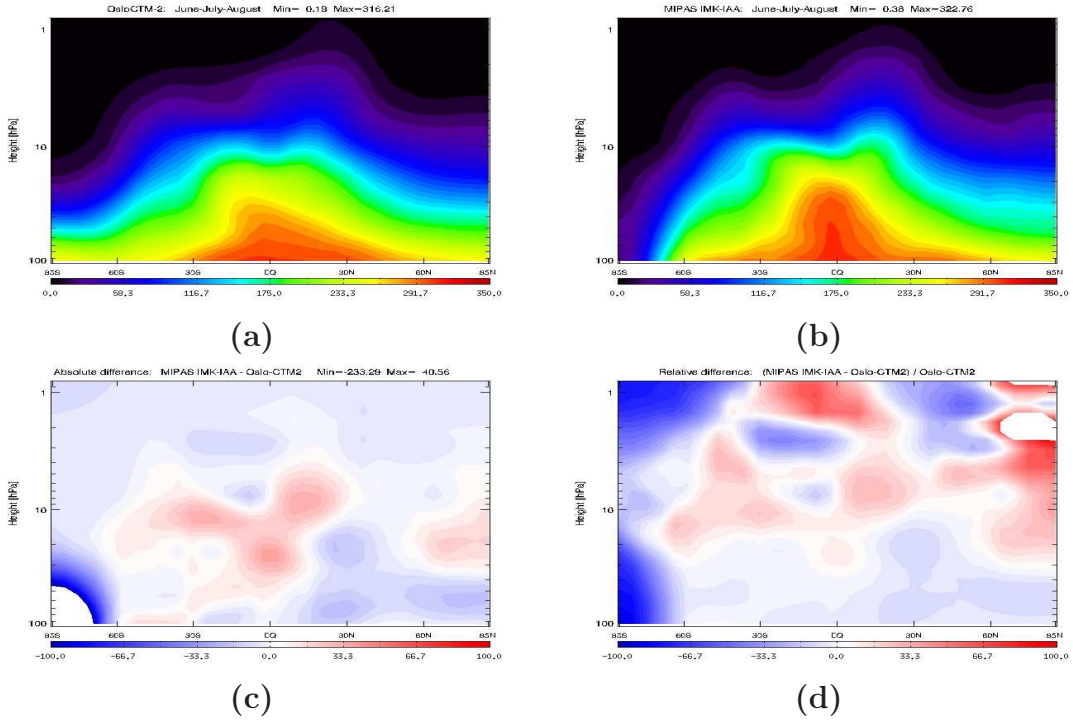

Figure 4.12: Meridional distribution of N_2O for JJA. a) Oslo-CTM2, b) MIPAS IMK-IAA, c) absolute difference and d) relative difference.

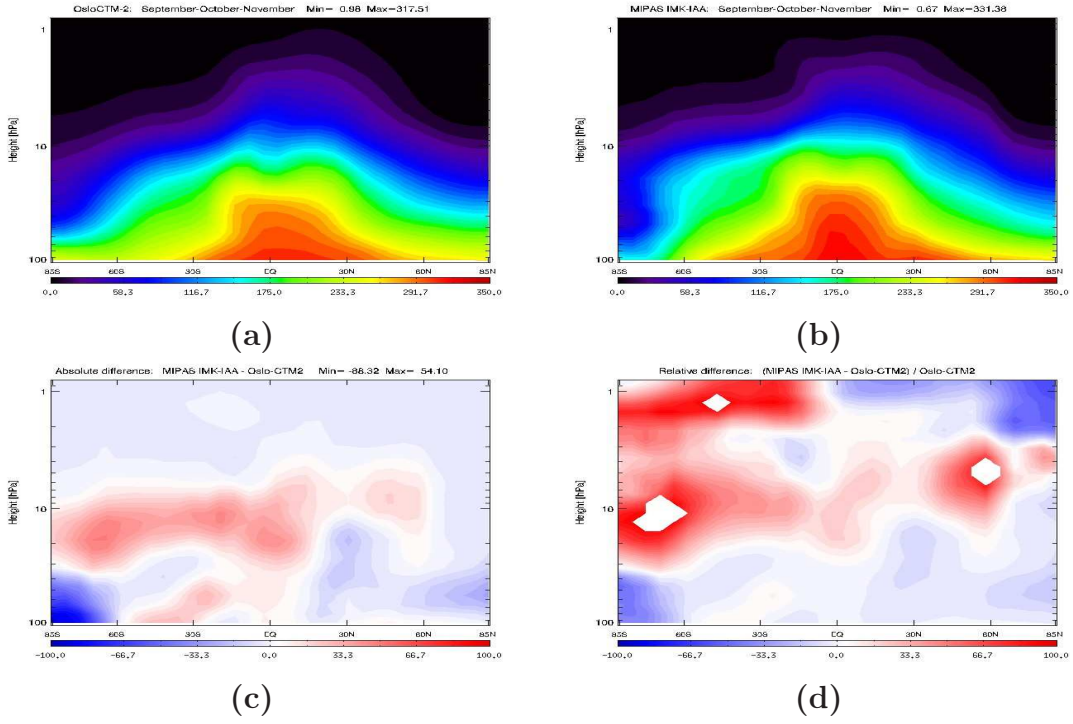

Figure 4.13: Meridional distribution of N_2O for SON. a) Oslo-CTM2, b) MIPAS IMK-IAA, c) absolute difference and d) relative difference.

4.3 Chlorofluorocarbon - 11 (CCl_3F)

Chlorofluorocarbons (CFCs) are solely man-made molecules which contain carbon, fluorine and chlorine atoms, and some of the most commonly occurring variants are CFC-11 (CCl_3F), CFC-113 (CCl_2FCClF_2) and CFC-12 (CCl_2F_2). CFCs were introduced to the atmosphere in the late 1940's, and they were principally used as blowing agents for foams and packaging materials and as refrigerants in large commercial chillers and air condition systems. The problem with CFCs begins as they migrate up into the stratosphere where the high energy UV radiation breaks them down resulting in atomic chlorine. The discovery of the link between CFCs and the springtime ozone-depletion led to "The Montreal Protocol" that was established in the late 1980's. The main objective of this protocol is to lower stratospheric chlorine and bromine concentrations by regulation of many ozone depleting and radiatively powerful greenhouse gases, among others the CFCs. Due to "The Montreal Protocols" widespread adoption and implementation it has been hailed as an example of exceptional international cooperation with Kofi Annan quoted as saying it is "Perhaps the single most successful international agreement to date...".

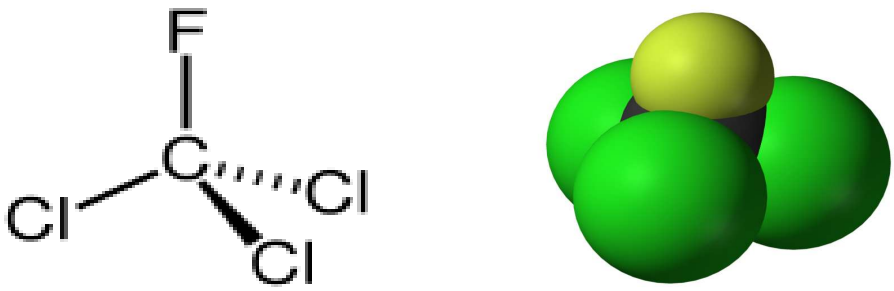

(a) **(b)**

Figure 4.14: Molecular structure of CFC-11 (http://www.Wikipedia.com)

CFCs are compounds with relatively long lifetimes with 45 and 100 years for CFC-11 and CFC-12, respectively, and their only known sink is photolysis by short-wave radiation in the stratosphere resulting in considerable release of chlorine. Most CFCs are also significant greenhouse gases, with an especially severe negative enviromental effect because they absorb radiation in a region of the electromagnetic spectrum where almost no other gases actively absorbs radiation, known as "the atmospheric window". Due to the restrictions regarding the use of CFCs in "The Montreal Protocol", hydrochlorofluorocarbons (HCFCs) have replaced many of the areas of utilization og CFCs. HCFCs ozone-depleting effects are only about 10% of CFCs, and their sinks are both photolysis and oxidation with OH and accordingly they have significantly lower atmospheric lifetimes than CFCs.
The only CFC included in both Oslo-CTM2 and MIPAS IMK-IAA datasets is $CFC-11$, which consists of one carbon, one fluorine and three chlorine

atoms (Figure 4.14). In Oslo-CTM2 the source of $CFC-11$ is emissions from the surface (POET), while the sink is photolysis in the stratosphere. MIPAS IMK-IAA retrieves VMR for $CFC-11$ in a quite large analysis window ranging from 838 to 853 cm^{-1} (Glatthor et al., 2005).

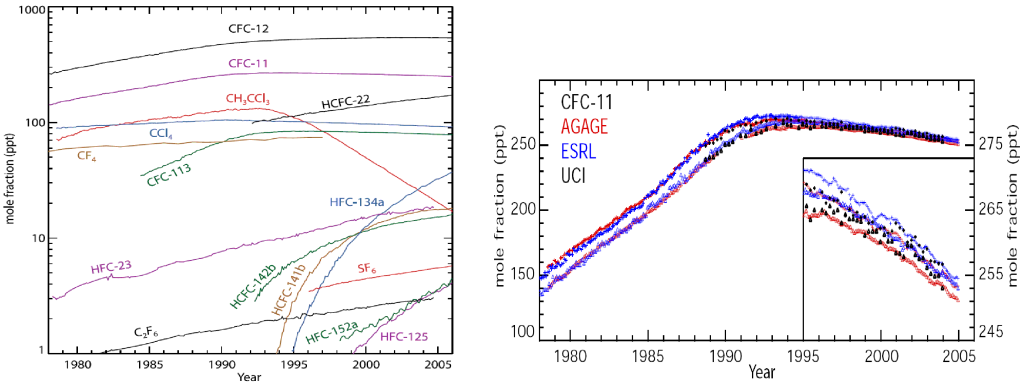

(a) (b)

Figure 4.15: a) Shows temporal evolution of the global average dry-air mole fractions (ppt) of the major halogen-containing long lived greenhouse gases. These are mainly derived using monthly mean measurements from the AGAGE and NOAA/GMD networks (Source: (Forster et al., 2007, page 145)). Whereas b) shows hemispheric monthly means of $CFC-11$ (crosses for NH and triangles for SH). Measurements from the AGAGE, the NOAA/ESRL and UCI. To increase visibility, recent measurements are depicted on a larger scale in the inserts (the scale is on the right-hand sides of the panel) (Source: (Clerbaux et al., 2007, page 1.8)).

4.3.1 Meridional distributions

As for the two preceding components the mean meridional circulation will produce a meridional gradient with higher values in the tropics. This implies that isolines of VMR will slope downwards from equator to the poles as one can observe in the meridional distributions for all these components. Due to the Earth's characteristic orbit around the Sun and its inclination, this slope will be steeper in the winter than in the summer hemisphere. We observe that $CFC-11$ (Figures 4.16 to 4.19) does not reach as high in the atmosphere as CH_4 and N_2O. This is because its shortwave photolytic destruction happens at relatively longer wavelenghts than for CH_4 and N_2O, and in general the longer the wavelenght, the deeper the UV radiation penetrates the atmosphere. The VMR in the meridional distributions for $CFC-11$ are presented in pptv for all four seasons.

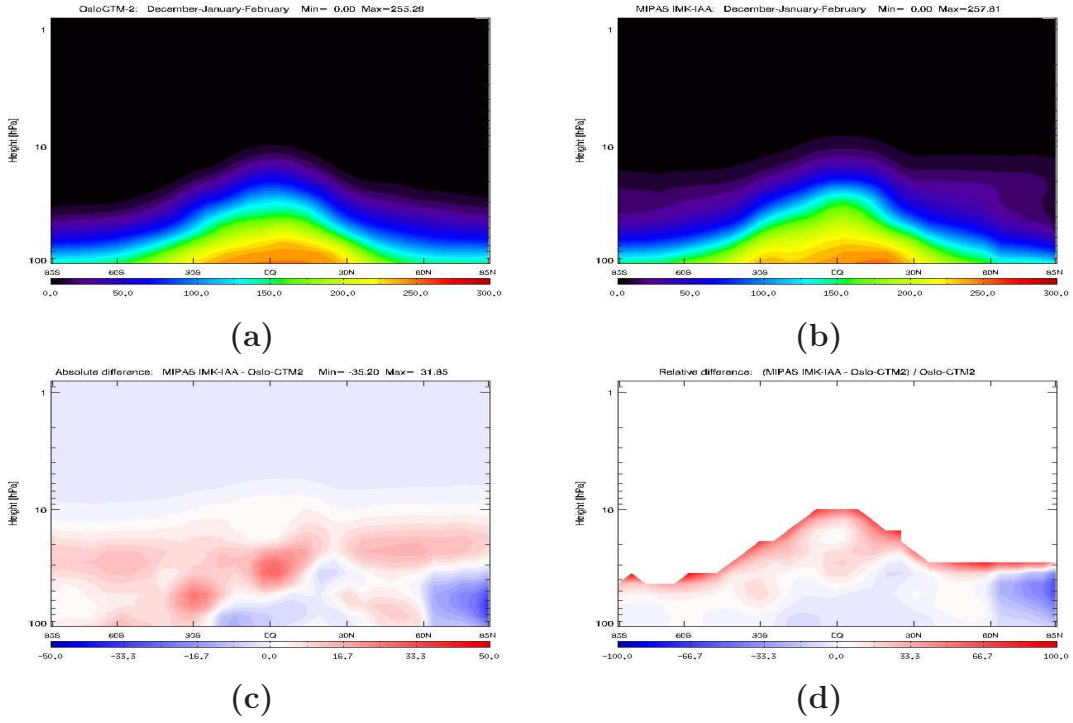

Figure 4.16: Meridional distribution of $CFC-11$ for DJF. a) Oslo-CTM2, b) MIPAS IMK-IAA, c) absolute difference and d) relative difference.

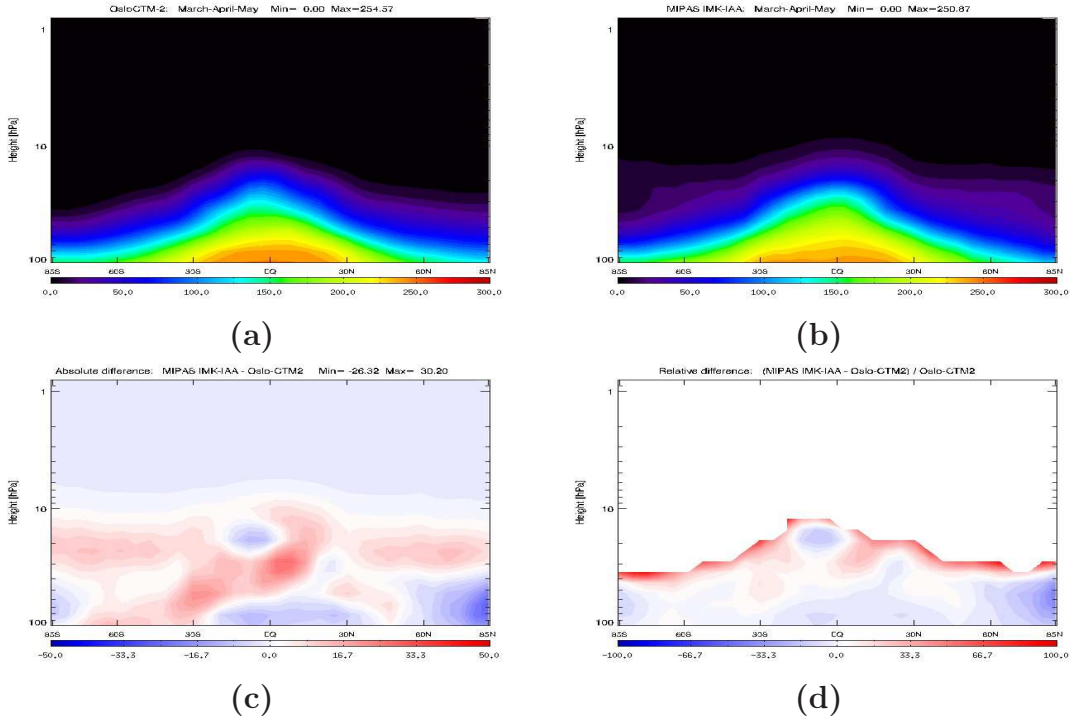

Figure 4.17: Meridional distribution of $CFC-11$ for MAM. a) Oslo-CTM2, b) MIPAS IMK-IAA, c) absolute difference and d) relative difference.

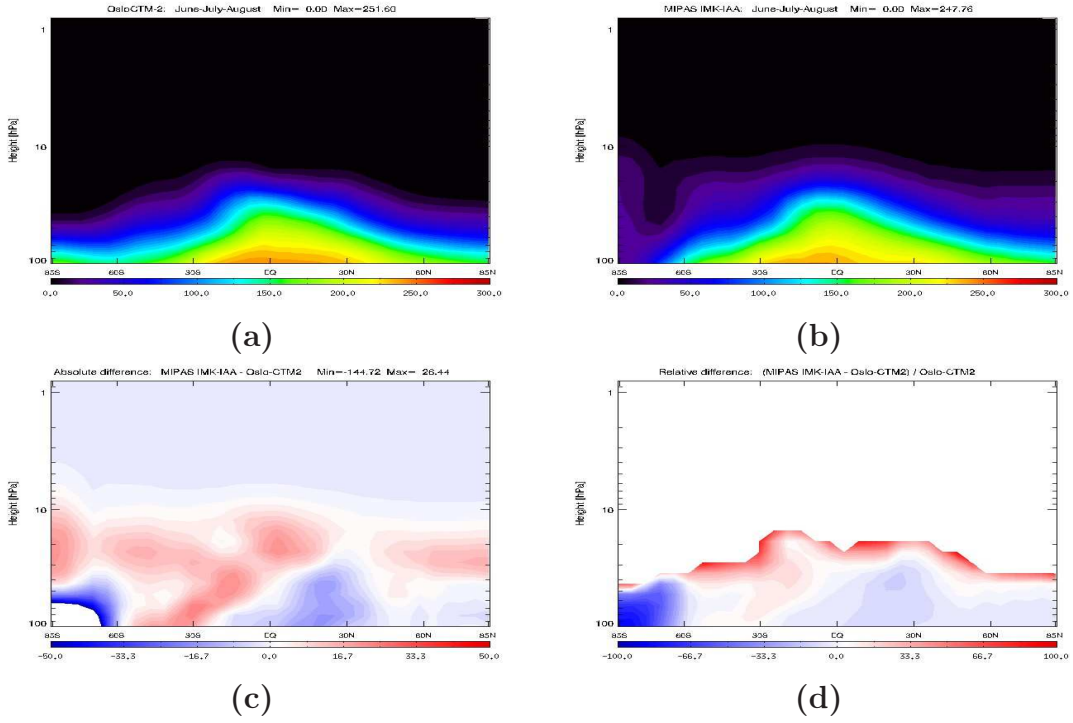

Figure 4.18: Meridional distribution of $CFC-11$ for JJA. a) Oslo-CTM2, b) MIPAS IMK-IAA, c) absolute difference and d) relative difference.

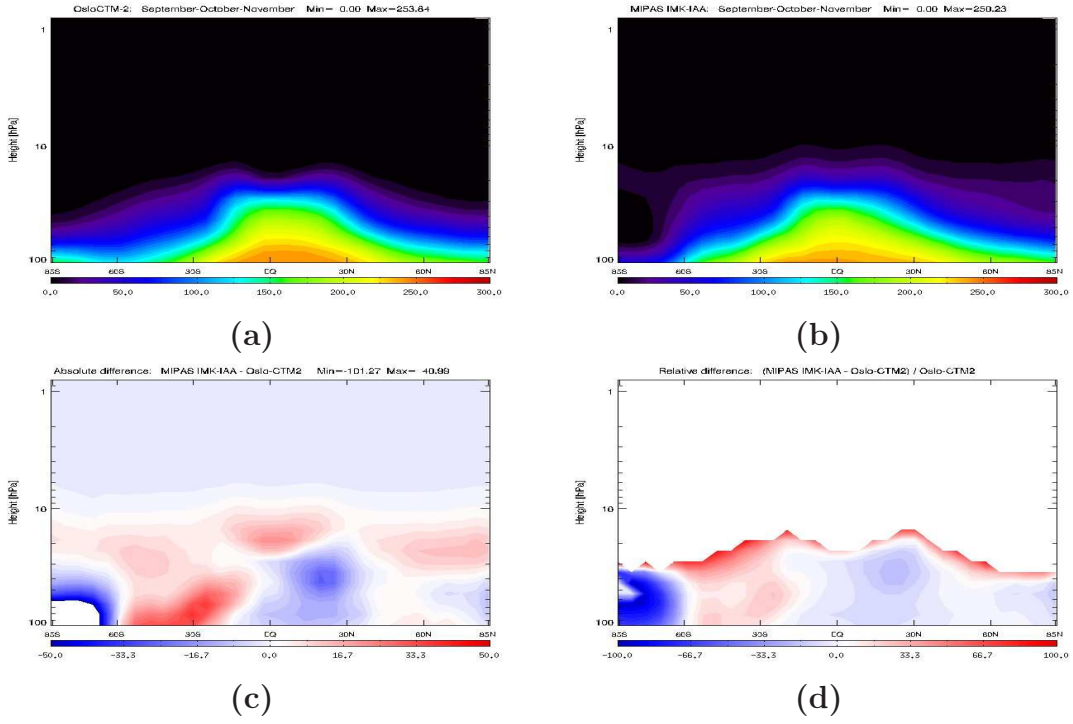

Figure 4.19: Meridional distribution of $CFC-11$ for SON. a) Oslo-CTM2, b) MIPAS IMK-IAA, c) absolute difference and d) relative difference.

4.4 Considerations about transport

As mention earlier in this thesis the transport of atmospheric components in Oslo-CTM2 are calculated based on ECMWFs IFSL60 dataset. Common features for CH_4, N_2O and $CFC-11$ are that their major sources are emissions from the surface, that they have relatively long lifetimes in the troposphere and that they enter the stratosphere mainly in tropical regions driven by the convection in the Hadley cell and the Brewer Dobson circulation. In the stratosphere their abundance are mainly influenced by the Brewer Dobson circulation and their individual chemical sinks. Accordingly, these components may be used as basis for discussing vertical transport across the tropopause in the model, also known as Stratosphere-Troposphere Exchange (STE) and stratospheric transport in general.

From the meridional distributions of these three components we find that Oslo-CTM2 generally underestimates the VMR in the lower stratosphere over tropical regions and overestimates the VMR in the lower stratosphere on high latitudes. We have not been in the position that we could do additional test runs with Oslo-CTM2, but these discrepancies could indicate that the meridional transport is somewhat weak in lower stratospheric regions, overestimating both vertical gradients in the upwelling circulation associated with the tropics and horizontal gradients in the lower stratosphere on both hemispheres simultaneously.
On the other hand, in the upper stratosphere modelled abundancies are consistently overestimated, indicating a somewhat strong meridional circulation in this region, e.g. underestimating vertical gradients in the upwelling regions. These patterns seem to be rather consistent for these three components, presented in the previous sections, throughout the year.

It has earlier been shown that the Brewer Dobson circulation and STE associated with the ECMWF's ERA-40 dataset were enhanced when applied in numerical models (Søvde and Isaksen, 2006; van Noije et al., 2004). However, the study described by Søvde and Isaksen (2006) showed a clear improvement of the transport, when they investigated the age of stratospheric air, using IFSL60 instead of ERA-40 in Oslo-CTM2.

4.5 Temperature

Temperature is a very important parameter in atmospheric chemistry. It determines the conditions for both atmospheric reaction rates and for which components reacting with eachother.

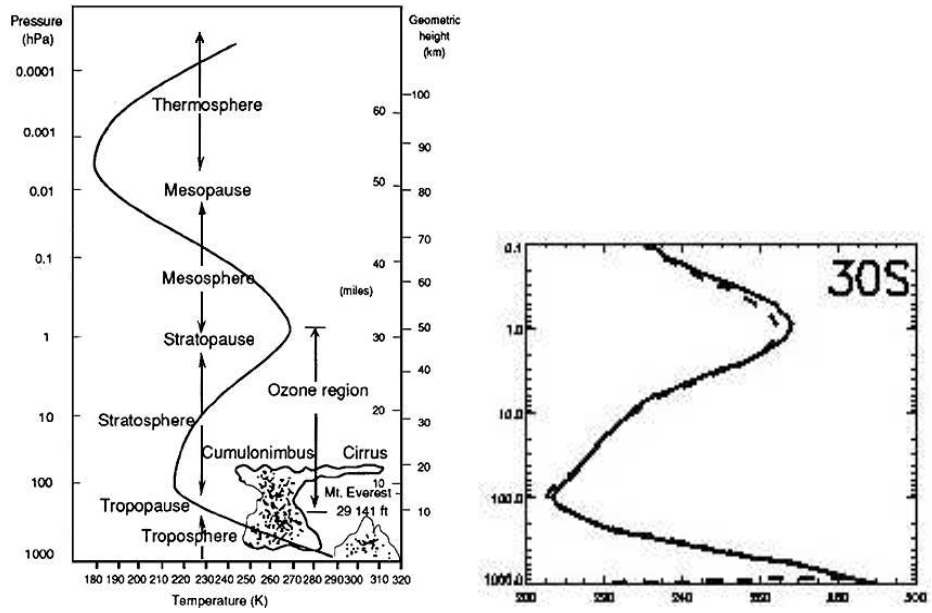

Figure 4.20: a) Vertical profile of temperature in the main atmospheric regions. Adopted from Butler et al. (1987). b) shows one example of vertical profiles from Oslo-CTM2 (solid line) and MIPAS IMK-IAA (dashed line).

Figure 4.20a shows the vertical profile of the Standard Atmosphere and the different vertical regions based upon whether the temperature gradients are positive or negative with increasing height. Figure 4.20b shows an example of vertical temperature profiles used in Oslo-CTM2 (solid line) and retrived by MIPAS IMK-IAA (dashed line), and we find that both datasets generally correspond well to the current theory.

Oslo-CTM2 interpolates the temperatures from ECMWFs IFSL60 dataset, while MIPAS IMK-IAA retrives temperatures using KOPRA (Stiller, 2000) for the forward solution of the radiative transfer equation. The retrieval of temperature preceeds retrival of abundances of atmospheric components (von Clarmann et al., 2003b) in the MIPAS IMK-IAA processing sequence. Consequently, one has to be very cautious when selecting a microwindow for this retrival since no reliable information of atmospheric state parameters is available from a previous retrival step. Traditionally, both in absorption and emission spectroscopy, small spectral regions that only contains CO_2 lines are used for these purposes.

4.5.1 Meridional distributions

The meridional distributions clearly show the seasonal variations in temperature. This variability is mainly caused by the differences in shortwave radiative heating associated with earths axial inclination of approximately 23.5 degrees in its yearly orbit around the Sun (Figure 2.1b). From the meridional distributions we find that there in general is good agreement between the two temperature products (Figures 4.21 to 4.24). The relatively small differences between the datasets are most probably mainly due to the sparse temporal resolution and that some parts of a season are biased in MIPAS IMK-IAA's dataset, meaning that it consists of more data than other parts of the same season. To confirm this phenomenon, one can take a closer look on the SON seasons meridional and global distributions (Figures 4.24 and 4.25). Here we observe that the ECMWF data used in Oslo-CTM2 to a certain extent has a cold bias in the SH, especially on higher latitudes. For this season most of MIPAS IMK-IAA temperature retrivals are in late October and November (Figure 3.7 botton panel, temperature are available on the same dates as O_3) whereas Oslo-CTM2 produces monthly means for the entire season. Due to the differences in daylight hours, the temperatures are significantly higher in the latter part than in the beginning of the SON season. This will obviously have an impact on the seasonal means, and accordingly appear as differences in both global and meridional distributions.
From the meridional distribution figures we find that the ECMWF data used in Oslo-CTM2 have lower temperatures in the upper stratosphere than the MIPAS IMK-IAA data, around 5 hPa, especially in tropical and polar regions. In tropical regions we also find that ECMWF temperatures around the tropopause are slightly cold biased compared to MIPAS IMK-IAA, while in the mesosphere the opposite is the case. Other consistent overestimations are found in the lower stratospheric region around 30°S and north of approximately 45°S.

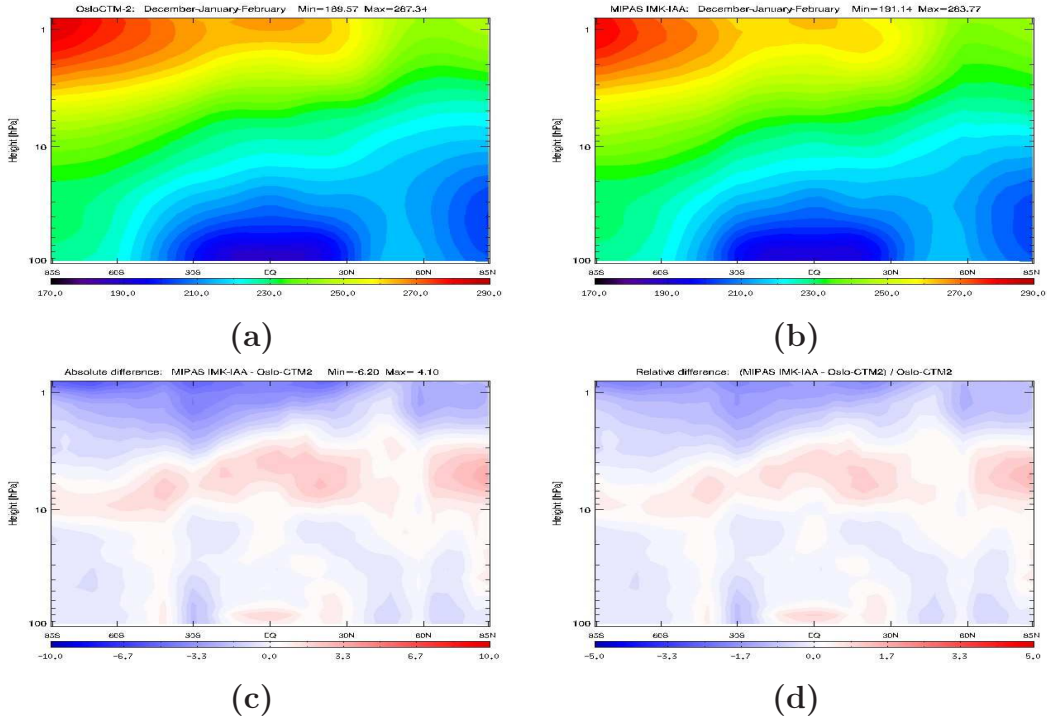

Figure 4.21: Meridional distribution of temperature in K for DJF. a) Oslo-CTM2, b) MIPAS IMK-IAA, c) absolute difference and d) relative difference.

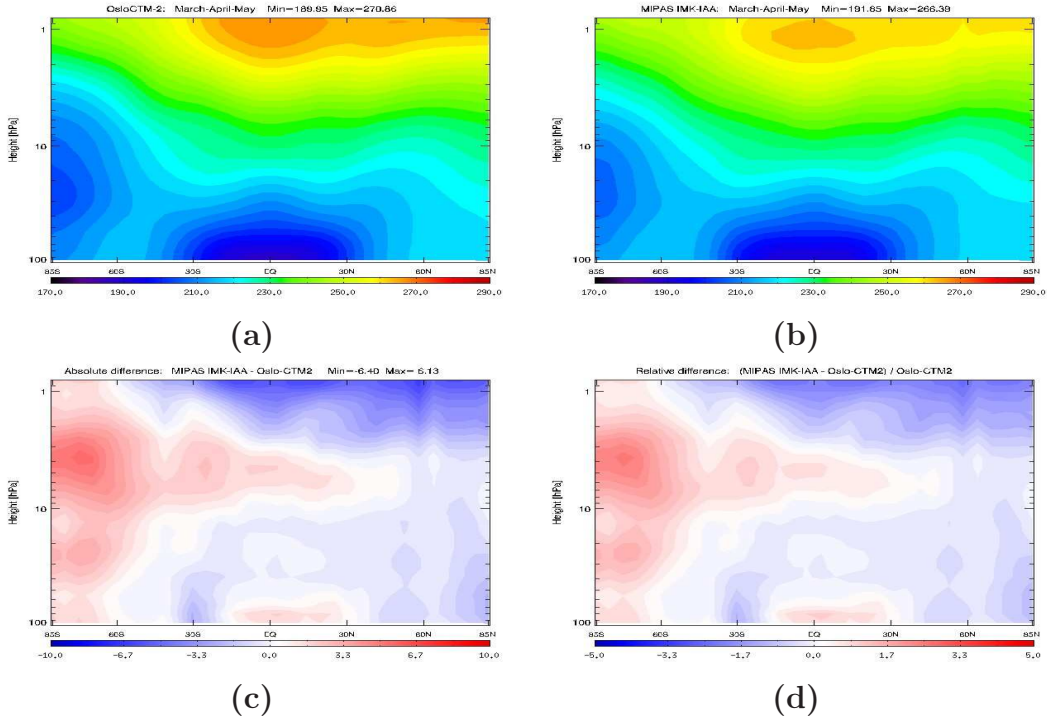

Figure 4.22: Meridional distribution of temperature in K for MAM. a) Oslo-CTM2, b) MIPAS IMK-IAA, c) absolute difference and d) relative difference.

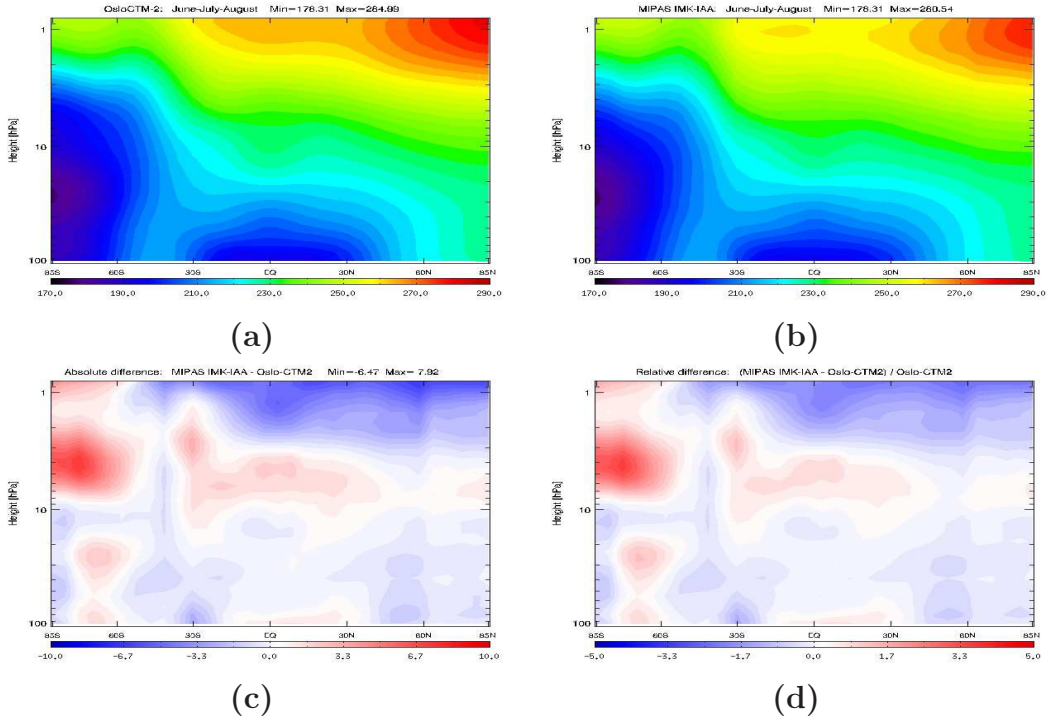

Figure 4.23: Meridional distribution of temperature in K for JJA. a) Oslo-CTM2, b) MIPAS IMK-IAA, c) absolute difference and d) relative difference.

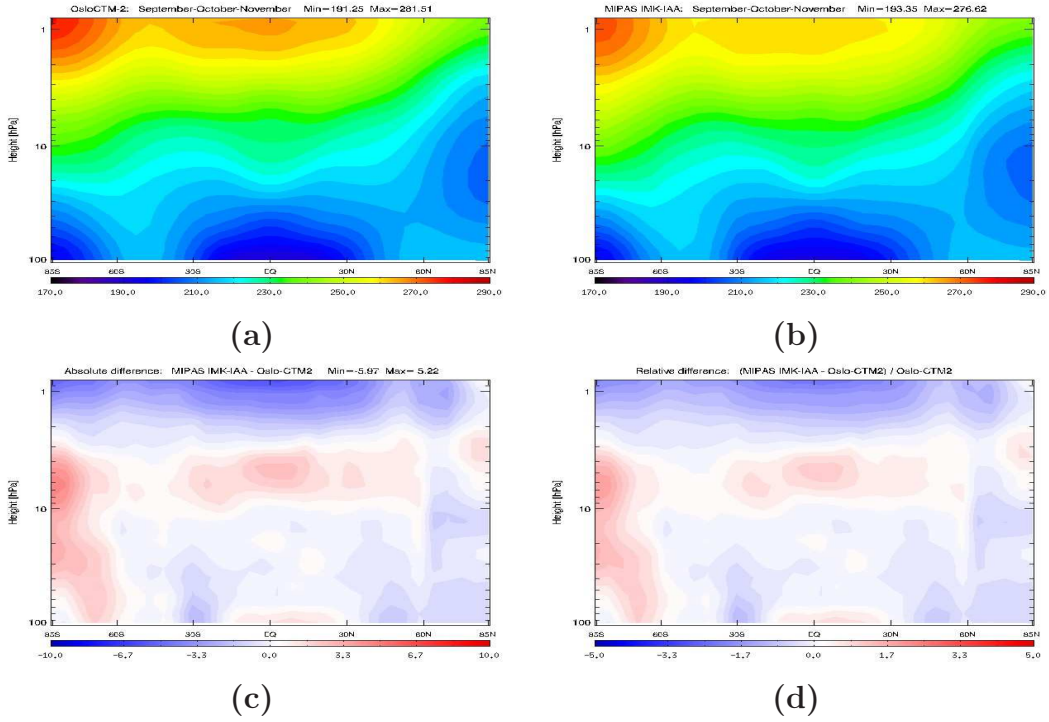

Figure 4.24: Meridional distribution of temperature in K for SON. a) Oslo-CTM2, b) MIPAS IMK-IAA, c) absolute difference and d) relative difference.

4.5.2 Temperatures at ≈5 hPa

Geographical distributions

The structure in geographical distribution fields for temperature at approximately 5 hPa shows that there are generally good correlation between the two products. The MIPAS IMK-IAA figures shows some signs of discontinued temporal resolution, but we still find some regional minima and maxima that to some exctent are comparable. The discrepancies are first and foremost visible in polar regions on the geographical distribution figures where we find that the ECMWF data used in Oslo-CTM2 generally has a cold bias compared to MIPAS IMK-IAA.

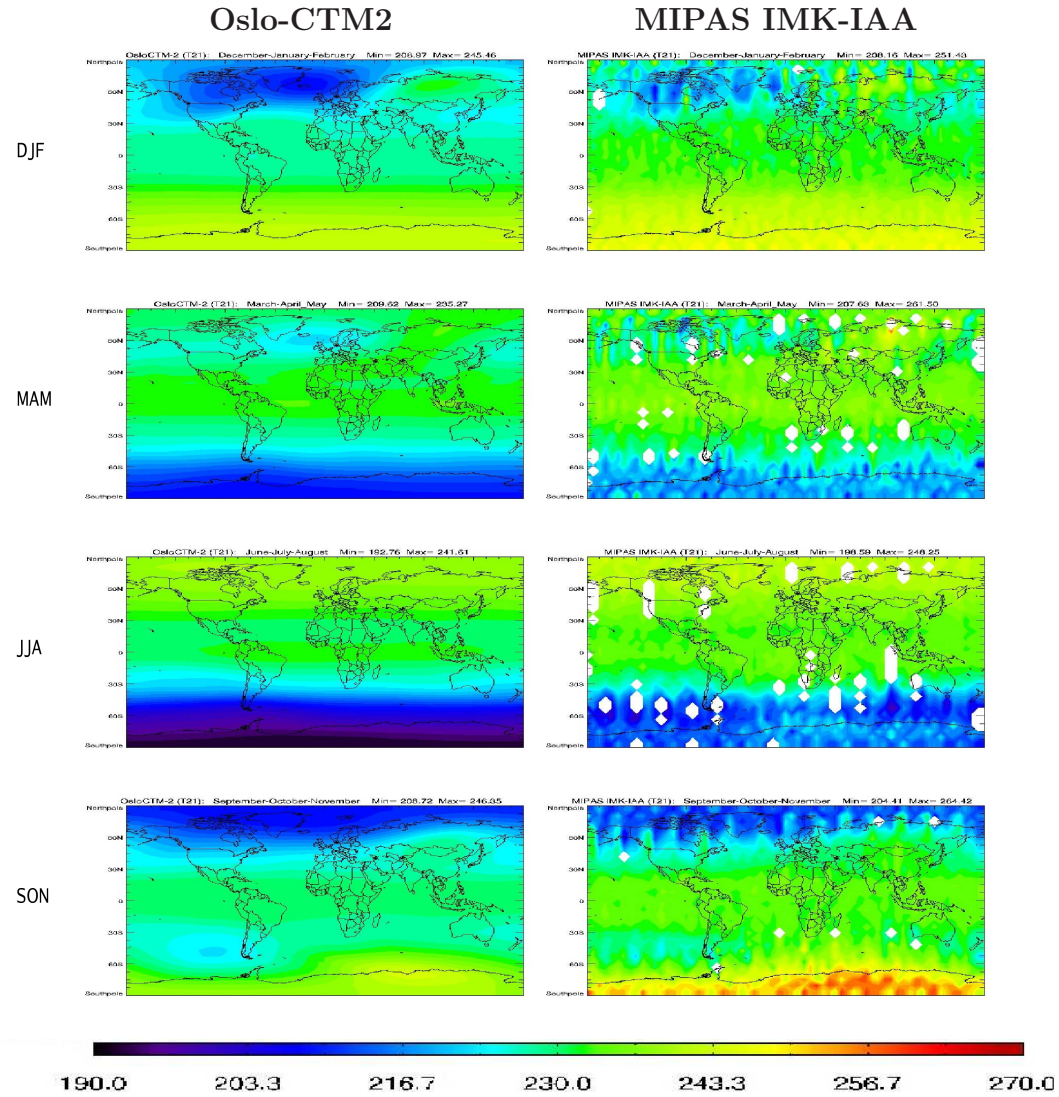

Figure 4.25: Seasonally averaged global distributions of temperature in K at approximately 5 hPa from Oslo-CTM2 and MIPAS IMK-IAA.

4.6 Nitrogen oxides (NO_x)

NO_x (NO + NO_2) do not directly affect the Earth's radiative balance, but are essential in several important atmospheric processes, such as the determination of both tropospheric and stratospheric O_3 consentrations and OH production.
Stratospheric abundances of NO_x are mainly produced by various photolytic reactions in the UV region of the electromagnetic spectrum and associated with rapid convertions between NO_x's reservoir species (NO_y). Occasionally, during major Solar Proton Events (SPEs), vast amounts of NO_x are produced in polar mesospheric regions, transported downward into the winter hemispheres upper stratosphere (Figure 2.1c) where it is converted to NO_y. In Oslo-CTM2, the chemical sources for stratospheric NO_x are various photolytic reactions involving nitric acid (HNO_3), dinitrogen pentoxide (N_2O_5), peroxynitric acid (HO_2NO_2), nitrate (NO_3) and Bromine nitrate ($BrONO_2$). There are also three-body, bimolecular and thermal decomposition reactions involving members from the NO_y, active chlorine species (ClO_x) and active bromine species (BrO_x) families. Together with oxidation of N_2O by $O(^1D)$ these components altogether complement the chemical sources of NO_x. For tropospheric NO_x, emissions from the surface (POET), lightning discharges and aircraft activities (NASA inventory) are significant sources in the model. The major stratospheric chemical sinks of NO_x in Oslo-CTM2 are photolysis as well as various three-body and bimolecular reactions that convert molecules from the NO_x family to its reservoir species in the NO_y family. See Appendix B for a complete summary of reactions included in the Oslo-CTM2 model.

4.6.1 Nitrogen oxide (NO)

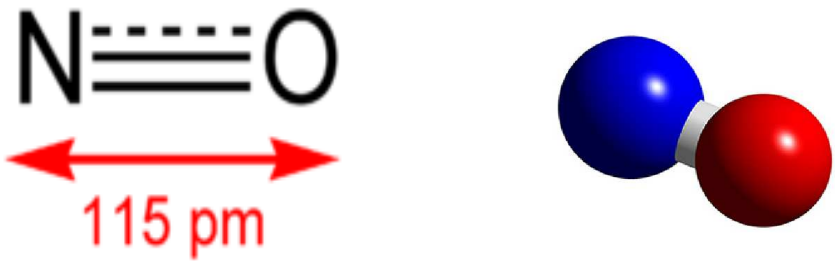

(a) (b)

Figure 4.26: Molecular structure of NO (http://www.3Dchem.com)

The NO molecule is a free radical, implying that it has a high reactivity. It consists of one nitrogen and one oxygen atoms (Figure 4.26). The lifetime of NO_x are always short, but in general one can say that it increases

with increasing height, being hours or less in the polluted boundary layer and typically 5 to 10 days in the upper troposphere and stratosphere. The dramatic increase in the use of various combustion engines has significantly increased the emissions of NO in the Earth-atmosphere system. In addition to its roles as source for O_3 and tropospheric OH, NO may be converted to HNO_3, which is associated with the formation of acid rain through wet deposition.
MIPAS IMK-IAA retrieves VMR of NO from its 1→0 fundamental band using microwindows in the 1845-1915 cm^{-1} spectral region (Funke et al., 2005b). As of today, using the MIPAS IMK-IAA spectra version V30, data are only available for the latter part of the SON season.

Height (km)	NO	NO_2
15		**0.3**
20	**0.3**	**0.3**
25	**0.6 (0.7)**	**0.3**
30	**1.1 (1.4)**	**0.5**
35	**1.3 (2.0)**	**0.9 (1.5)**
40	**1.4 (2.3)**	**0.6 (1.2)**
45	**1.8 (3.2)**	**0.3 (0.5)**
50	**1.5 (4.7)**	**0.3 (0.6)**
55	**1.3 (3.2)**	**0.3 (0.6)**
60	**0.7 (1.2)**	**0.3 (0.4)**
65		**0.3 (0.4)**

Table 4.2: Total error for NO and NO_2 retrival for a single scan. The errors are given in absolute (ppbv) units. For NO, the numbers in brackets correspond to errors in polar conditions whenever they are different from errors in midlatitude conditions, while for NO_2 the numbers in brackets correspond to nighttime errors whenever they are different from daytime errors. The complete error budget are presented in Funke et al. (2005b).

Table 4.2 shows the total absolute errors for retrival of NO and NO_2. We see that in general, the absolute errors are smaller for NO_2 than for NO, but the total errors are relatively low for both components.

Meridional distributions

Since MIPAS IMK-IAA only provides data for NO abundance from the SON season this is the only season presented in this section. We observe that there are some differences between the two datasets in the lower mesosphere and upper stratosphere which will be further discussed in Section 4.13. Apart from these large discrepancies the general structure of the fields seems to be comparable both in size and in abundance. However, we find from the meridional distributions that Oslo-CTM2 underestimates the NO abundance somewhat in the regions with low abundance, around 10 hPa (Figure 4.27). The VMR in the meridional distributions for NO are presented in ppbv for the SON season.

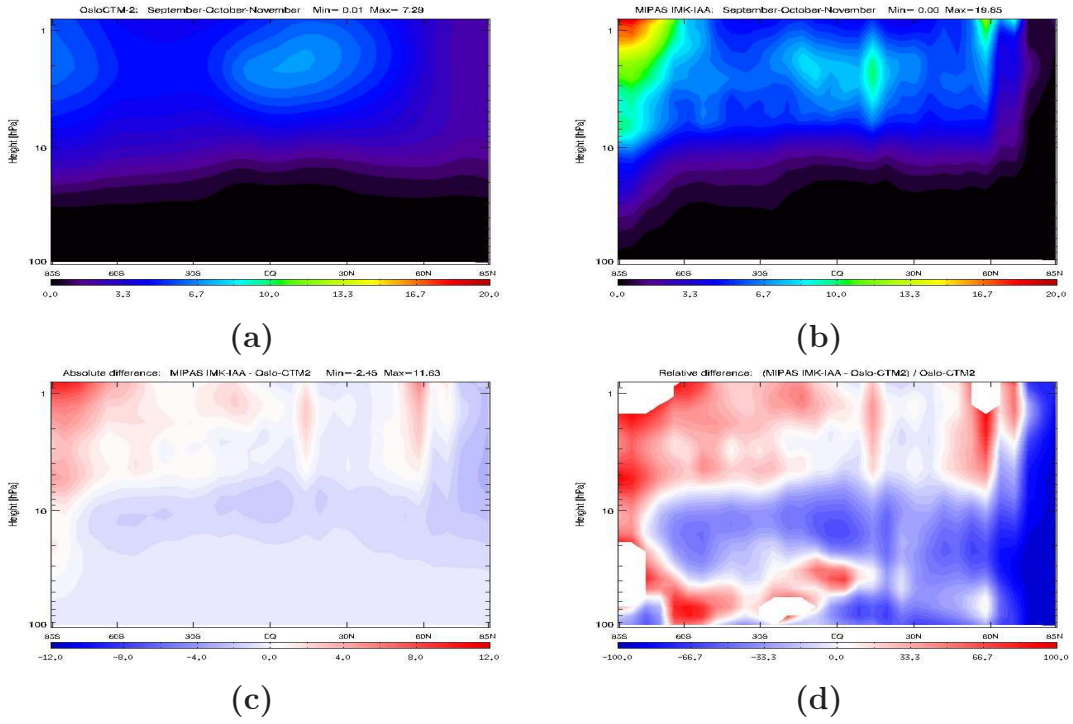

Figure 4.27: Meridional distribution of NO for SON. a) Oslo-CTM2, b) MIPAS IMK-IAA, c) absolute difference and d) relative difference.

4.6.2 Nitrogen dioxide (NO_2)

NO_2 consists of one nitrogen and two oxygen atoms (Figure 4.28) and just as for NO, it has several indirect, but significant, effects on the climate system. The most important anthropogenic source for NO_2 is via NO that is emitted from combustion engines and reacts rapidly with O_3, but another major industrial source for NO_2 is pulp mills. NO_2 has received much scientific attention due to the catalytic cycling with NO that serves as a major sink of odd oxygen species (O and O_3). NO reacts with O_3 producing NO_2 and O_2. When NO_2 is in the presence of UV radiation, it breaks down into NO and $O(^3P)$, which is very reactive and attaches to among others O_2 or NO_2. When $O(^3P)$ reacts with O_2 it has no net effect on O_3, and this form of cycling is refered to as the "null cycle", but when it reacts with NO_2 both $O(^3P)$ and O_3 are depleted. This is the mechanism for the NO_x catalytic cycle responsible for some of the reduction of the ozone layer.

Meridional distributions

From the meridional distribution of NO_2 for the SON season, we see in general that there is very good correlation between the two datasets, except in the nothern hemisphere lower mesospheric region (Figure 4.29). In this area there are processes associated with SPEs that are not included in Oslo-CTM2. In addition, we also find that Oslo-CTM2 slightly underestimates

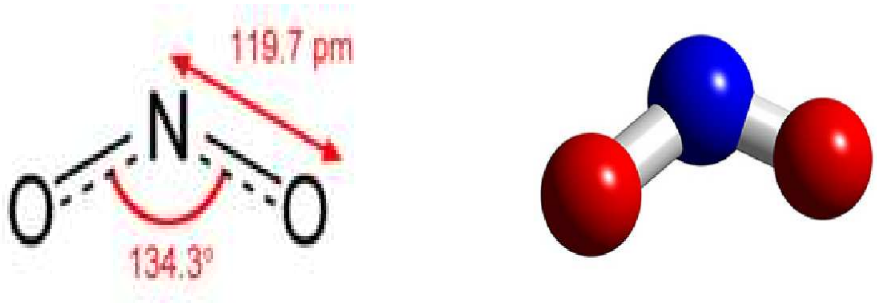

(a) (b)

Figure 4.28: Molecular structure of NO_2 (http://www.3Dchem.com)

the abundance of NO_2 in the middle stratosphere (around 10 hPa) similar for the observations for NO. This is not surprising based on their strong dependenceof eachother. The VMR in the meridional distributions for NO_2 are presented in ppbv for the SON season.

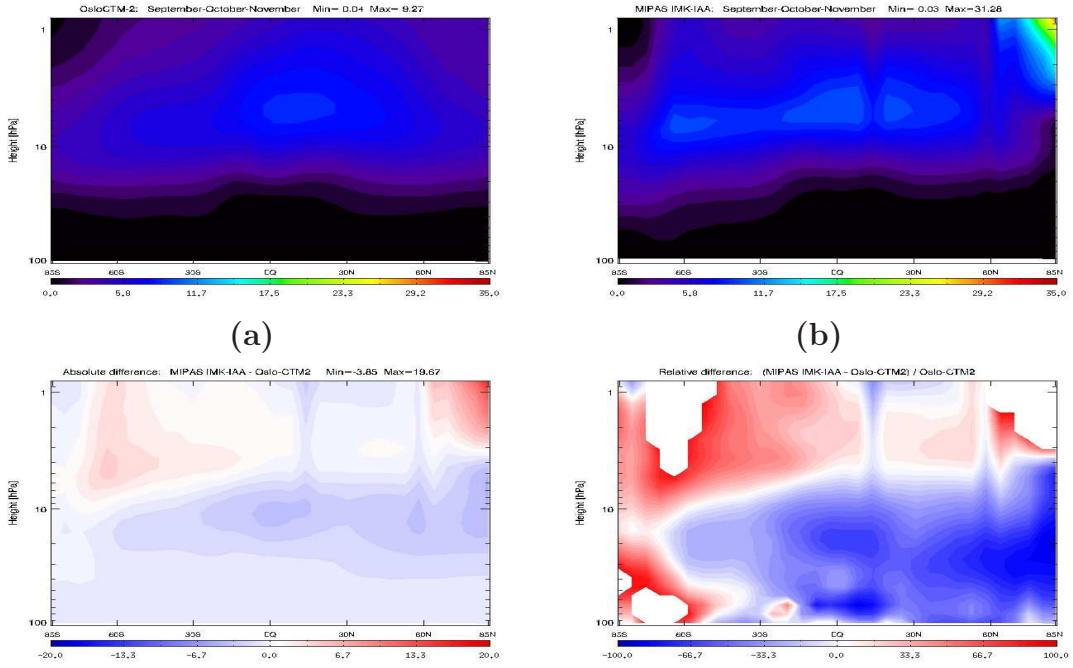

(a) (b)

(c) (d)

Figure 4.29: Meridional distribution of NO_2 for SON. a) Oslo-CTM2, b) MIPAS IMK-IAA, c) absolute difference and d) relative difference.

4.7 Dinitrogen pentoxide (N_2O_5)

N_2O_5 is a non-radical species that has a relatively long atmospheric lifetime (from hours to days). N_2O_5 is one of the most dominant nighttime reservoirs for NO_x in the stratosphere, and it consists of two nitrogen and five oxygen atoms (Figure 4.30). The catalytic destruction of ozone by NO and NO_2 is reduced by the formation of N_2O_5 because it "occupies" a NO_2 molecule.

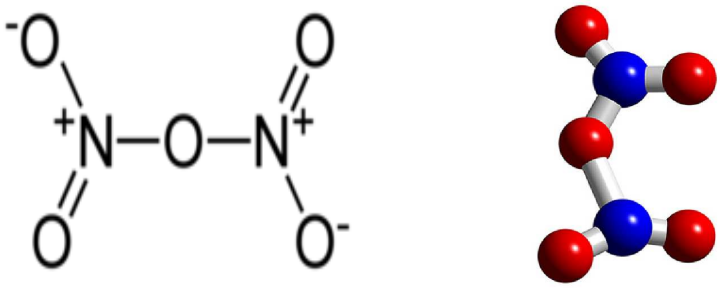

(a) **(b)**

Figure 4.30: Molecular structure of N_2O_5 (http://www.3Dchem.com)

N_2O_5 is a member of the chemical family, NO_y. The ultimate removal of NO_y is by transport to the troposphere where it is rapidly removed by wet deposition. It accumulates during nighttime and acts as a source for HNO_3. Consequently, it is indirectly responsible for some of the springtime ozone depletion over the polar regions.

In Oslo-CTM2 the main source for N_2O_5 is the three-body reaction between NO_2 and NO_3, whereas the main sinks are various heterogeneous reactions that converts N_2O_5 to HNO_3 and a thermal decomposition reaction (Appendix B consists of a complete summary of reactions included in Oslo-CTM2). The MIPAS IMK-IAA retrieval of N_2O_5 is described in Mengistu Tsidu et al. (2004). The spectroscopic data are taken from the HITRAN database, which includes cross-section data. The target analysis window covers 1239.0-1243.0 cm^{-1} and 1275.0-1276.0 cm^{-1} of the electromagnetic spectrum, accordingly it covers the N_2O_5's ν_{12} vibration-rotation band. The species that are assumed to interfere in the microwindows selected for N_2O_5 are O_3, CO_2, sulfur dioxide (SO_2), NO_2, HNO_3, hypochlorous acid ($HOCl$), hydrogen peroxide (H_2O_2), acetylene (C_2H_2), carbonyl fluoride (COF_2), $F14$ and $ClONO_2$.

Table 4.3 shows a representative example of total errors in retrival of HNO_3 and N_2O_5. It shows that the absolute error associated with MIPAS IMK-IAA retrival of N_2O_5 are most significant above 30 km, while the relative errors in the atmospheric region where the abundance is highest are approximately 10% during daytime and approximately 20% during night time.

Height (km)	HNO_3 **N midlat**	HNO_3 **N pv**	N_2O_5 **D midlat**	N_2O_5 **N pv**
10	**77 (56)**	**54 (7)**		
15	**110 (7)**	**81 (3)**	**19 (76)**	**34 (78)**
20	**380 (6)**	**390 (16)**	**47 (28)**	**73 (36)**
25	**680 (6)**	**310 (7)**	**71 (9)**	**83 (16)**
30	**790 (11)**	**250 (24)**	**150 (12)**	**140 (24)**
35	**630 (37)**	**110 (27)**	**230 (27)**	**150 (32)**
40	**150 (50)**	**50 (40)**	**210 (53)**	**170 (42)**
44	**63 (53)**	**24 (58)**		

Table 4.3: Total error for retrival of HNO_3 and N_2O_5 at daytime (D) and night time (N), in the midlatitudes (midlat) and inside the Polar vortex (pv). The errors are given in absolute (pptv) and relative units (% in brackets). For the complete error budget for these components see Mengistu Tsidu et al. (2005, 2004).

4.7.1 Meridional distributions

In the meridonal distributions we find that Oslo-CTM2 overestimates the abundance of N_2O_5 in regions associated with the local maximum value. This is especially evident in the seasons that include the solstices (Figures 4.31 to 4.34). We also find that Oslo-CTM2 calculates the N_2O_5 abundance slightly too low in the stratosphere, but that the main structures in the fields are in relatively good agreement with the MIPAS IMK-IAA retrivals for all four seasons. The VMR in the meridional distributions for N_2O_5 are presented in ppbv for all four seasons.

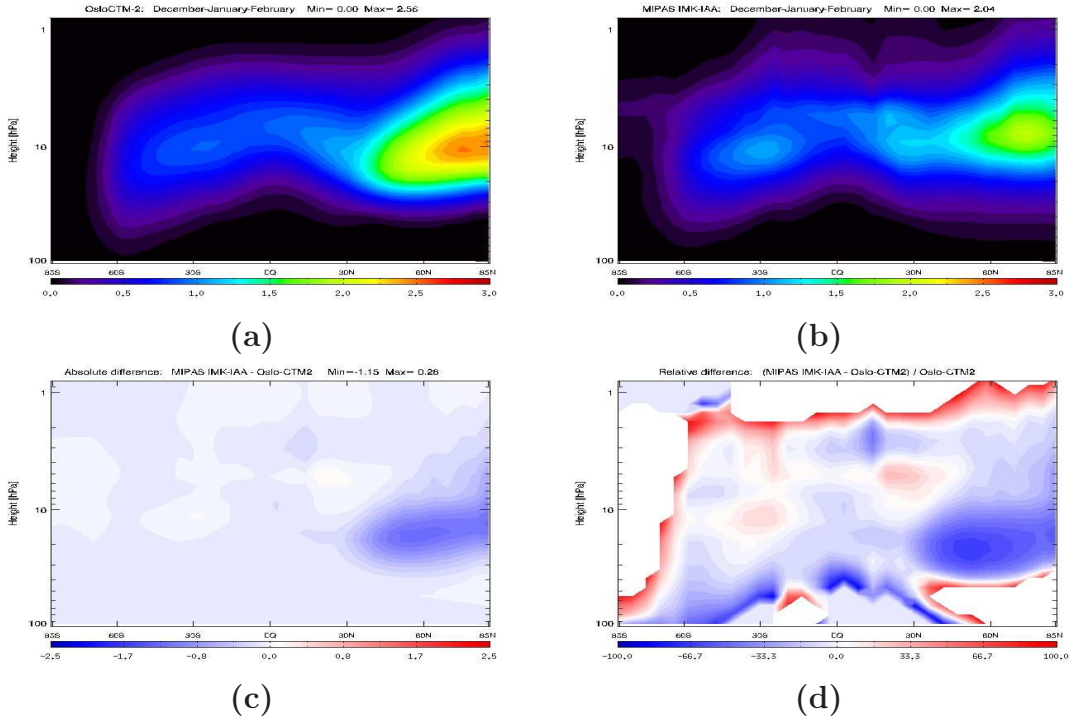

Figure 4.31: Meridional distribution of N_2O_5 for DJF. a) Oslo-CTM2, b) MIPAS IMK-IAA, c) absolute difference and d) relative difference.

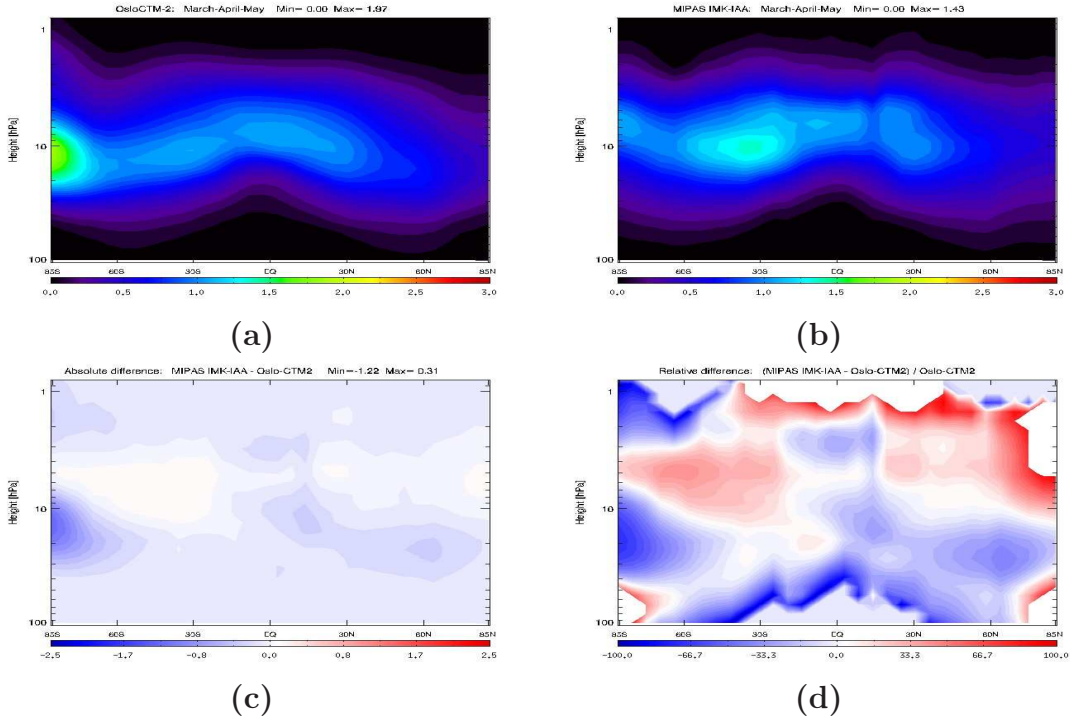

Figure 4.32: Meridional distribution of N_2O_5 for MAM. a) Oslo-CTM2, b) MIPAS IMK-IAA, c) absolute difference and d) relative difference.

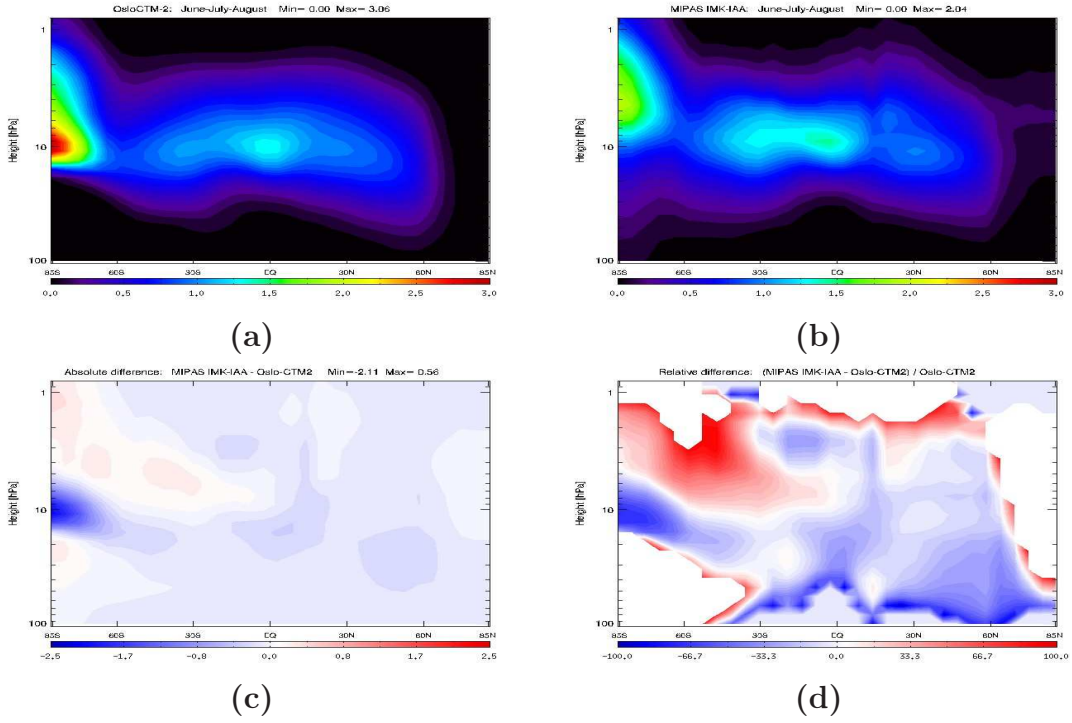

Figure 4.33: Meridional distribution of N_2O_5 for JJA. a) Oslo-CTM2, b) MIPAS IMK-IAA, c) absolute difference and d) relative difference.

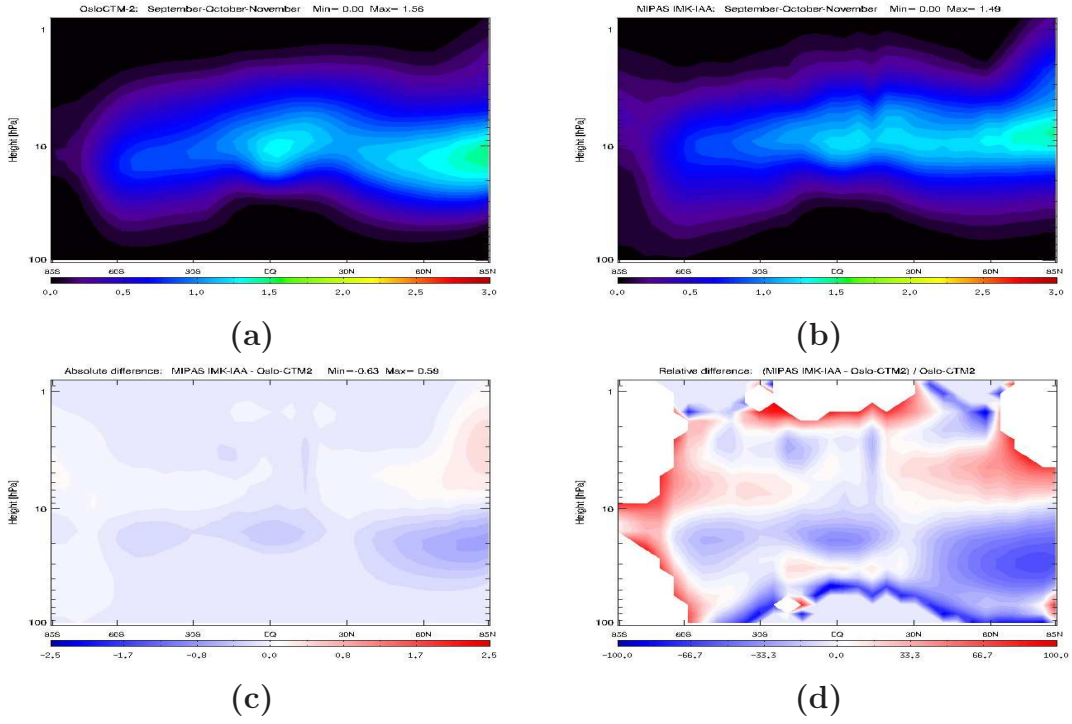

Figure 4.34: Meridional distribution of N_2O_5 for SON. a) Oslo-CTM2, b) MIPAS IMK-IAA, c) absolute difference and d) relative difference.

4.8 Nitric acid (HNO_3)

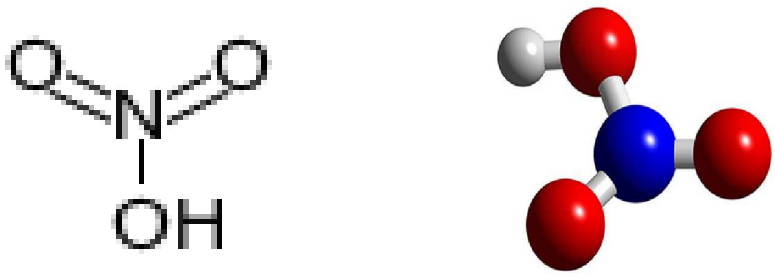

(a) **(b)**

Figure 4.35: Molecular structure of HNO_3 (http://www.3Dchem.com)

HNO_3 is a non-radical member of the NO_y family that has an even longer atmospheric lifetime than N_2O_5 (up to weeks) in the stratosphere. It is a major reservoir for NO_x in the lower stratophere and due to its direct photochemical link to NO_x it plays an important role in processes that control ozone abundance in these regions of the atmosphere. Oxidization with OH is also a considerable sink for HNO_3. HNO_3 is highly soluble, and the ultimate removal of NO_y is by transport to the troposphere where HNO_3 is rapidly removed by wet deposition. These removal processes are significant for the dinitrification of the atmosphere which is central for the formation of the "ozone hole" in especially the SH's springtime (SON). Sulfuric acid (H_2SO_4) and HNO_3 are together the most dominant contributors to the precipitation acidity that among several effects leads to strong decline of fish population in lakes.
Sources of HNO_3 in Oslo-CTM2 are various heterogeneous reactions, while sinks are photolysis, oxidization with OH and removal through wet deposition (Appendix B). In MIPAS IMK-IAA, the dataset for HNO_3 is retrived jointly with ozone using two different spectral regions, 741-798 cm^{-1} and 1020-1108 cm^{-1}, which cover HNO_3's ν_5 and $2\nu_9$ bands (Mengistu Tsidu et al., 2005). The species that are assumed to interfere with HNO_3 in these microwindows are H_2O, O_3, CO_2, NO_2, N_2O, CH_4, ethane (C_2H_6), $CFC-11$, $CFC-12$, ClO, carbonul sulfide (OCS) and amonia (NH_3). Table 4.3 shows the total errors in retrival of HNO_3 and N_2O_5. We see that the absolute errors are most significant in the region between 20 and 35 km, corresponding to approximately 50 and 5 hPa, respectively. The relative errors are lower than 10% in the region where the abundance of HNO_3 is highest.

4.8.1 Meridional distributions

The Meridional distributions in Figures 4.36 to 4.39 show the seasonal variability for HNO_3, and its characteristic maxima in the autumn and winter

hemisperes. It seems that the HNO_3 field's upper limit is to a large exctent controlled by decomposition by UV radiation, wheras its lower limit are controlled by oxidation by OH and that it is highly soluble and consequently washed out with precipitation. We find that Oslo-CTM2 consistently underestimates the amount of stratospheric HNO_3 on both hemispheres in all four seasons compared to MIPAS IMK-IAA. A Major contributor to this underestimation, especially in the upper stratospheric regions, are effects from SPEs which are not resolved in the model. This phenomenon will be discussed further in section 4.13. We also find that Oslo-CTM2 generally seems to overestimate the VMR in the lower stratospheric regions on the SH's midlatitudes, whereas in the NH we observe that the model consistently underestimates the VMR in the lower stratosphere. Besides these discrepancies the HNO_3 fields seems to be comparable in the general structure. The VMR in the meridional distributions for HNO_3 are presented in ppbv for all four seasons.

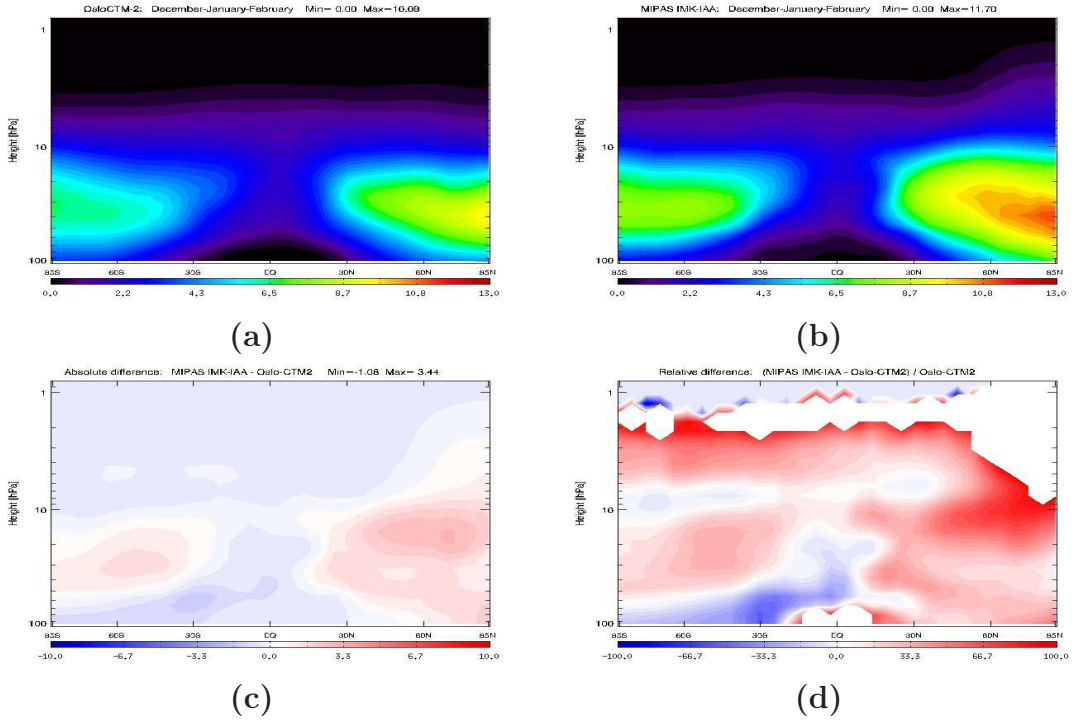

Figure 4.36: Meridional distribution of HNO_3 for DJF. a) Oslo-CTM2, b) MIPAS IMK-IAA, c) absolute difference and d) relative difference.

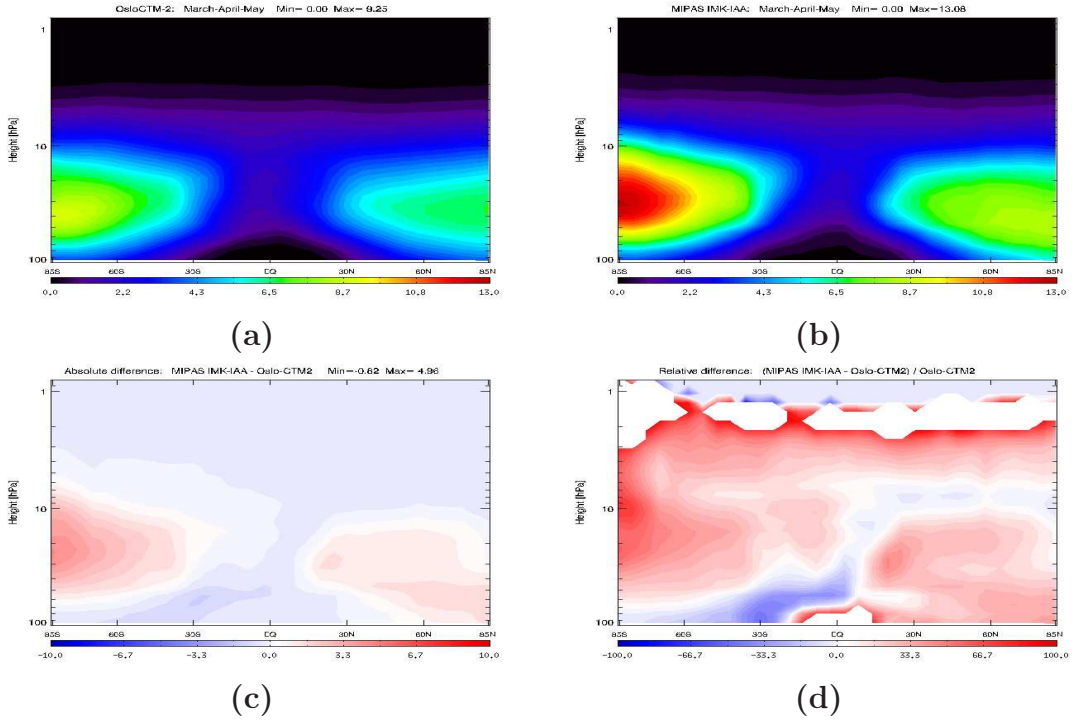

Figure 4.37: Meridional distribution of HNO_3 for MAM. a) Oslo-CTM2, b) MIPAS IMK-IAA, c) absolute difference and d) relative difference.

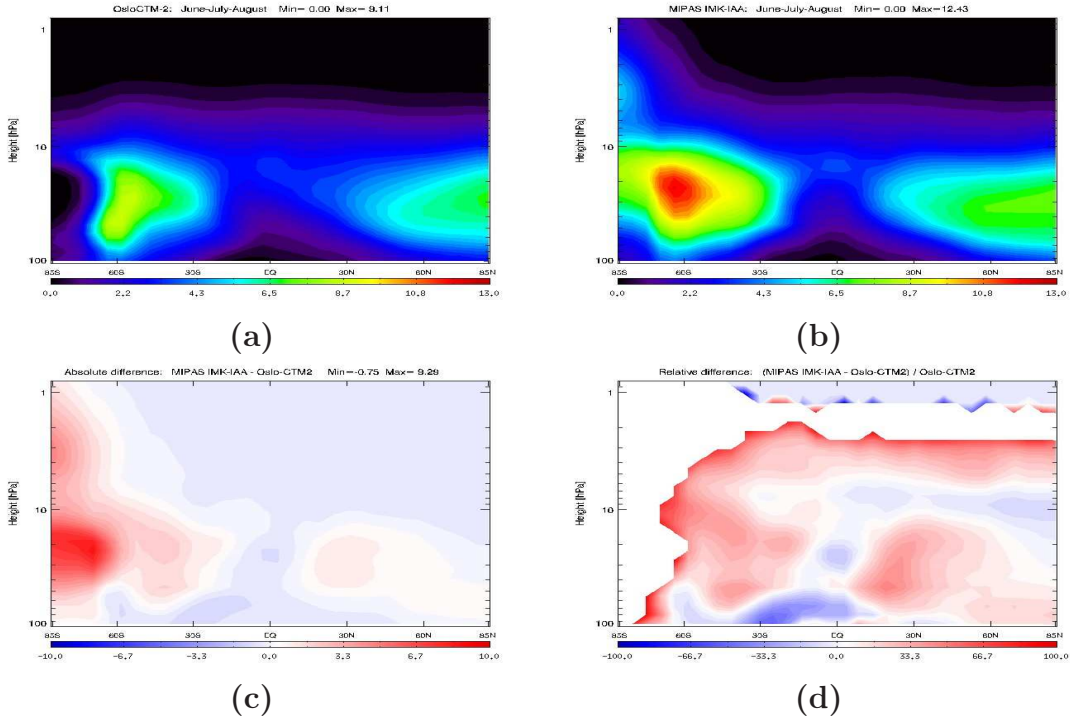

Figure 4.38: Meridional distribution of HNO_3 for JJA. a) Oslo-CTM2, b) MIPAS IMK-IAA, c) absolute difference and d) relative difference.

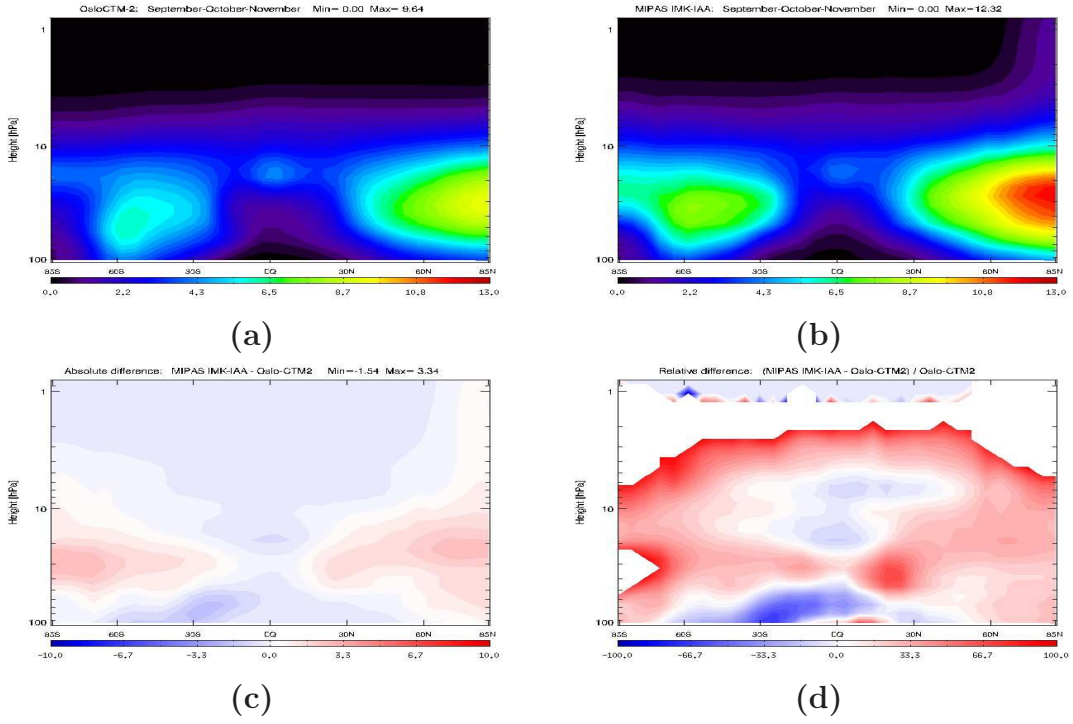

Figure 4.39: Meridional distribution of HNO_3 for SON. a) Oslo-CTM2, b) MIPAS IMK-IAA, c) absolute difference and d) relative difference.

4.8.2 Vertical column Nitric acid

Geographical distributions

From the Geographical distributions of HNO_3's vertical column abundance (Figure 4.40) we find the same discrepancies as in the meridional distributions. The structure in the fields seems to correspond well, but the model generally underestimates the values, this will be discussed further in Section 4.13.

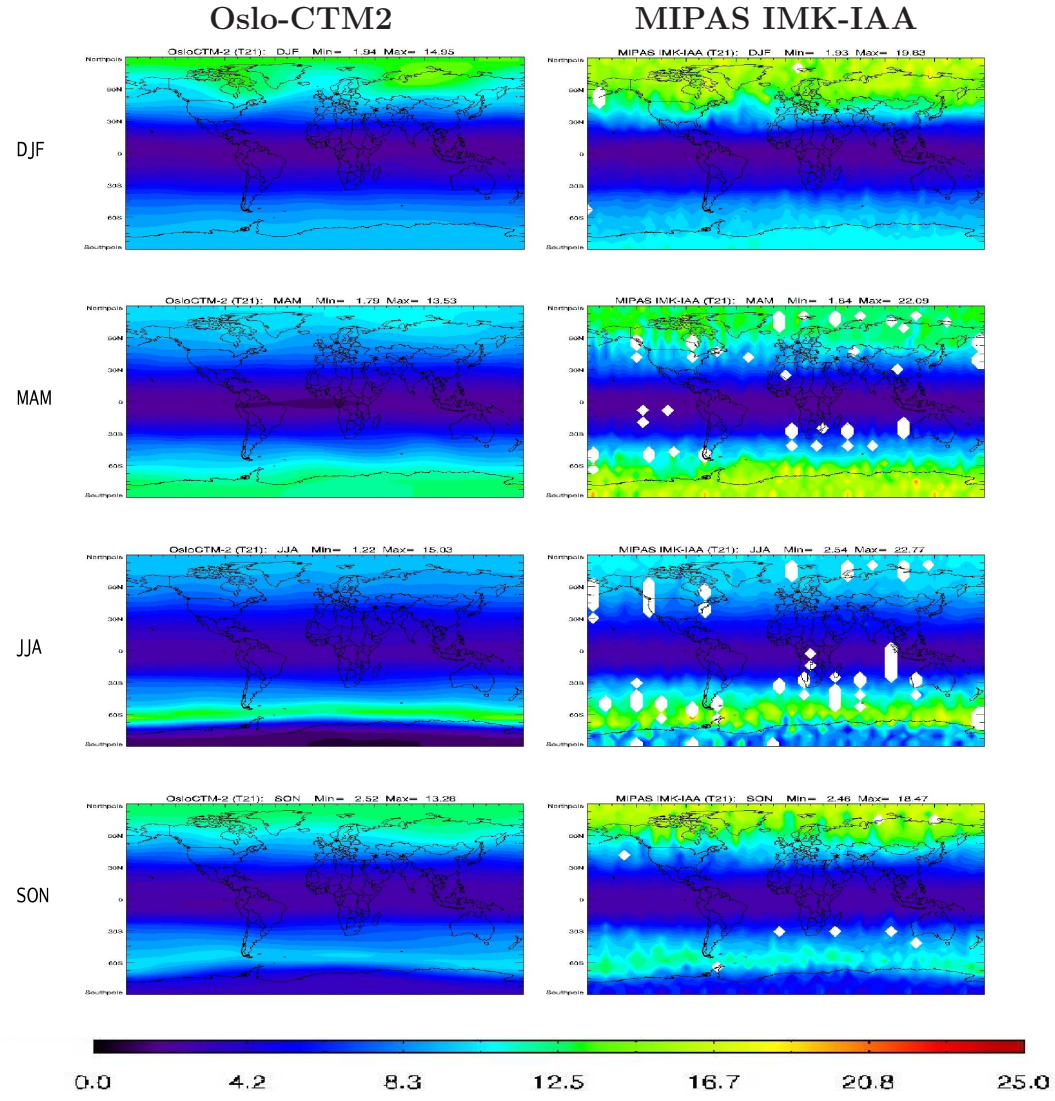

Figure 4.40: Seasonally averaged global distributions of stratospheric nitric acid Oslo-CTM2 and MIPAS IMK-IAA.

4.9 Peroxynitric acid (HO_2NO_2)

HO_2NO_2 is an important molecule for the understanding of stratospheric ozone depletion since it is an important reservoir for both NO_x and HO_x (OH and $HO2$). It acts as a link between the catalytic cycles of NO_x and HO_x, which are responsible for a major part of ozone destruction. HO_2NO_2 is thought to be formed exclusively in the gas phase via the three-body reaction involving NO_2 and HO_2. The processes that control its removal from the atmosphere are thermal decomposition, UV, VIS and near IR photolysis and oxidation by OH. Because it is very weakly bound and rapidly dissociated at temperatures over 240 K, abundances of HO_2NO_2 are most significant in the lower stratosphere and upper troposphere.
In Oslo-CTM2 the source for stratospheric HO_2NO_2 is as expected the three-body reaction involving NO_2 and HO_2, while the sinks are photolysis, oxidation by OH and thermal decomposition reactions. MIPAS IMK-IAA retrieves VMR for HO_2NO_2 from the Q branch of its ν_6 band at 802.7 cm^{-1}, and according to Stiller et al. (2007) a single profile precision in the altitude range between 20 and 34 km is in the order of 15.0 to 34 pptv.

4.9.1 Meridional distributions

The meridional distribution figures (Figures 4.41 to 4.44) shows that Oslo-CTM2 generally overestimates the VMR in the lower stratospheric regions on high latitudes. The discrepancy is most significant on the winter hemisphere (DJF and JJA seasons), but are apparent throughout the entire year. The difference will be discussed further in Section 4.13. Apart from this distinct discrepancy the fields seems to be comparable both in location and size. We observe from the figures that the upper boundary of the VMR field especially on the winter hemispheres (DJF and JJA seasons) follows approximately the shape of the 240 K isoterm from the meridional distributions (Figure 4.21 and 4.23) of temperature. On the corresponding summer hemispheres the abundance are controlled by photolysis and oxidation. The VMR in the meridional distributions for HO_2NO_2 are presented in ppbv for all four seasons.

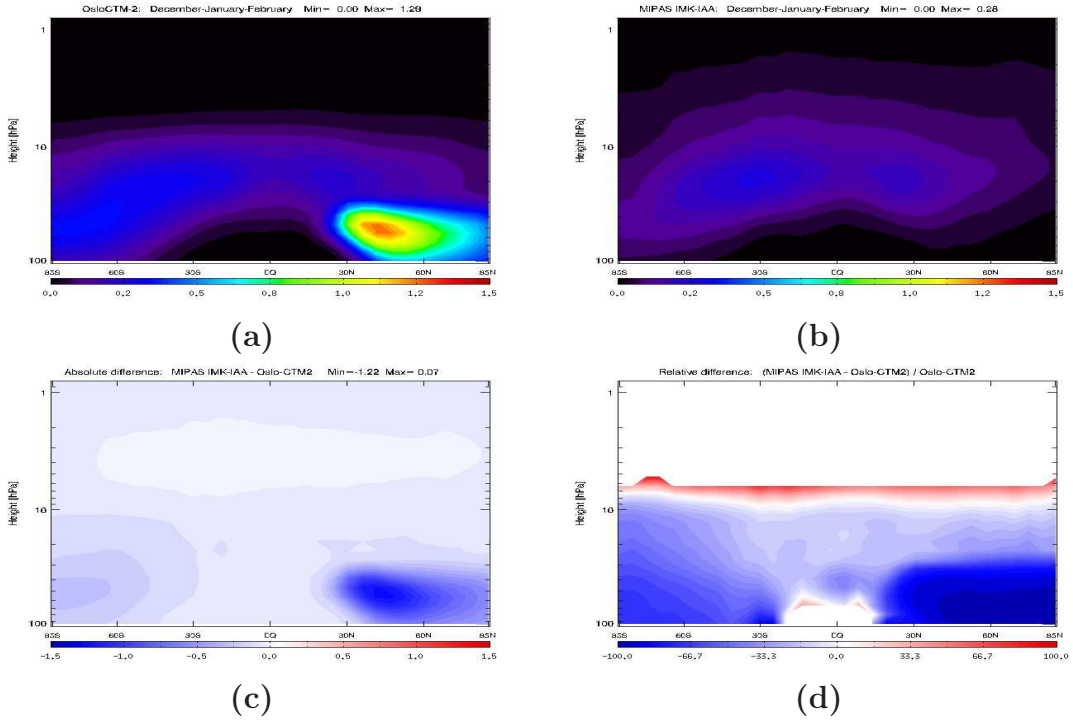

Figure 4.41: Meridional distribution of HO_2NO_2 for DJF. a) Oslo-CTM2, b) MIPAS IMK-IAA, c) absolute difference and d) relative difference.

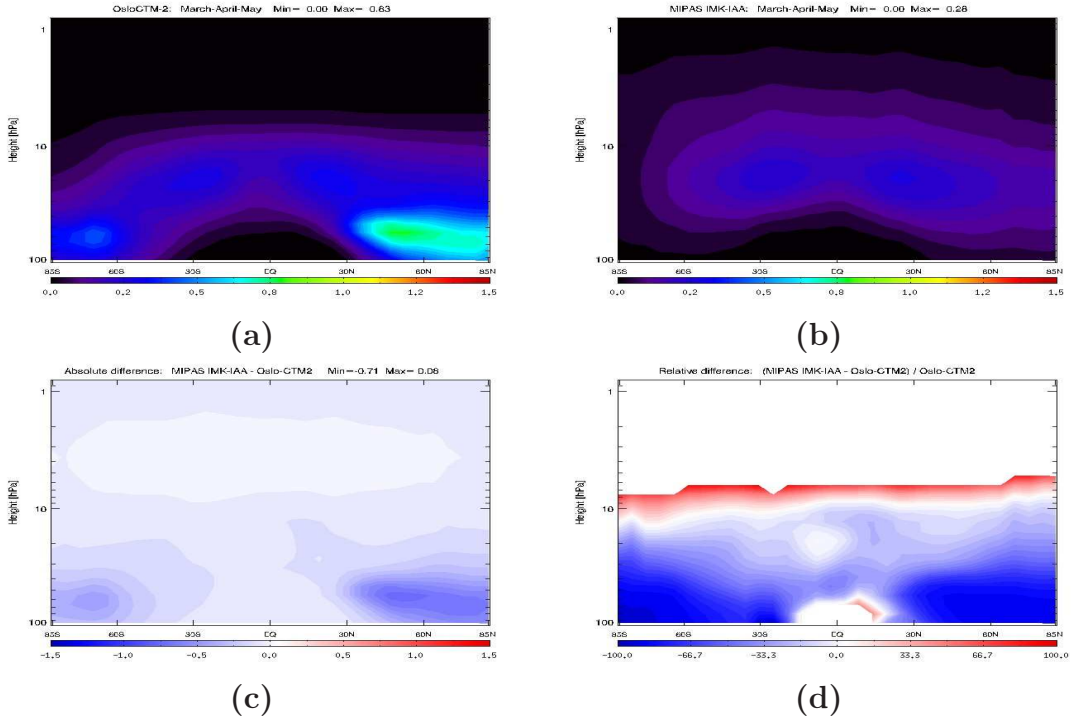

Figure 4.42: Meridional distribution of HO_2NO_2 for MAM. a) Oslo-CTM2, b) MIPAS IMK-IAA, c) absolute difference and d) relative difference.

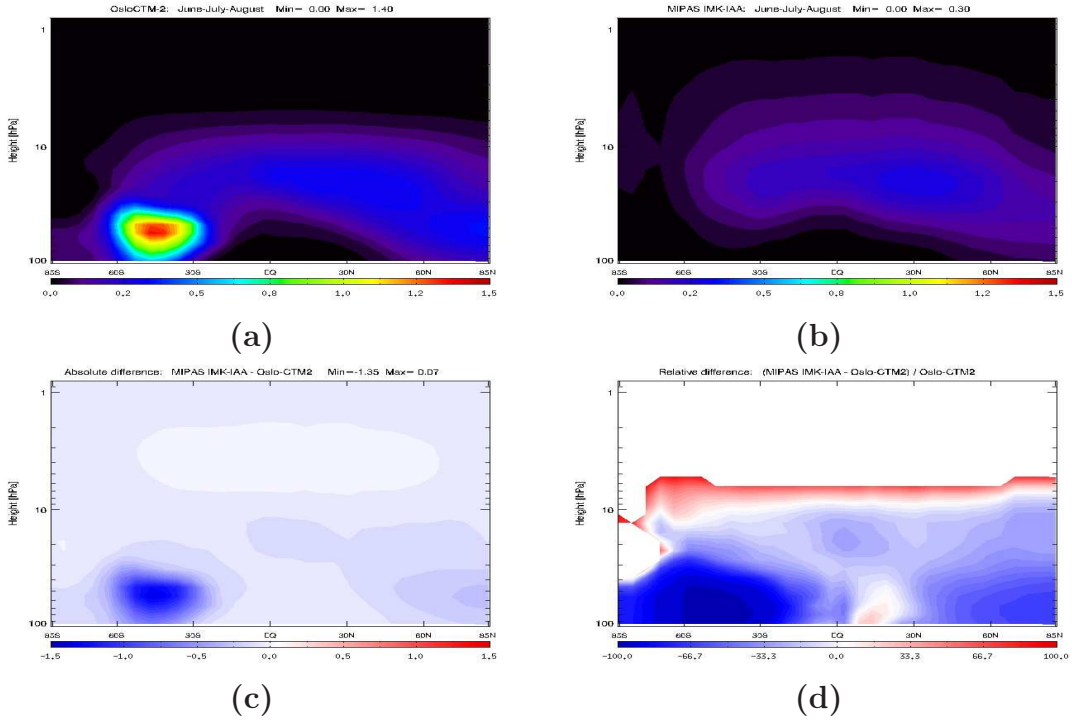

Figure 4.43: Meridional distribution of HO_2NO_2 for JJA. a) Oslo-CTM2, b) MIPAS IMK-IAA, c) absolute difference and d) relative difference.

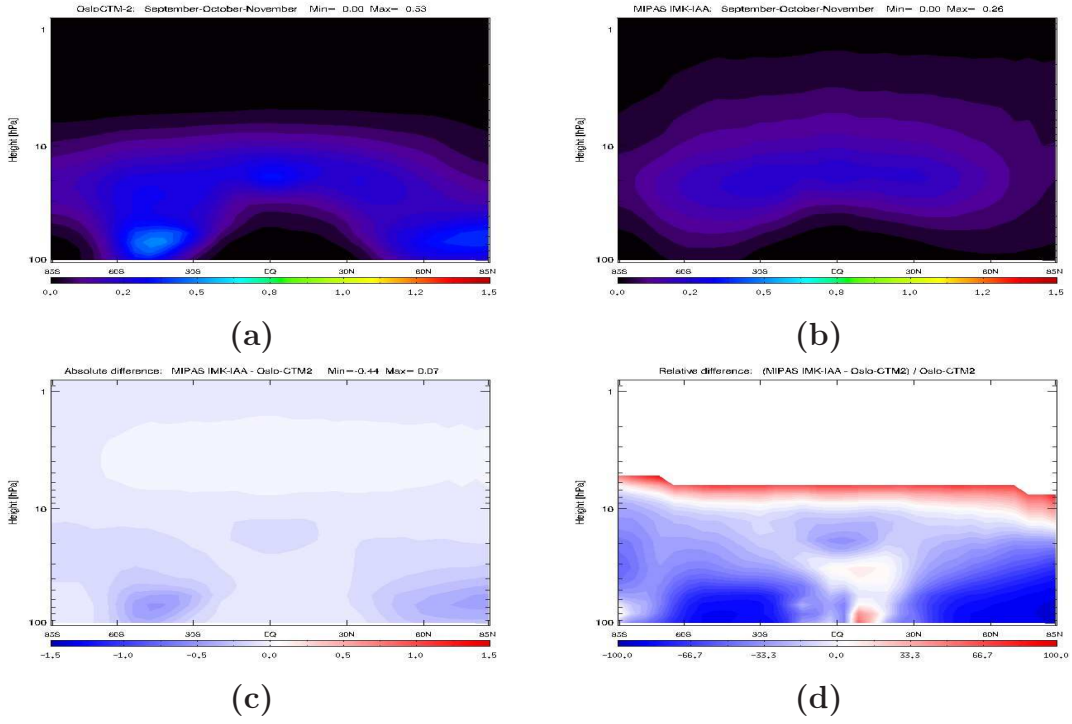

Figure 4.44: Meridional distribution of HO_2NO_2 for SON. a) Oslo-CTM2, b) MIPAS IMK-IAA, c) absolute difference and d) relative difference.

4.10 Chlorine oxide (ClO)

ClO is a very strong oxidant and consists of one chlorine and one oxygen atom (Figure 4.45). Catalytic reactions of O_3 and Cl via ClO and Cl_2O_2 are the main contributors causing the Antarctic "ozone hole". When polar atmospheres become sunlit again in the hemispheric springtime, Cl_2 is photolysed to Cl that forms ClO by reaction with ozone. Most of the ClO is converted to its dimer Cl_2O_2 at nighttimes, which again undergoes photolysis into ClO after sunrise.

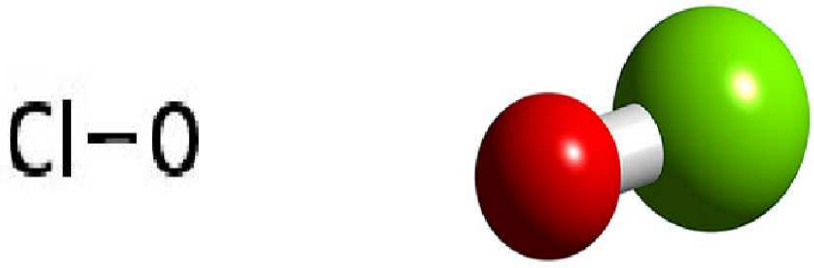

(a) **(b)**

Figure 4.45: Molecular structure of ClO (http://www.3Dchem.com)

In Oslo-CTM2 sources for stratospheric ClO are photolysis of $OClO$, various bimolecular and three-body reactions involving Cl and the thermal decomposition reaction of Cl_2O_2. Sinks for ClO in the stratosphere are photolysis and bimolecular and three-body reactions involving the ClO_x and BrO_x families. The only ClO absorption band in the mid-IR is the weak 1→0 fundamental band centered at 844 cm^{-1}, and due to overlapping with components such as HNO_3, CO_2 and O_3 the suitable microwindows for retrival of ClO with MIPAS IMK-IAA are in the 820.975-846.175 cm^{-1} spectral region.

Height (km)	$High - ClO$	$Low - ClO$
12	**66 (36)**	**58 (79)**
14	**290 (34)**	**260 (72)**
16	**410 (29)**	**270 (71)**
18	**590 (30)**	**310 (157)**
20	**600 (28)**	**350 (678)**
22	**530 (49)**	**400 (261)**
25	**280 (458)**	**260 (133)**
30	**280 (198)**	**260 (98)**

Table 4.4: Total error for ClO retrival scans for High and Low ClO abundances. The errors are given in absolute (pptv) and relative units (% in brackets). A complete summary over the error budget for ClO in the UTLS region are included in Glatthor et al. (2004).

Table 4.4 shows two examples of total error for the retrival of *ClO*. The High-abundance-ClO scan was performed on the 20. September 2002 (Orbit 2910), while the Low-abundance-ClO scan was performed on the 26. September 2002 (Orbit 2994). The table shows that the errors linked to retrival of ClO are relatively large in the UTLS region. The tables range corresponds to the lower stratospheric maximum associated with formation of PSCs, implying that errors in the atmospheric levels with the most significant *ClO* abundances are excluded from the table. Since *ClO* has a strong diurnal variability, and because both day and night retrivals are included in the seasonal means we ensured that there were no bias due to more day than night retrivals in the MIPAS IMK-IAA datasets. This was accomplished by calculating the mean of the solar zenit angle for each MIPAS IMK-IAA retrival included in the seasonal mean.

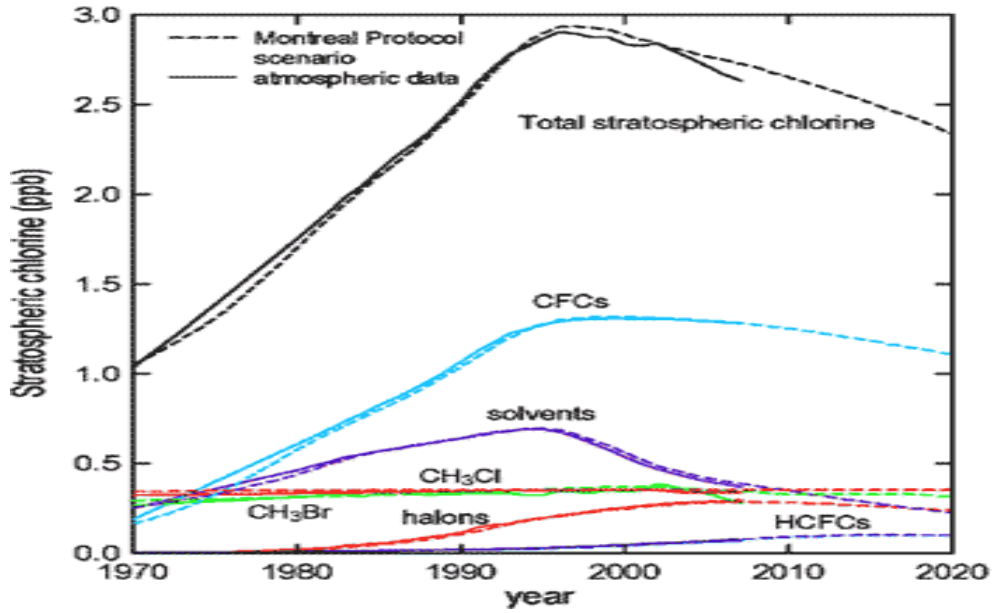

Figure 4.46: Observed and projected abundance of stratospheric chlorine in ppb from the major ozone depleting substances (CFCs, chlorinate solvents, halons, metyl bromine, metyl chloride and HCFCs). (Source: http://www.environment.gov.au).

We see in Figure 4.46 that the stratospheric chlorine abundance peaked in the mid 1990s and is now in decline by about one percent per year. These observed reductions are associated with the restrictions in the industrial use of ozone depleting substances regulated by the "Montreal Protocol".

4.10.1 Meridional distributions

Because the formation of *ClO* is highly dependent of photolysis by UV radiation it has a strong diurnal variability. The same processes are prevailing in the areas both north and south of the polarcircle, but on a longer timescale

(polarday/polarnight). This feature can clearly be seen in the upper stratosphere (Figures 4.47 to 4.50), with distinct VMR maximum in polarday regions, while ClO abundance is low in the corresponding polarnight regions. From the figures we can easily identify the regions where the heterogeneous chemistry is active as maxima of ClO abundances in the lower stratosphere. We observe that these regions are associated with regions covered by the "polar vortex" on the winter hemisphere, and that they in general are in good agreement with the ClO abundance from the MIPAS IMK-IAA dataset. The VMR in the meridional distributions for ClO are presented in ppbv for all four seasons. In general we find that Oslo-CTM2 reproduces the ClO abundance in a satisfactory way in regions dominated by heterogenous chemistry and regions with low abundance, but in the upper stratospheic tropical regions Oslo-CTM2 seems to have a significant low bias compared to the MIPAS IMK-IAA product. The main discrepancy for this component will be further discussed in Section 4.13.

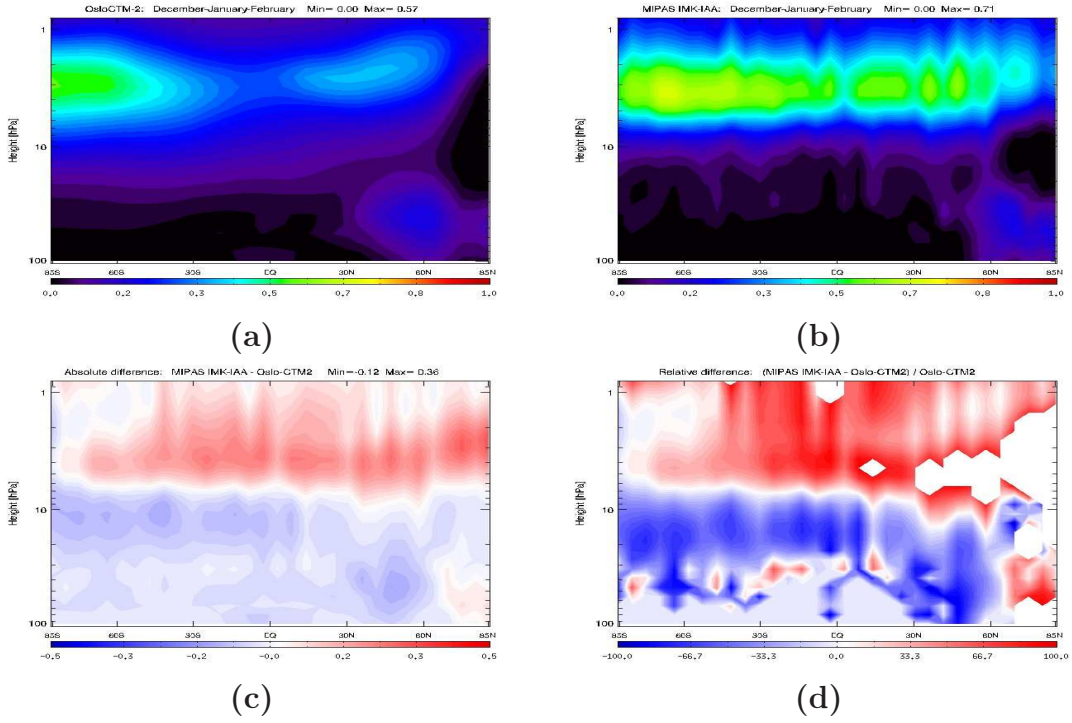

Figure 4.47: Meridional distribution of *ClO* for DJF. a) Oslo-CTM2, b) MIPAS IMK-IAA, c) absolute difference and d) relative difference.

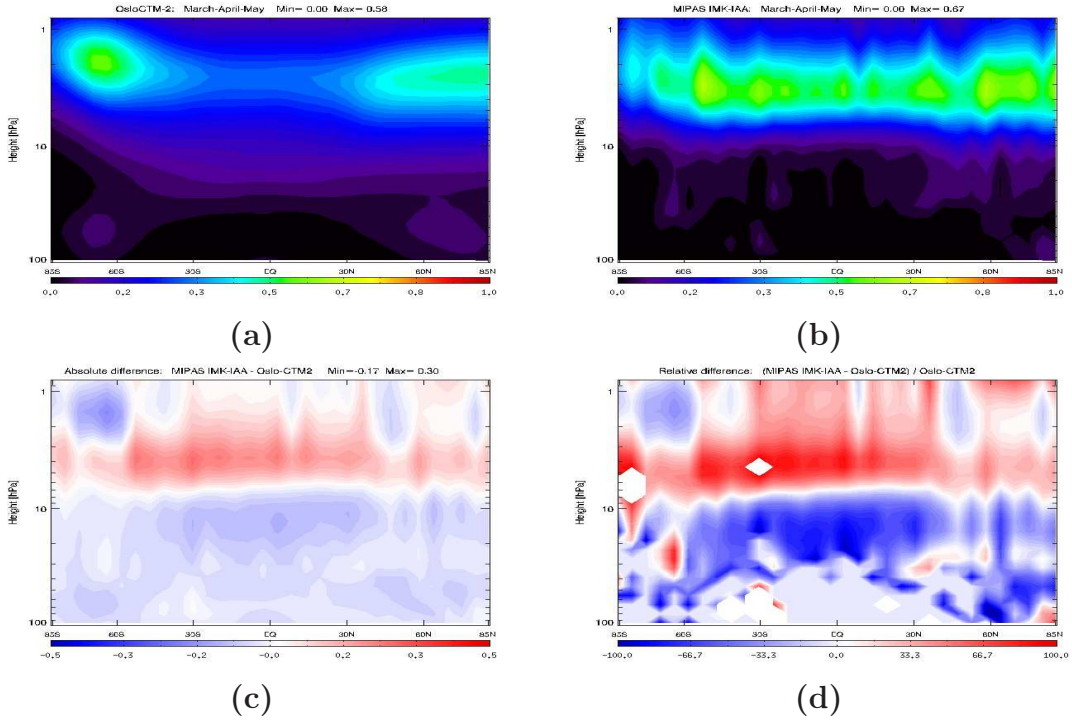

Figure 4.48: Meridional distribution of *ClO* for MAM. a) Oslo-CTM2, b) MIPAS IMK-IAA, c) absolute difference and d) relative difference.

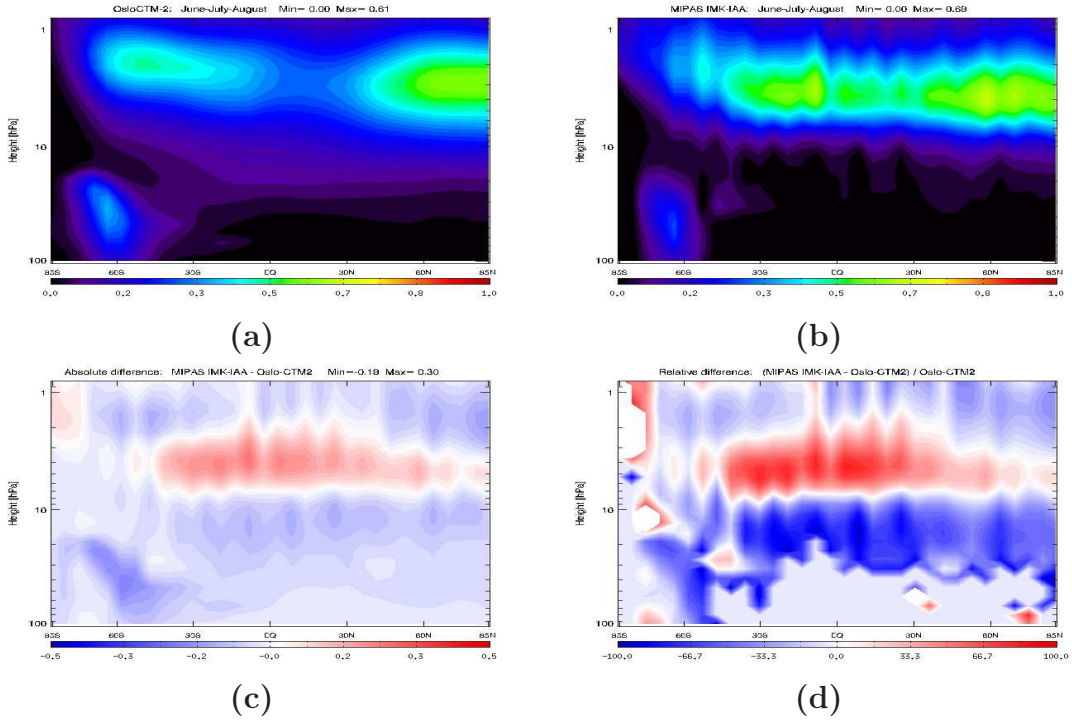

Figure 4.49: Meridional distribution of *ClO* for JJA. a) Oslo-CTM2, b) MIPAS IMK-IAA, c) absolute difference and d) relative difference.

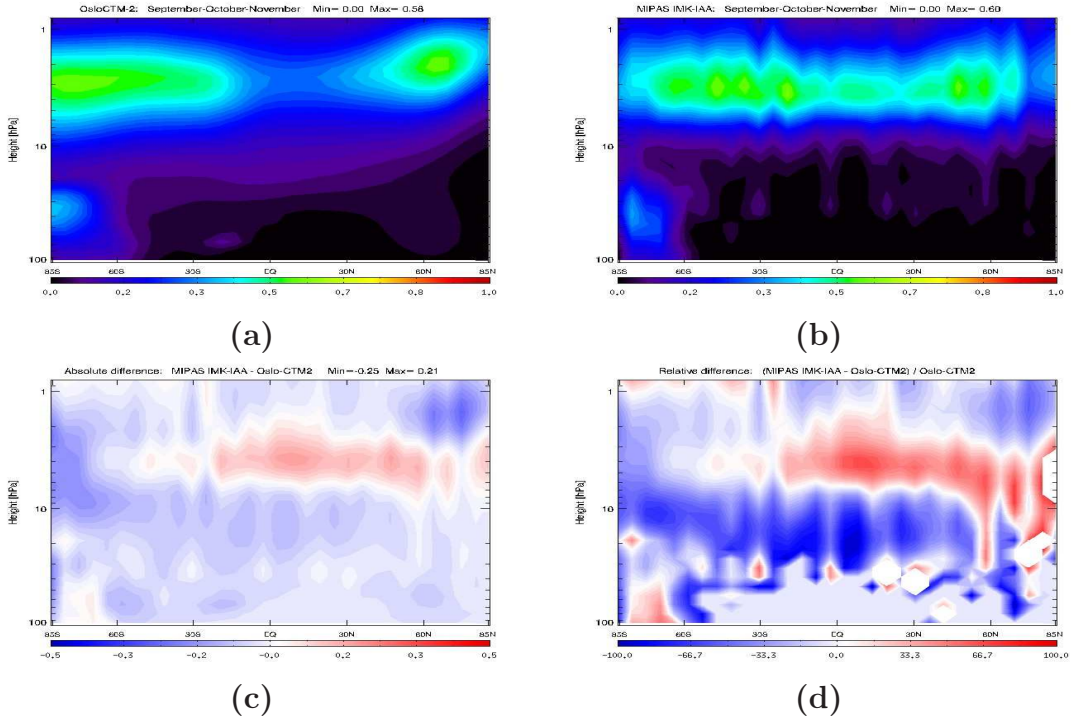

Figure 4.50: Meridional distribution of *ClO* for SON. a) Oslo-CTM2, b) MIPAS IMK-IAA, c) absolute difference and d) relative difference.

4.11 Chlorine nitrate ($ClONO_2$)

$ClONO_2$ is one of the major reservoir gases for Cl in the stratosphere. During polar winter it is converted into ClO_x by heterogeneous reactions in PSCs, This is a prerequisite for the fast catalytic destruction of ozone in springtime polar regions.
In Oslo-CTM2, the source for $ClONO_2$ is the three-body reaction between ClO and NO_2, whereas sinks are various heterogenous reactions and a bimolecular reaction between $ClONO_2$ and Cl. MIPAS IMK-IAA used the Q branch of the ν_4 band of $ClONO_2$ for their analysis, and the spectral window used for retrival are between 779.5-781.0 cm^{-1}. In order to reduce error propagation due to uncertainties of O_3, which has spectral signatures in the selected window, they are jointly fitted in the retrival process (Höpfner et al., 2004).

Height (km)	$ClONO_2$
15	**21 (5)**
18	**45 (8)**
21	**80 (11)**
24	**140 (6)**
27	**130 (10)**
30	**110 (13)**
33	**86 (17)**
36	**51 (15)**
39	**22 (12)**

Table 4.5: Total error for $ClONO_2$ retrival for a scan on 20. Sept 2002, profiles were taken inside the polar vortex. The errors are given in absolute (pptv) and relativ units (% in brackets). For a complete summary of the error budget see Höpfner et al. (2004).

4.11.1 Meridional distributions

The general impression of the Oslo-CTM2 models reproduction of the $ClONO_2$ abundance are good, the model seems to overestimate the abundance slightly in the entire stratosphere except in the polar wintertime regions where it to a certain degree underestimates. We also observe that it seems as if MIPAS IMK-IAA retrives some $ClONO_2$ associated with downward transport from the mesosphere where NO_x caused by SPEs may be converted to $ClONO_2$ in the three-body reaction between ClO and NO_2. The general discrepancies between the datasets will be discussed further in Section 4.13. The VMR in the meridional distributions for $ClONO2$ are presented in ppbv for all four seasons.

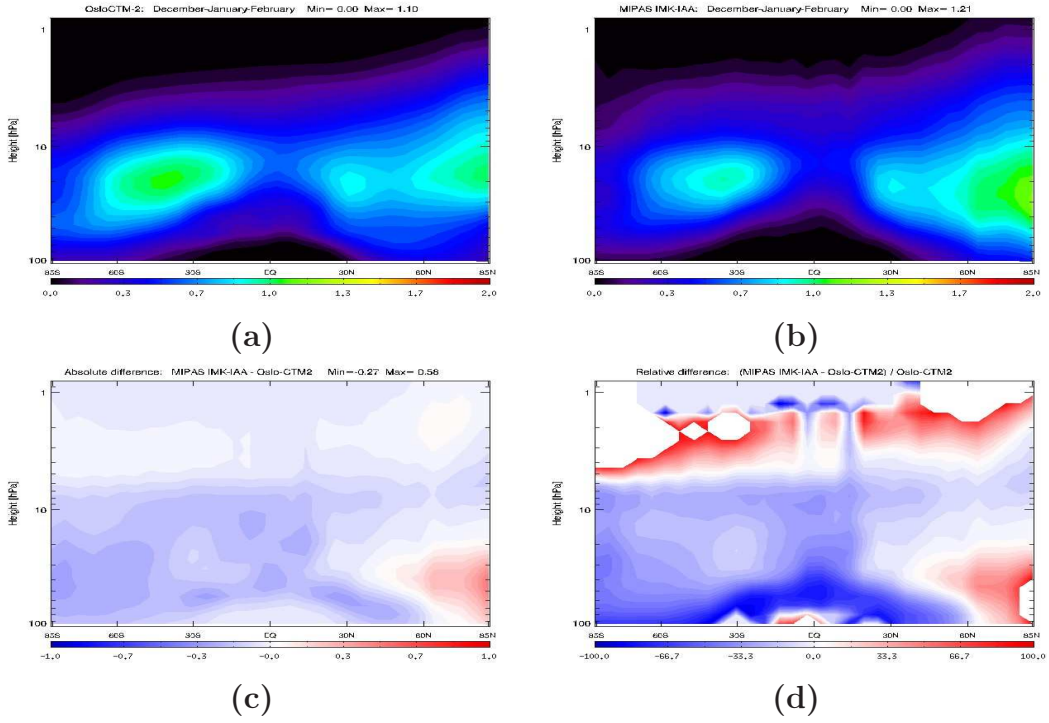

Figure 4.51: Meridional distribution of $ClONO_2$ for DJF. a) Oslo-CTM2, b) MIPAS IMK-IAA, c) absolute difference and d) relative difference.

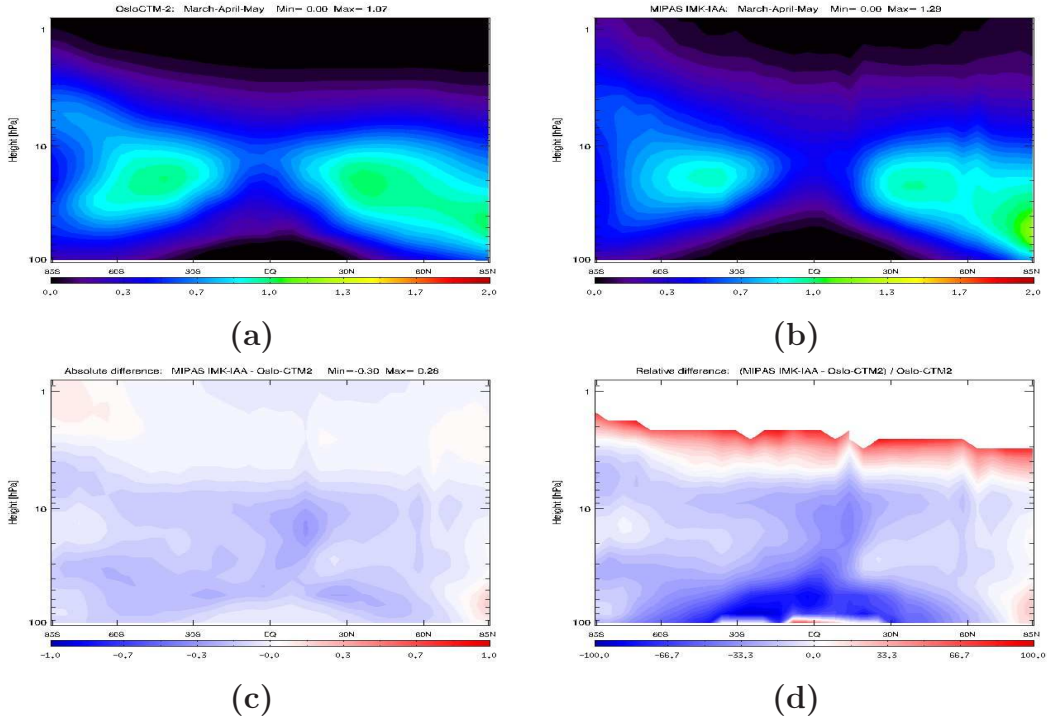

Figure 4.52: Meridional distribution of $ClONO_2$ for MAM. a) Oslo-CTM2, b) MIPAS IMK-IAA, c) absolute difference and d) relative difference.

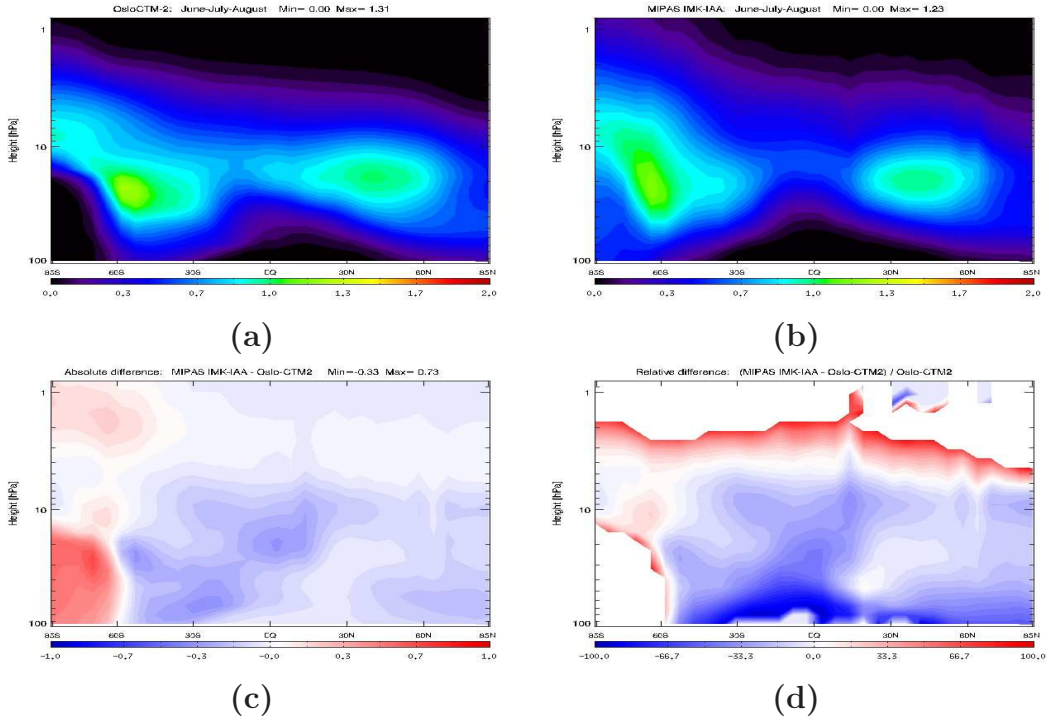

Figure 4.53: Meridional distribution of $ClONO_2$ for JJA. a) Oslo-CTM2, b) MIPAS IMK-IAA, c) absolute difference and d) relative difference.

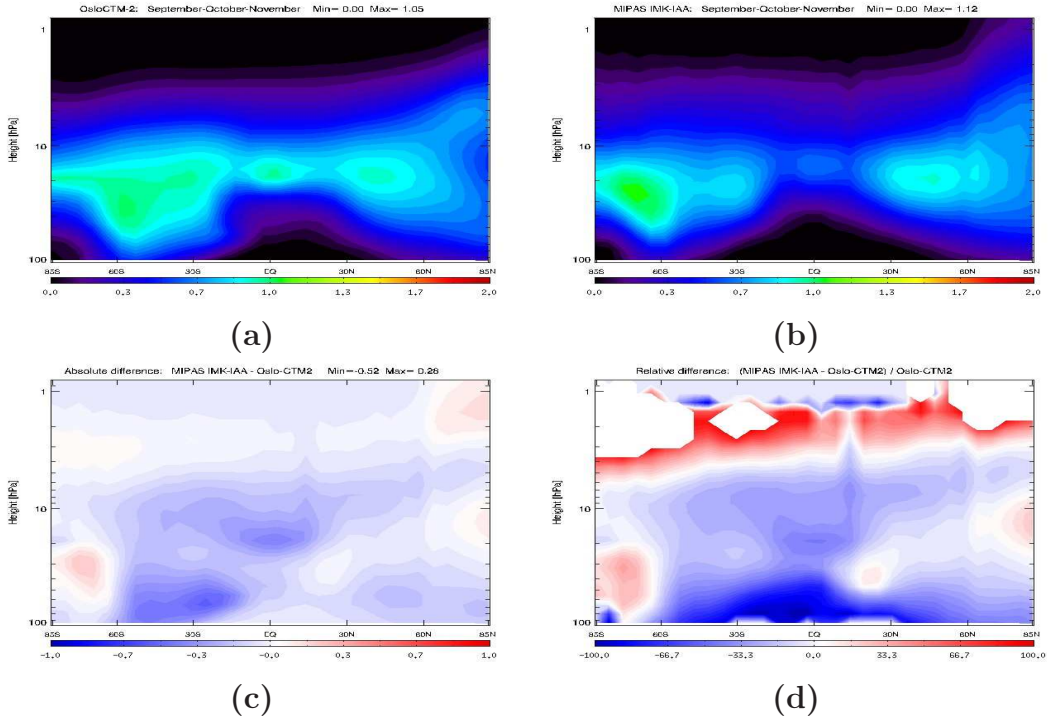

Figure 4.54: Meridional distribution of $ClONO_2$ for SON. a) Oslo-CTM2, b) MIPAS IMK-IAA, c) absolute difference and d) relative difference.

4.12 Ozone (O_3)

Due to its importance as an ultraviolet (UV) radiation absorber, being a greenhouse gas and having disadvantageous health effect on living species, O_3 is an atmospheric component of major interest. It is central in the highly coupled chemical, radiative and dynamical processes in the stratosphere. O_3 protects life on Earth by absorbing potentially harmful UV and VIS radiation from the Sun and is also an absorber of Earth-emitted IR radiation. The absorptive effect of UV, VIS and IR radiation leads to local heating and consequently the temperature profile (increasing temperature with increasing altitude) associated with the dynamically stable stratosphere.

(a) **(b)**

Figure 4.55: Molecular structure of O_3 (http://www.3Dchem.com)

In Oslo-CTM2 the source for stratospheric O_3 is the three-body reaction involving oxygen atoms in ground-level triplet state ($O(^3P)$) and O_2, while the sinks involve more complex processes. O_3 is decomposed in bimolecular reaction with $O(^3P)$, in photolysis and in catalytic cycles involving species in the HO_x, NO_x, ClO_x and BrO_x families (Appendix B consists of a complete summary of the chemical reactions included in Oslo-CTM2). MIPAS IMK-IAA retrieves VMR for O_3 in two different spectral regions, 741-798 cm^{-1} and 1020-1108 cm^{-1}, depending on scan altitude. The first of these regions cover the most energetic ν_1 and ν_3 bands, commonly used in the middle atmosphere, whereas the second region cover the weaker ν_2 fundamental band, which is used at lower altitudes (Glatthor et al., 2006). Figure 4.56a compares global O_3 values (annual averages) with the average from the periode 1964 to 1980. It shows that the global total abindance decreased each year between 1980 and the early 1990s with a minimum value in 1993. Now global O_3 abundances are approximately 4 % below the 1964-to-1980 average. Figure 4.56b compares O_3 changes between 1980 and 2004 for different latitudes, and it shows that the largest decreases have occured at the higest latitudes and that the losses are greatest in the SH due to the Antarctic "ozone hole".

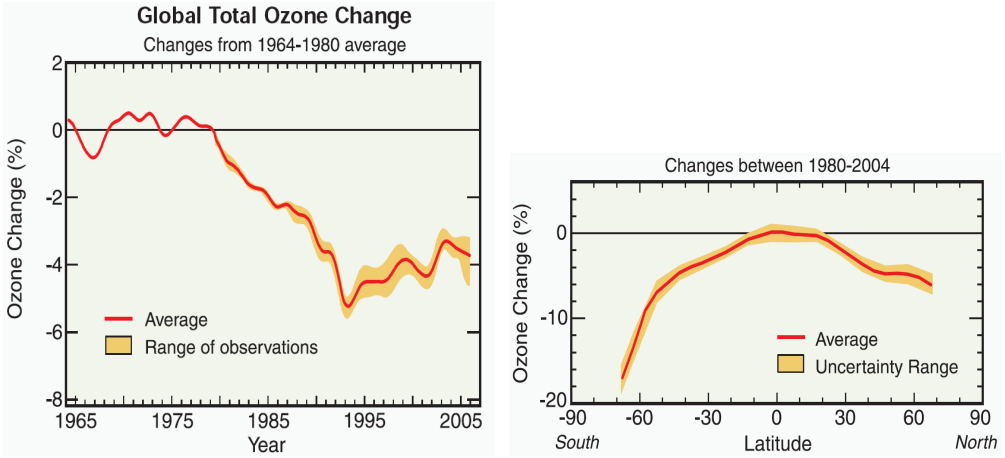

(a) (b)

Figure 4.56: Global total O_3 changes from satelite observations (Source: (Fahey, 2007, page Q.28)).

4.12.1 Meridional distributions

In this section the meridional distributions of O_3 VMR (in ppmv), for all four seasons are presented. The Figures 4.57 to 4.60 shows that the abundance of O_3, known as the "ozone layer", is situated between approximately 30 and 2 hPa. We recognice the characteristic maxima in the tropical stratosphere in all seasons with only minor seasonal variabilities in strenght and location.

The basic shape shown in the figures, with a distinct stratospheric maximum, is characteristic of any gas in which concentration is dependent on the balance between photochemical production driven from above and the atmospheric density that declines with increasing altitude. The mixing ratio is 0.1-0.5 ppmv near the tropopause, 3 ppmv at 50 hPa, 8-10 ppmv at 10 hPa and 2 ppmv near the stratopause (approximately 1 hPa). In the upper stratosphere we find that the O_3 abundance is generally higher in the winter than in the summer hemisphere.

The figures show a generally good correlation between the meridional distribution produced by the Oslo-CTM2 and the MIPAS IMK-IAA datasets, and the main discrepancies will be discussed in Section 4.13.

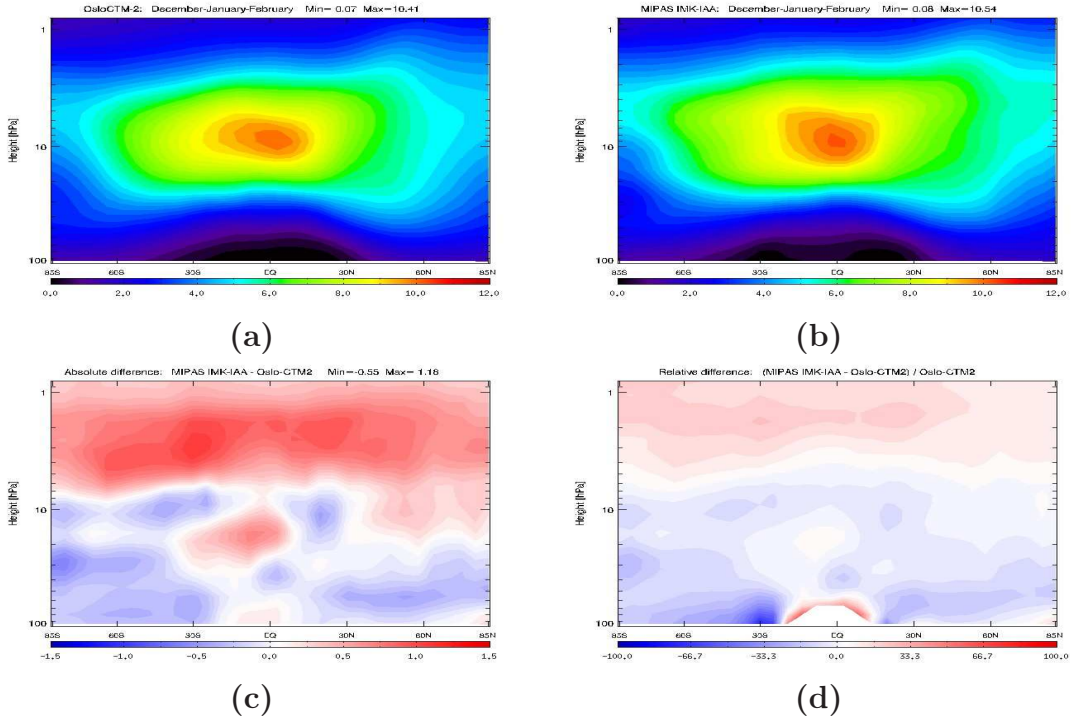

Figure 4.57: Meridional distribution of O_3 for DJF. a) Oslo-CTM2, b) MIPAS IMK-IAA, c) absolute difference and d) relative difference.

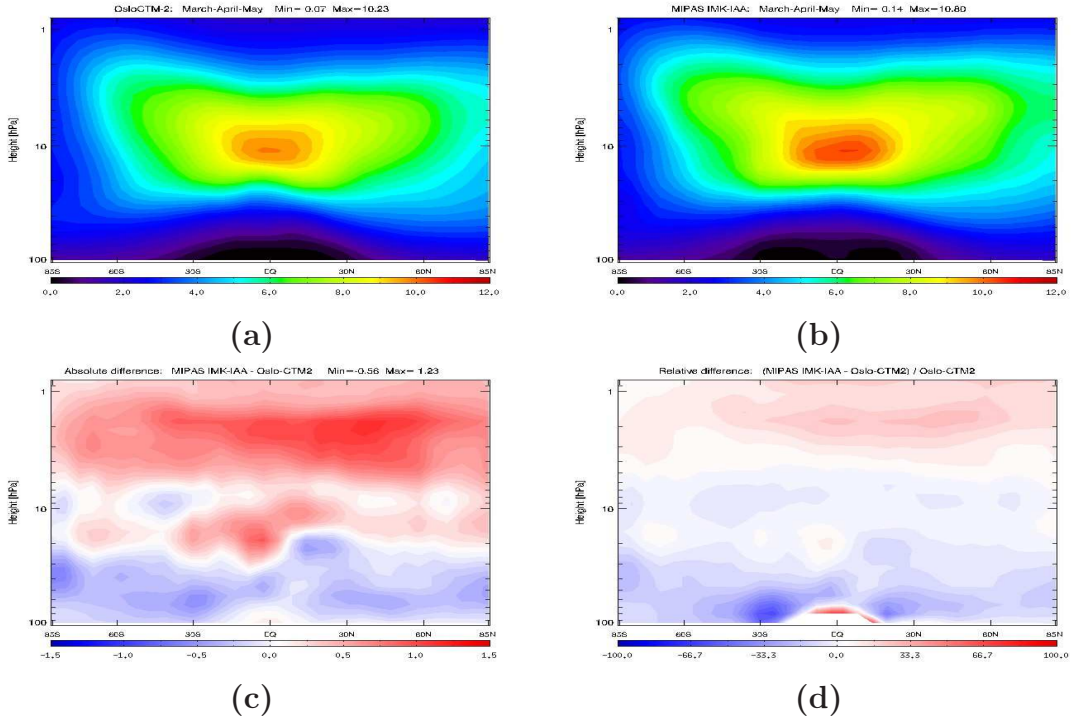

Figure 4.58: Meridional distribution of O_3 for MAM. a) Oslo-CTM2, b) MIPAS IMK-IAA, c) absolute difference and d) relative difference.

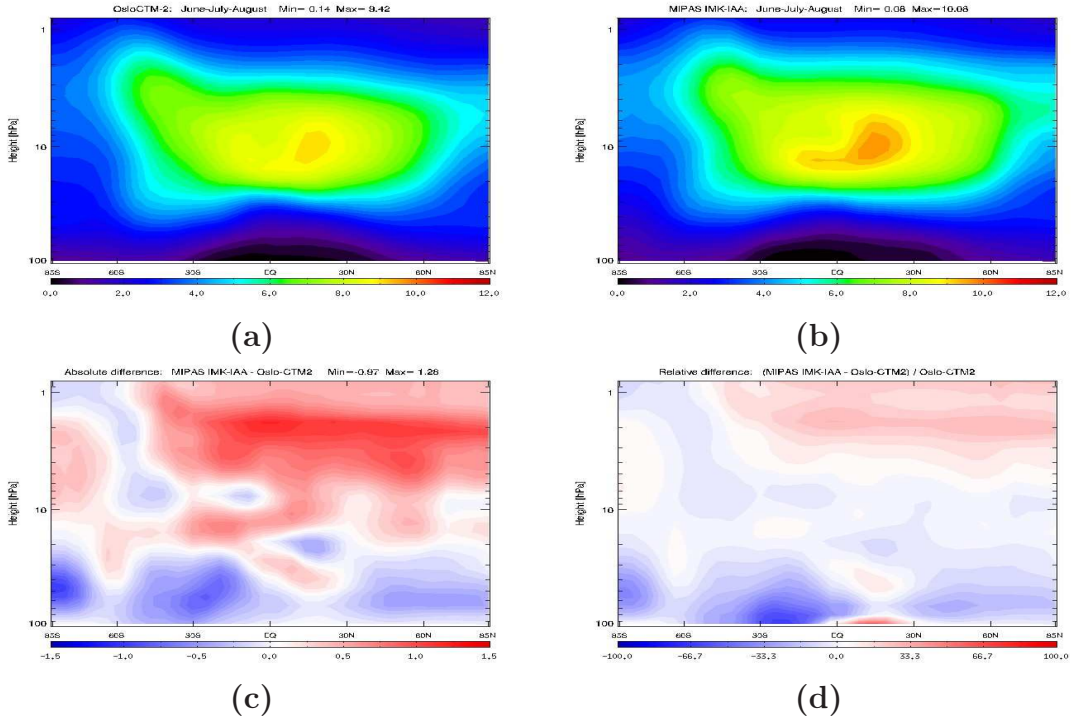

Figure 4.59: Meridional distribution of O_3 for JJA. a) Oslo-CTM2, b) MIPAS IMK-IAA, c) absolute difference and d) relative difference.

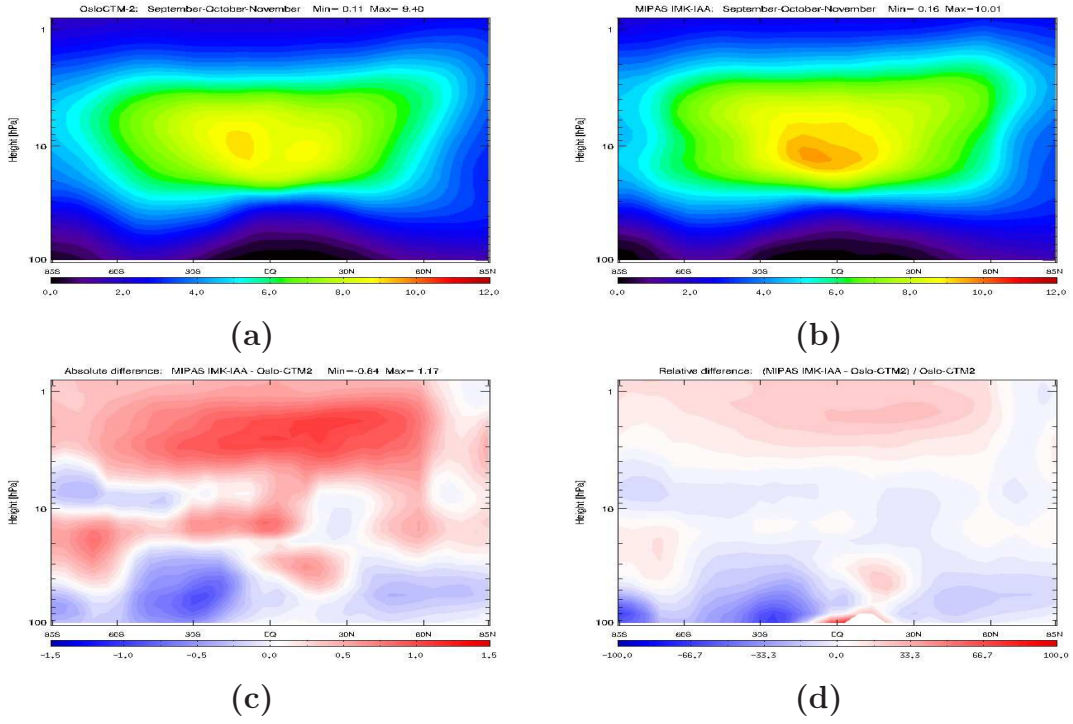

Figure 4.60: Meridional distribution of O_3 for SON. a) Oslo-CTM2, b) MIPAS IMK-IAA, c) absolute difference and d) relative difference.

4.12.2 Vertical column Ozone

Annual cycle

Figure 4.61 shows the 2003 total column O_3 abundance in DU as a function of time of the year and latitude from Oslo-CTM2 based on daily O_3 data in the entire atmospheric column. The highest O_3 abundances are found at high latitudes in winter and early spring, whereas the lowest values, apart from in the "Ozone hole", are found in the tropics (Figure 4.61). This distribution is the result of strong poleward and downward transport in the stratosphere during winter, and is in accordance with current theory.

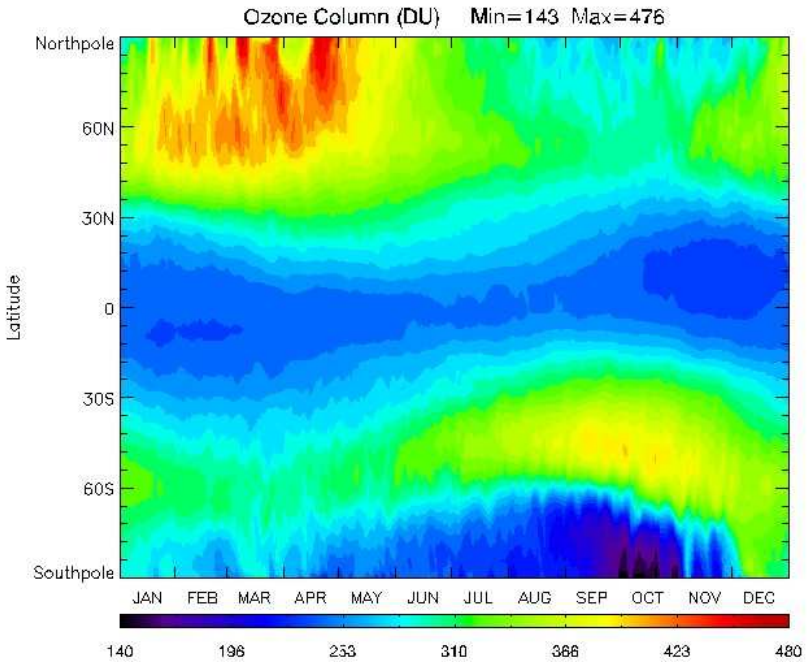

Figure 4.61: Total column O_3 abundance (Dobson units) versus latitude and season

Geographical distributions

The geographical distribution of stratospheric O_3 in DU is presented in Figure 4.62. In general we find good correlation between the Oslo-CTM2 and the MIPAS IMK-IAA datasets. The global distribution of O_3 abundance show similar features as those observed in the annual cycle figure with strong poleward and downward transport in the stratosphere during winter giving the maxima on both hemispheres. The weakest maximum is in the SH due to the "polar vortex" and the associated O_3 depletion. The Antarctic "Ozone hole" can clearly be seen in the SON season associated with very low O_3 column values. Its size and position correspond relatively well between the two datasets, but the minimum value of the Oslo-CTM2 is approximately 30 DU higher than the value obtained by MIPAS IMK-IAA. This difference

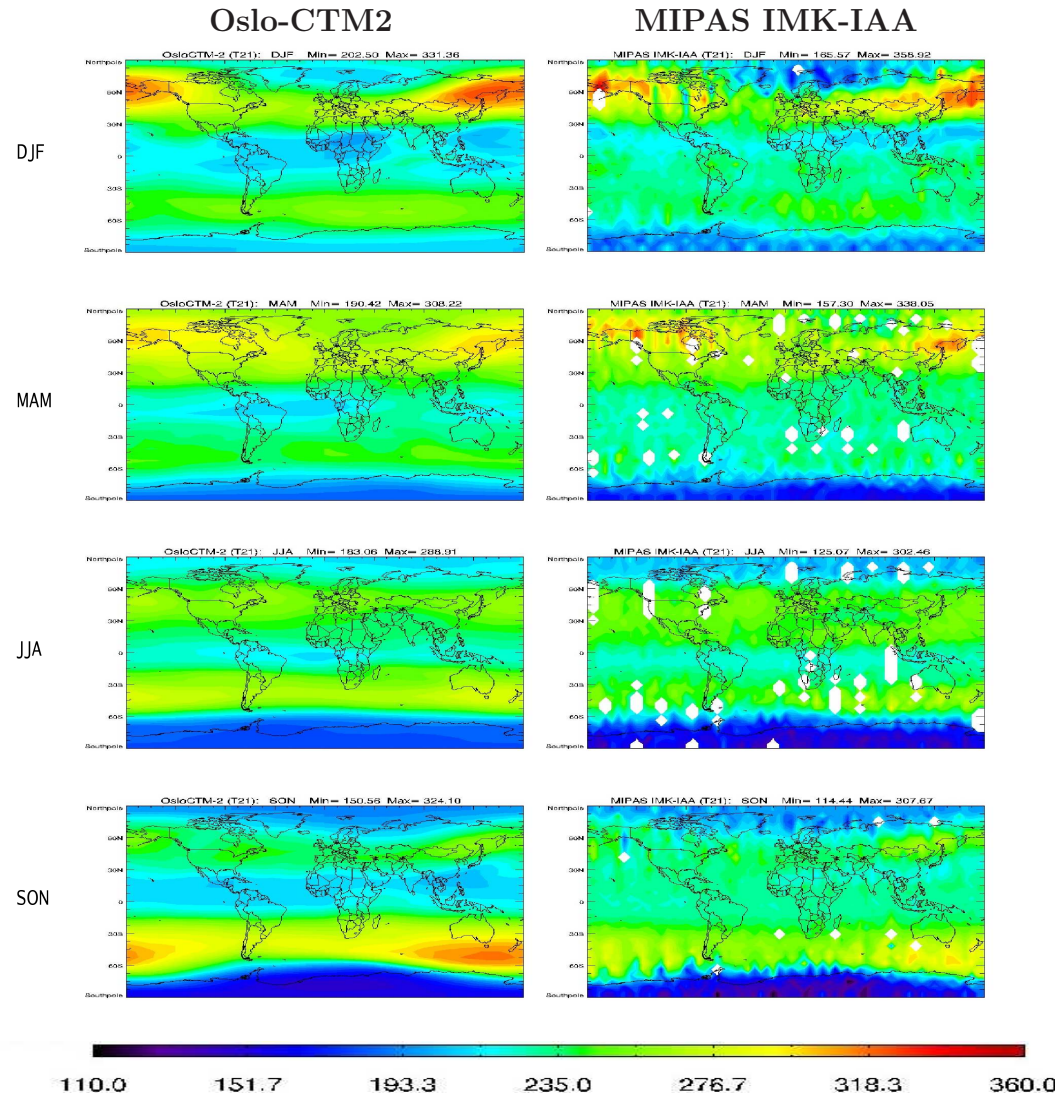

Figure 4.62: Seasonally averaged global distributions of stratospheric O_3 in DU from Oslo-CTM2 and MIPAS IMK-IAA.

is most probably associated with model resolution issues, and has to some degree been investigated by A. Søvde (UiO, MetOs).
The main differences between the two datasets are found in the tropical region where Oslo-CTM2 underestimates the VMR of O_3 compared to MIPAS IMK-IAA. This may be due to incomplete convection, mainly caused by coarse resolution, implying that the strong vertical advection associated with solar heating of the surface may not be sufficiently resolved in the model.

4.12.3 Antarctic "Ozone hole"

The O_3 depletion in the SH during springtime (SON) over Antarctica has traditionally received much scientific attention in the field of atmospheric chemistry since it first was reported by the British Antarctic Survey in 1985.

This depletion is chiefly caused by chemical reactions between O_3 and Cl or bromine species orginating from industrially manufactured gases. The extremely rapid depletion of O_3 can not be explained by transport processes or by gas phase reactions alone, accordingly there has to exist other mechanisms. These mechanisms are chemical reactions on the surface of cloud particles in the stratosphere, known as heterogeneous reactions (see Section 2.2). Thus, the Antarctic O_3 depletion appears to be connected with the extremely low prevailing temperatures associated with the "polar vortex", which in turn lead to condensation of water vapour and HNO_3 to form PSCs. Paul Crutzen, Mario Molina and Sherwood Rowland received the Nobel Prize in chemistry in 1995 for their work concerning the formation and decomposition of O_3.

The Secretariat of the WMO issues bulletins containing information on the state of the O_3 layer in Antarctica with roughly two week intervals from August to November. The information is based on data provided by WMO members which operate O_3 monitoring stations in the SH and satellites that observe global abundances. According to WMO Antarctic Ozone Bulletin for 2003 the city of Ushuaia, Argentina, located on the southern tip of South America were localized under the "Ozone hole" during four periods, with the first in early september, two times it occured in latter part of September and the final incident during the first week of October. Figure 4.63 shows that Oslo-CTM2 reproduces the size and position of the "Ozone hole" for all four periods.

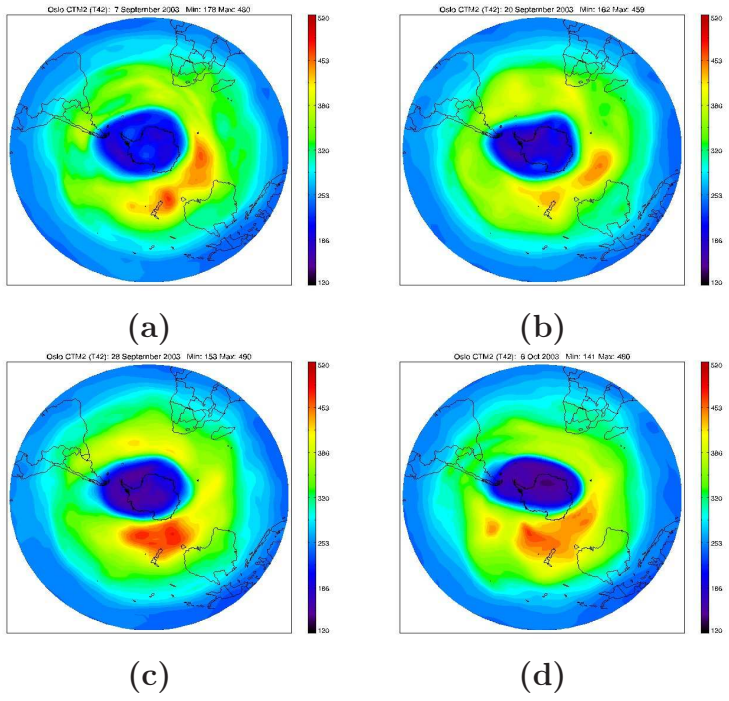

Figure 4.63: The "Ozone hole" covering the southern regions of South America on a) 7. Sept, b) 20. Sept, c) 28. Sept and d) 6. Oct 2003

4.13 Considerations about stratospheric chemistry

4.13.1 General reflections

The chemistry scheme used in Oslo-CTM2 is based upon QSSA. Temperatures are provided by the ECMWFs IFSL60 dataset and tropopause data from NCEP are used to separate between tropospheric and stratospheric modules (Section 3.1.1).
Stratospheric chemistry is complex. It involves a vast number of different molecules and their interaction with eachother. Radiation (UV and VIS) from the Sun is the primary energy source and is necessary to produce the species that are chemically active in the atmospheric region. STE and downward transport from the mesosphere, particularly during SPEs, are additional sources for species involved in the stratospheric chemistry. SPEs occurs when high-energy protons ejected from the Sun's surface during a solar flare get caught by the Earth's magnetic field (Figure 4.64).

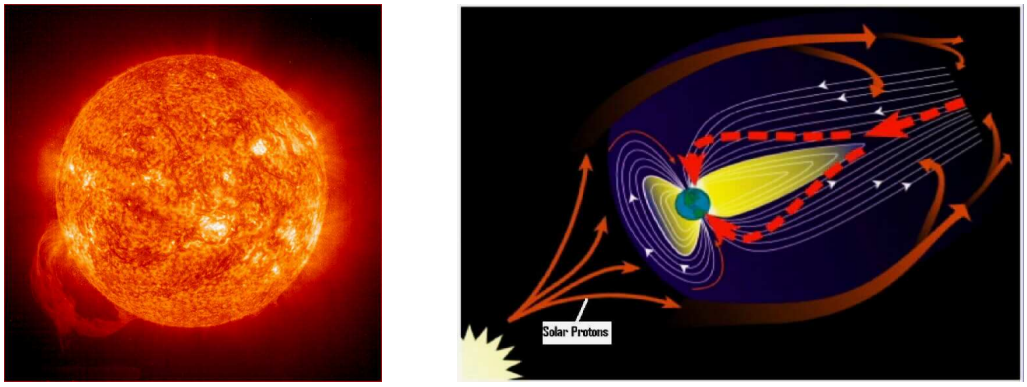

(a) **(b)**

Figure 4.64: a) Sun flares. b) Schematic overwiev of how solar protons are caught by the Earth's magnetic field (Source: NASA).

4.13.2 NO_y components

Figur 4.65 (upper panels) shows meridional distributions of total VMR in ppbv for all the NO_y family members (NO, NO_2, N_2O_5, HNO_3, HO_2NO_2 and $ClONO_2$) that are included in both Oslo-CTM2 (left panel) and MIPAS IMK-IAA (middel panel) datasets, and the absolute difference between them (right panel). The lower panels show the fractional distribution among the members for Oslo-CTM2 (left panels), MIPAS IMK-IAA (middel panels) and the difference between the two datasets (right panels).

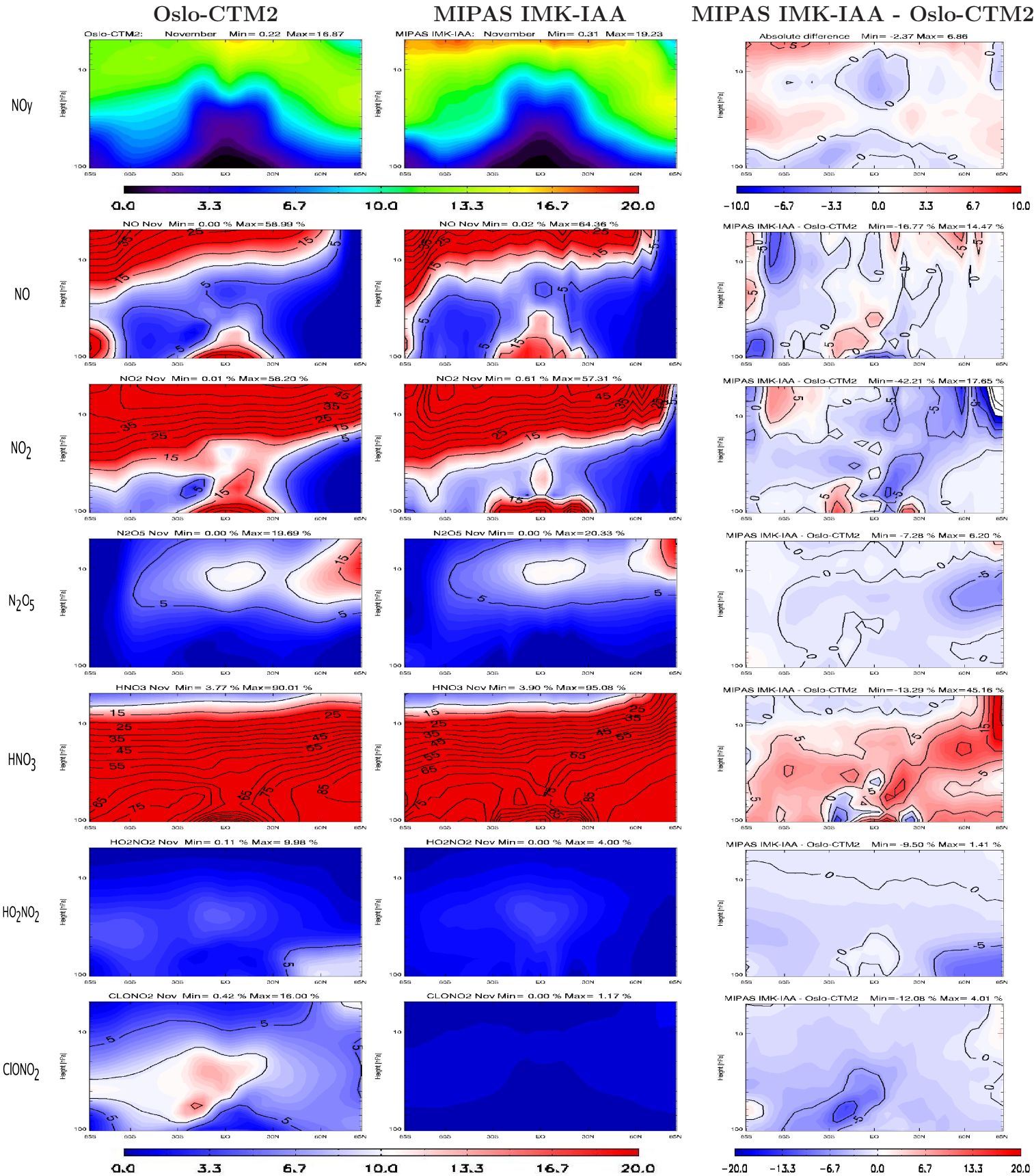

Figure 4.65: Total abundance (upper panels) of NO_y and fractional distribution among the nitrogen components included in this study (lower panels) from Oslo-CTM2 (left panels), MIPAS IMK-IAA (middel panels) and the difference between them (right panels). Data are from the month of November 2003.

Since the temporal resolution from the dataset provided by MIPAS IMK-IAA is relatively good for the month of November 2003 we have chosen to present this as a monthly mean for the stratosphere (vertical range from 100 to 5 hPa).
Both the meridional and the geographical distributions, presented in the previous sections, and the fractional distribution of NO_y (Figure 4.65) show that there in general is good agreement between the Oslo-CTM2 model and MIPAS IMK-IAA datasets. For the NO_y members we find the most pronounced absolute differences in the upper and middle stratospheric regions where Oslo-CTM2 underestimates the total abundance. From the meridional distributions of VMR for each component, presented in previous sections, we find that these discrepancies mainly are associated with increases in NO_x and HNO_3 abundances associated with the effects of SPEs.
During late October and early November 2003, three active solar regions produced major solar flares. This incident was described by Jackman et al. (2005a,b) as the fourth largest SPE observed in the past 40 years. Orsolini et al. (2005) reported HNO_3 enhancements and related them to particle precipitation caused by the intense solar storms. MIPAS IMK-IAA dataset consistes of an almost instant increase in the stratospheric HNO_3 abundance of about 1-2 ppbv. This was by López-Puertas et al. (2005) attributed to the acceleration of the tree-body reaction between NO_2 and OH due to increased production of stratospheric OH (Jackman and McPeters, 2004). A large second increase (1-5 ppbv) of the HNO_3 abundance occured later, and it was attributed to NO_x production in the mesosphere which was transported and converted to N_2O_5 and HNO_3 in the stratosphere (López-Puertas et al., 2005).
Since Oslo-CTM2 has a fixed upper boundary provided by climatological mixing ratios from the Oslo-2D model, the effects of SPEs are not taken into account in the model domain. Accordingly, many of the differences (especially for the NO_y members) in the meridional and geographical distributions between Oslo-CTM2 and MIPAS IMK-IAA datasets can be associated with SPEs. However, this phenomenon does not explain all the differences in fractional distributions of the NO_y families.

NO_x

In the upper stratosphere the NO_y discrepancies between the datasets are clearly linked to the increase in NO and NO_2 abundances, as shown in the meridional distribution figures in Section 4.6, caused by the SPEs that occurred during the SON season.
Additionally, we find in the meridional distributions from Section 4.6 that the model slightly underestimates NO_2 abundances in the SH polar lower stratospheric region. This low bias corresponds well with the overestimation of N_2O (Figure 4.13c) that may be caused by weak vertical transport and incomplete STE in Oslo-CTM2. Another effect that may be associated with the high N_2O bias in this region can be found in the fractional distribution

of NO in Figure 4.65. Since the abundance of N_2O are overestimated the oxidation with $O(^1D)$ will occur to often, accordingly too much NO will be produced.
In the middle stratosphere Oslo-CTM2 generally seems to overestimate the abundance of NO_x (Figure 4.13). However, since NO and NO_2 are very reactive the possible reasons for this overestimation remain unexplained.

N_2O_5

In Oslo-CTM2 the overestimation of N_2O_5 associated with the winter hemispheric maxima seems to be clearly connected with polar night conditions where the decomposition by photolysis is inactive. The maxima are situated at too high atmospheric levels for heterogenous and thermal decomposition reactions to have significant effects. The most probable explanation for this high bias in N_2O_5 is associated with the three-body reaction between NO_2 and NO_3, which act as a source for N_2O_5. From the temperature distributions we find that, during polar nights, the use of ECMWF's IFSL60 data produces a cold bias. Accordingly, due to this effects influence on the three-body reaction, the abundance of N_2O_5 will be overestimated.
From the fractional distribution figures we find that in NH's upper stratosphere the N_2O_5-fraction are somewhat overestimated in the model compared to the N_2O_5-fraction in the MIPAS IMK-IAA dataset. The amount and location seems to correspond well with the low bias of HNO_3. This strengthens the argumentation for the connection with the three-body reaction since NO_2 are occupied by N_2O_5 leading to underepresentation of HNO_3 in the NO_y fractional distribution.

HNO_3

The largest discrepancies between Oslo-CTM2 and MIPAS IMK-IAA datasets are found for the HNO_3 molecule. The main structures in the fields seem to be comparable, but Oslo-CTM2 consistently underestimates the abundance in both hemispheres for all seasons compared to MIPAS IMK-IAA especially on high and in midlatitudes (Figures 4.36 to 4.39). In addition to the major SPEs occuring in late October and early November 2003 MIPAS IMK-IAA also report of increased production of mesospheric NO_x during the 2002/2003 Artic winter in Funke et al. (2005a). However, they report that due to major midwinter warmings caused by high planetary wave activity the downward transport from mesosphere was rather inefficient.
A large part of the HNO_3 low bias in the model may be related to increased production of NO_x and HNO_3 caused by SPEs that are not resolved in the model domain. Both the instantanous increase in stratospheric abundance and the transport from mesospheric regions contribute to the differences found in the meridional distributions. However, this can not fully explain the discrepancies (up to $\approx$9 ppbv in JJA) found in Section 4.8, and accordingly there have to be additional processes involved.

HNO_3 is a molecule with complex sources and sinks. It is involved in heterougenous chemistry in the UTLS regions, while in other parts of the stratosphere oxidation by OH and photolysis dominate the total HNO_3 budget. This makes it increasingly difficult to conclude when trying to explain reasons for the discrepancies observed between the datasets.
However, from the difference panels in Figure 4.65 we observe a strong correlation between the fractional distribution of HNO_3 and NO_2 in the lower stratosphere of the tropics and in the NH's upper stratospheric polar regions. Accordingly, the generally low bias in Oslo-CTM2 may be associated with the oxidation process of NO_2 by OH being to slow resulting in insufficient production of HNO_3.
Another finding from the fractional distributions of HO_2NO_2 and HNO_3 is that the discrepancies for these components, in NH's lower stratosphere polar regions, seems to correspond remarkably well both in size and location. Hence, some of the HNO_3 underestimation by Oslo-CTM2 may probably be associated with an amount of HO_2NO_2 that "occupies" NO_2 abundances in this region of the model domain.

HO_2NO_2

For HO_2NO_2, the largest discrepancies between the two datasets are found in the lower stratospheric polar regions, where Oslo-CTM2 overestimates the abundance compared to MIPAS IMK-IAA. The resent update of Oslo-CTM2 chemical kinetics and photochemistry shows significant improvements for this component in the region where we find the most pronounced overestimations (Figures 4.66 and 4.41 to 4.44). The differences in abundances for HO_2NO_2

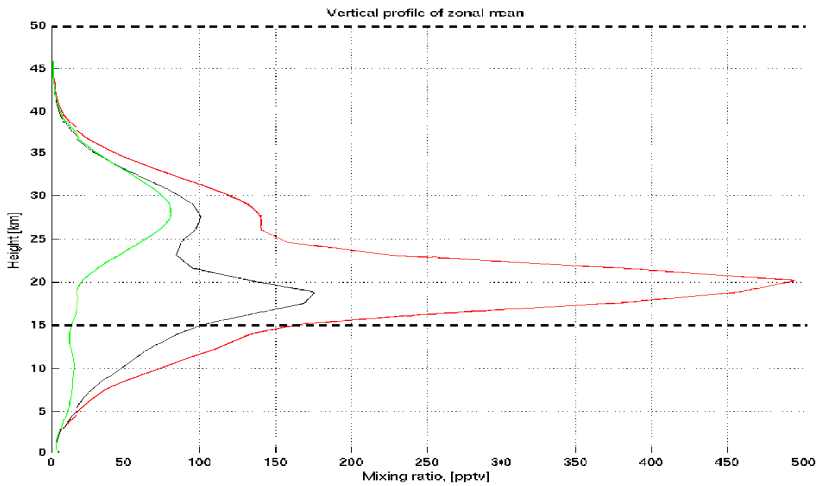

Figure 4.66: The improvement for HO_2NO_2 by updating J-values according to JPLs Publication No. 06-2. The red solid line shows abundance before, while the green line shows the abundance after the update. The dashed horizontal black lines shows approximately the vertical range used in the meridional distributions in this study. (Source: B.Rognerud).

in this study are most likely associated with incomplete descriptions of the photolytic reaction rates, especially in the IR region of the electromagnetic spectrum. Consequently, the abundances of NO_2 and HO_2 are expected to be underestimated. We recognize this feature in the relative difference figure in meridional distribution for NO_2 (Figure 4.29d). Because NO_2 is highly reactive with other species, the increase in abundance caused by the overestimation of HO_2NO_2 are not pronounced enought to be observed in the NO_2 absolute difference (Figure 4.29c).

$ClONO_2$

The meridional distributions of $ClONO_2$ show that Oslo-CTM2 consistently overestimates the abundance of this component, except in lower stratospheric winter hemisphere regions associated with the polar night. Here we find that Oslo-CTM2 underestimates $ClONO_2$. The three-body reaction between ClO and NO_2 is the only chemical source for $ClONO_2$, while the sinks are more complex involving photolysis, bimolecular reaction with Cl and heterogenous reactions with HCl and H_2O. For the SON season the models general high biases $ClONO_2$ field concures relatively well with the overestimations of both ClO and NO_2. A possible explanation for the overestimation is that the $ClONO_2$'s source reaction rate is too high due to the high abundances of ClO and NO_2. Another plausible explanation is linked to the photolysis loss reaction for decomposition of $ClONO_2$. Since O_3 and $ClONO_2$ absorb UV radiation in the approximately same spectral region and O_3 is underestimated by the model in the upper stratospheric regions (as shown in Figure 4.60c), the reaction rate for photolytic decomposition of $ClONO_2$ becomes to high. As a result of this the photolysis decomposes too much $ClONO_2$ and consequently its VMR is high biased compared to MIPAS IMK-IAA. However, the underestimation in the lower stratospheric polar winter hemisphere is most probably due to incomplete processing in the heterogenous chemistry. Heterogenous chemistry is important for all chlorine species especially where the "polar vortex" contributes to create temperatures cold enough for PSCs formation. Linking this phenomenon to heterougenous chemistry is plausible since the underestimation is stronger in the SH winter (JJA) than in the NH winter (DJF) season. Due to hemispheric differences, the SH's "polar vortex" is more consistent and stronger than in the NH. Consequently the heterogenous chemistry has a stronger impact in the SH polar regions.

4.13.3 *ClO*

From the meridional distributions in Section 4.10 we find that in general the regions dominated by heterogenous chemistry and low abundances (UTLS) are reproducedes in a satisfactory manner by Oslo-CTM2 (Figures 4.47 to 4.50) compared to the rerival by MIPAS IMK-IAA. However, in the upper stratosphere we find that Oslo-CTM2 consistently underestimates the abundance, especially in tropical regions. Since ClO is involved in various chemical

processes the reasons for the observed low bias are difficult to identify, but since ClO reacts with both NO and NO_2 some of it may be associated with the increase in these componds due to SPEs. The low ClO bias in this atmospheric region also corresponds well with the cold bias shown in Figures 4.21 to 4.24, accordingly the three-body reaction between ClO and NO_2 are to fast and ClO are underestimated in the model. To further complicate the matter the retrival errors for this component seem to be relatively high (Table 4.4) compared to other compounds retrived by MIPAS IMK-IAA.

4.13.4 O_3

The VMR meridional distribution shows a generally good agreement between Oslo-CTM2 and MIPAS IMK-IAA regarding the stratospheric O_3 abundance. The structure in the fields are comparable, and the maxima seems to be in the approximately same location. We find that differences between size, shape and location of the field in the vicinity of the maxima values vary slightly. However, the relative differences in these regions are less than 10 %, which is within the range of accuracy for the satellite retrival.
The main difference between the model and the satellite retrived VMR fields is in the upper part of the stratosphere, especially on the summer hemisphere. In this region the model underestimates the abundance of O_3 compared to MIPAS IMK-IAA. However, the update on Oslo-CTM2 chemical kinetics and photochemistry shows significant improvements for O_3 in this region (Figure 4.67). This indicates that at least some of the discrepancies between the

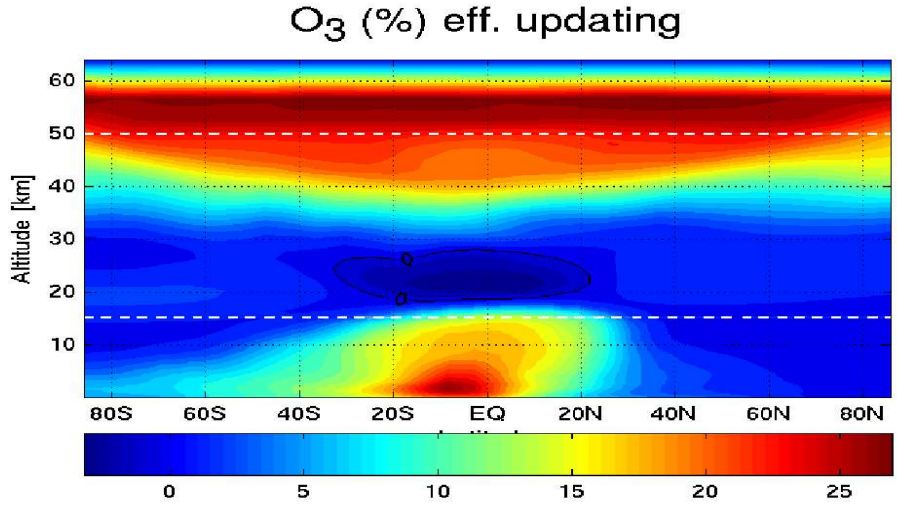

Figure 4.67: The improvement for O_3 by updating J-values according to JPLs Publication No. 06-2. The dashed horizontal white lines shows the approximate vertical range used in the meridional distributions in this study. (Source: B.Rognerud).

datasets are related to incomplete description of the photochemistry in the model version of Oslo-CTM2 used in this work.

Chapter 5

Summary and conclusion

Comparisons of abundances of various atmospheric components between Oslo-CTM2 model and MIPAS IMK-IAA satellite retrived datasets have been reported in this study. The atmospheric region of interest has been the stratosphere and the very lowest part of the mesosphere. Results have mostly been presented as seasonal means, and the period of interest stretches from December 2002 through November 2003. The main objectives have been validation of the Oslo-CTM2 chemical transport model in addition to investigating the quality of satellite retrived products provided by MIPAS IMK-IAA.

Overall, this study shows that the model and the satellite datasets describe the stratospheric chemical state rather consistently. The general structures in the distribution of many compounds are found to be reproduced relatively well by the model compared to abundances retrived and reanalysed by ESA's MIPAS instrument and IMK-IAA. The fact that a model based on first principles and an observational dataset agree to a large extent places confidence in current scientific knowledge of the distribution of trace species and in current understanding of the processes governing the chemical composition of the stratosphere.

Obviously, because of the complexity of the methods and the task, there are differences between the two datasets. However, this study has shown that the discrepancies generally are small and to a certain extent can be connected to differences between temporal and spatial resolution of the datasets.

The MIPAS IMK-IAA seasonal means are based on all the vertical soundings done during each season. The amount of data is influenced by the prioritizing of periods with most scientific value (for example the major SPEs that ocurred in October and November 2003) done by scientists at IMK and IAA. However, in the Oslo-CTM2 seasonal means are based upon monthly means which include the diurnal cycle. This difference in sampling of data makes the MIPAS IMK-IAA dataset biased compared to the Oslo-CTM2 dataset. In some cases it therefore becomes difficult to fully explain the observed discrepancies. To decrease the uncertainty, and most probably some of the discrepancies, between the two datasets regarding this temporal and spatial

bias an improvement would be to calculate the Oslo-CTM2 seasonal means based on only the days with good data coverage provided by MIPAS IMK-IAA. This has not been done in this thesis and can only be done by re-running the Oslo-CTM2 and store appropriate model results.

From the meridional distribution figures it seems that the discrepancies between Oslo-CTM2 and MIPAS IMK-IAA for the NO_y family members, first and foremost, may be connected to the distribution within the family. This feature suggests that some of the discrepancies are due to inaccuracies in the description of chemical processes in the model domain. In more recent experiments (not shown in this thesis) with the Oslo-CTM2 model, with updated chemical kinetics, some of the problems that have been pointed to in this study have, at least partly, been solved.

The comparisons between Oslo-CTM2 and MIPAS IMK-IAA further points to some inaccuracies in the advection of species in the Oslo-CTM2 in the stratosphere. Apparently the ECMWF IFSL60 data used in the model results in a meridional circulation which seems to be too weak (e.g. underestimates vertical gradients for abundances) in the lower stratosphere and too strong (e.g. overestimates vertical gradients abundances) in the upper stratosphere to some extent.

Finally, the MIPAS IMK-IAA dataset show evidence of effects from SPEs in the mesosphere and middle stratsophere. These events are not described in Oslo-CTM2, yielding large discrepancies between the two products during parts of the period of interest.

Appendix A

Chemical Species in Oslo-CTM2

All components included in the Oslo CTM2 are listed below, with molecular weight (M_w), CTM2 number (Nr), whether they are transported (T=Y) or not (T=N) along with the chemical domain of interest (C): T is troposphere only, S is stratosphere only and B is both.

Name	M_w	Nr.	T/C	Remarks
O_3	48.0	01	Y/B	
NOX	30.0	02	Y/T	NO+NO_2+NO_3+2N_2O_5 +HO_2NO_2+PAN
NOZ	62.0	03	N/T	NO_3+N_2O_5
HNO_3	63.0	04	Y/B	
PANx	121.0	05	Y/T	PAN+CH_3COO_2
CO	28.0	06	Y/B	
C_2H_4	28.0	07	Y/T	
C_2H_6	30.0	08	Y/T	
C_3H_6	42.0	09	Y/T	
C_4H_{10}	58.0	10	Y/T	
C_6H_{14}	86.0	11	Y/T	
C_6HXR	106.0	12	Y/T	m-xylene
CH_2O	30.0	13	Y/B	
CH_3CHO	44.0	14	Y/T	
H_2O_2	34.0	15	Y/B	
CH_3O_2H	48.0	16	Y/B	
HO_2NO_2	79.0	17	Y/B	
CH_3COY	86.0	18	Y/T	$CH_3COCOCH_3$
CH_3COX	64.0	19	Y/T	$CH_3COC_2H_5$
Isoprene	68.0	20	Y/T	C_5H_8
HO_2	33.0	21	Y/B	
CH_3O_2	47.0	22	N/B	
$C_2H_5O_2$	61.0	23	N/T	
$C_4H_9O_2$	89.0	24	N/T	
$C_6H_{13}O_2$	117.0	25	N/T	
CH_2O_2OH	63.0	26	N/T	
CH_3COB	103.0	27	N/T	$CH_3COCH(O_2)CH_3$
CH_3XX	91.0	28	N/T	$CH_3CH(O_2)CH_2OH$

Name	M_w	Nr.	T/C	Remarks
AR1	100.0	29	N/T	first RO_2 radical from the reaction of m-xylene with OH
AR2	100.0	30	N/T	a C-5 carbonyl compound formed by reaction of AR1 with NO
AR3	100.0	31	N/T	a C-5 RO_2 radical formed by reaction of AR2 with OH
ISOR1	100.0	32	N/T	first RO_2 radical by the reaction of isoprene with OH
ISOK	100.0	33	N/T	methylvinylketone (MVK) + methacrolein (MACR)
ISOR2	100.0	34	N/T	RO_2 radical formed from MVK + OH or MACR+OH
HCOHCO	61.0	35	Y/T	
RCOHCO	74.0	36	Y/T	
CH_3X	75.0	37	Y/T	CH3COO2
O(3P)	16.0	38	N/B	
O(1D)	16.0	39	N/B	
OH	17.0	40	N/B	
NO_3	62.0	41	Y/B	
N_2O_5	74.0	42	Y/B	
NO	30.0	43	Y/B	
NO_2	46.0	44	Y/B	
O_3NO	48.0	45	N/T	O3 minus NO
CH_4	16.0	46	Y/B	
DMS	62.0	47	N/T	dimethyl sulphide, $(CH_3)_2S$
C_3H_8	44.0	48	Y/T	
$C_3H_7O_2$	75.0	49	Y/T	
Acetone	58.0	50	Y/T	$CH_3C(O)CH_3$
CH_3COD	89.0	51	Y/T	$CH_3COCH_2(O_2)$
MCF	170.0	101	Y/S	CH_3CCl_3
HCFC-22	86.0	102	Y/S	CF_2HCl
CFC-11	137.0	103	Y/S	$CFCl_3$
CFC-12	121.0	104	Y/S	CF_2Cl_2
CCl_4	154.0	105	Y/S	
CH_3Cl	50.0	106	Y/S	
N_2O	44.0	107	Y/S	
Clx	35.0	108	Y/S	$Cl+ClO+OHCl+ClONO_2+2Cl_2$ $OClO+BrCl+ClOO+2Cl_2O_2$
NOx_str	30.0	109	Y/S	$NO+NO_2+NO_3+2N_2O_5$ $+HO_2NO_2+ClONO_2+BrONO_2$
SO	48.0	110	Y/S	$O_3+O(1D)+O(3P)-NO-Cl-Br$
HCl	36.0	111	Y/S	
Cly	35.0	112	Y/S	Clx+HCl
H_2	2.0	113	N/S	
H_2O	18.0	114	N/S	
SH	1.0	115	Y/S	$H+OH+HO_2+2H_2O_2$
CH_3Br	95.0	116	Y/S	

Name	M_w	Nr.	T/C	Remarks
H-1211	165.0	117	Y/S	CF_2ClBr
H-1301	149.0	118	Y/S	CF_3Br; 1 Br-atom
Bry	80.0	119	Y/S	Br+BrO+$BrONO_2$+OHBr +HBr+$2Br_2$+BrCl
H-2402	260.0	120	N/S	$C_2F_4Br_2$
CFC-113	187.0	121	Y/S	CCl_2FCClF_2
CFC-114	171.0	122	Y/S	$CClF_2CClF_2$
CFC-115	154.0	123	Y/S	$CClF_2CF_3$
HNO_3s	63.0	124	Y/S	solid phase (het. chemistry)
H_2Os	18.0	125	N/S	solid phase (het. chemistry)
HCFC-123	153.0	127	Y/S	CF_3CHCl_2
HCFC-141	117.0	128	Y/S	$CFCl_2CH_3$
HCFC-142	100.0	129	Y/S	CF_2ClCH_3
H	1.0	130	N/S	
Cl	35.0	132	N/S	
ClO	51.0	133	N/S	
OHCl	52.0	134	Y/S	
$ClONO_2$	97.0	135	Y/S	
Cl_2	71.0	136	Y/S	
OClO	67.0	137	Y/S	
Br	80.0	138	N/S	
BrO	96.0	139	N/S	
HBr	81.0	140	Y/S	
$BrONO_2$	142.0	141	Y/S	
OHBr	97.0	142	Y/S	
Br_2	160.0	143	Y/S	
ClOO	67.0	144	Y/S	
Cl_2O_2	103.0	145	Y/S	
BrCl	115.0	146	Y/S	
NOy_str	30.0	147	Y/S	NOx_str+HNO_3+HNO_3s

Appendix B

Reactions in Oslo-CTM2

Oslo-CTM2 takes into account all reactions listed on the following pages (i.e. both tropospheric and stratospheric chemistry). Reactions in bold type are included in both the tropospheric and the stratospheric modules.

Photolysis reactions

Tropospheric chemistry module

$O_3 + h\nu \rightarrow O_2 + O(3P)$
$O_3 + h\nu \rightarrow O_2 + O(1D)$
$NO_2 + h\nu \rightarrow NO + O(3P)$
$H_2O_2 + h\nu \rightarrow 2OH$
$HNO_3 + h\nu \rightarrow NO_2 + OH$
$CH_2O + h\nu \rightarrow H + HCO$
$CH_2O + h\nu \rightarrow H_2 + CO$
$CH_3CHO + h\nu \rightarrow CHO + CH_3$
$CH_3COCH_2CH_3 + h\nu \rightarrow CH_3CO + C_2H_5O_2$
$CH_3COCOCH_3 + h\nu \rightarrow 2\ CH_3CO$
$HCOHCO + h\nu \rightarrow CO + CH_2O$
$CH_3COHCO + h\nu \rightarrow CO + CH_3CHO$
$NO_3 + h\nu \rightarrow NO_2 + O(3P)$
$NO_2NO_3 + h\nu \rightarrow NO_2 + NO_3$
$CH_3O_2H + h\nu \rightarrow OH + CH_3O$
$HO_2NO_2 + h\nu \rightarrow NO_2 + HO_2$

Stratospheric chemistry module

$O_2 + h\nu \rightarrow O + O$
$O_3 + h\nu \rightarrow O_2 + O(3P)$
$O_3 + h\nu \rightarrow O_2 + O(1D)$
$H_2O + h\nu \rightarrow OH + h\nu$
$H_2O_2 + h\nu \rightarrow OH + OH$
$HNO_3 + h\nu \rightarrow NO_2 + OH$
$HO_2NO_2 + h\nu \rightarrow NO_2 + HO_2$
$N_2O + h\nu \rightarrow N_2 + O$
$NO_2 + h\nu \rightarrow NO + O(3P)$
$NO_3 + h\nu \rightarrow NO + O_2$
$NO_3 + h\nu \rightarrow NO_2 + O(3P)$
$N_2O_5 + h\nu \rightarrow NO_2 + NO_3$
$CH_2O + h\nu \rightarrow H + HCO$

$CH_2O + h\nu \rightarrow H_2 + CO$
$CF_2Cl_2 + h\nu \rightarrow Clx$
$CFCl_3 + h\nu \rightarrow Clx$
$CCl_4 + h\nu \rightarrow Clx$
$CHF_2Cl + h\nu \rightarrow Clx$
$CH_3Cl + h\nu \rightarrow Clx$
$ClONO_2 + h\nu \rightarrow Cl + NO_3$
$OHCl + h\nu \rightarrow OH + Cl$
$\mathbf{CH_3O_2H + h\nu \rightarrow CH_3O + OH}$
$HCl + h\nu \rightarrow H + Cl$
$ClO + h\nu \rightarrow Cl + O$
$CH_3CCl_3 + h\nu \rightarrow Clx$
$OClO + h\nu \rightarrow O + ClO$
$Cl_2 + h\nu \rightarrow Cl + Cl$
$BrO + h\nu \rightarrow Br + O$
$BrONO_2 + h\nu \rightarrow BrO + NO_2$
$Br_2 + h\nu \rightarrow Br + Br$
$HBr + h\nu \rightarrow H + Br$
$OHBr + h\nu \rightarrow OH + Br$
$CH_3Br + h\nu \rightarrow Bry$
$CF_2ClBr + h\nu \rightarrow Bry$
$CF_3Br + h\nu \rightarrow Bry$
$C_2F_3Cl_3 + h\nu \rightarrow Clx$
$C_2F_4Cl_2 + h\nu \rightarrow Clx$
$C_2F_5Cl + h\nu \rightarrow Clx$
$Cl_2O_2 + h\nu \rightarrow ClOO + Cl$
$CHCl_2CF_3 + h\nu \rightarrow Clx$
$CH_3CCl_2F + h\nu \rightarrow Clx$
$CH_3CClF_2 + h\nu \rightarrow Clx$
$NO + h\nu \rightarrow N + O$
$BrCl + h\nu \rightarrow Br + Cl$

Chemical reactions in the tropospheric module

$O(1D) + O_2 \rightarrow O(3P) + O_2$
$O(1D) + N_2 \rightarrow O(3P) + N_2$
$O(1D) + H_2O \rightarrow 2OH$
$O(3P) + O_2 + M \rightarrow O_3 + M$
$O(3P) + NO_2 \rightarrow NO + O_2$
$O_3 + NO \rightarrow NO_2 + O_2$
$O_3 + NO_2 \rightarrow NO_3 + O_2$
$O_3 + OH \rightarrow O_2 + HO_2$
$O_3 + HO_2 \rightarrow OH + 2O_2$
$HO_2 + HO_2 \rightarrow H_2O_2 + O_2$
$HO_2 + HO_2 + M \rightarrow H_2O_2 + O_2 + M$
$OH + H_2O_2 \rightarrow H_2O + HO_2$
$OH + NO_2 + M \rightarrow HNO_3 + M$
$NO + HO_2 \rightarrow NO_2 + OH$
$NO_2 + NO_3 \rightarrow NO + NO_2 + O_2$
$NO_2 + NO_3 + M \rightarrow N_2O_5 + M$
$N_2O_5 + M \rightarrow NO_2 + NO_3 + M$
$N_2O_5 + aq(aerosol) \rightarrow 2HNO_3(aq)$
$NO_2 + HO_2 + M \rightarrow HO_2NO_2 + M$
$HO_2NO_2 + M \rightarrow HO_2 + NO_2 + M$

$NO + NO_3 \rightarrow 2NO_2$
$OH + HO_2 \rightarrow H_2O + O_2$
$OH + HNO_3 \rightarrow NO_3 + H_2O$
$OH + HO_2NO_2 \rightarrow NO_2 + O_2 + HO_2$
$OH + CO + O_2 \rightarrow HO_2 + CO_2$
$OH + CH_4 \rightarrow CH_3 + H_2O$
$OH + C_2H_4 \rightarrow CH_3 + CH_2O$
$O_3 + C_2H_4 \rightarrow HCHO + 0.12HO_2 + 0.44CO$
$OH + C_2H_6 \rightarrow C_2H_5O_2 + H_2O$
$NO_3 + C_2H_6 \rightarrow C_2H_5O_2 + HNO_3$
$OH + C_3H_6 \rightarrow CH_3CH(O_2)CH_2OH$
$O_3 + C_3H_6 \rightarrow 0.25HO_2$
$+ 0.5(HCHO + CH_3CHO) + 0.15OH$
$+ 0.03CH_3O + 0.31CH_3 + 0.07CH_4 + 0.4CO$
$OH + C_3H8 \rightarrow C_3H_7O_2 + H_2O$
$OH + C_4H10 \rightarrow C_4H_9O_2 + H_2O$
$OH + C_6H_{14} \rightarrow C_6H_{13}O_2 + H_2O$
$OH + \text{m-Xylene} \rightarrow 0.6AR1$
$OH + \text{Isoprene} \rightarrow ISOR1$
$CH_3 + O_2 + M \rightarrow CH_3O_2 + M$
$CH_3O_2 + CH_3O_2 \rightarrow 0.4(2CH_3O + O_2)$
$\rightarrow 0.6CH_2O$
$CH_3O + O_2 \rightarrow HO_2 + CH_2O$
$OH + CH_2O \rightarrow CHO + H_2O$
$CHO + O_2 \rightarrow HO_2 + CO$
$CH_3O_2 + HO_2 \rightarrow 0.5CH_3O_2H + O_2$
$OH + CH_3O_2H \rightarrow CH_3O_2 + H_2O$
$OH + CH_3O_2H \rightarrow CH_2O + OH + H_2O$
$OH + AR2 \rightarrow AR3$
$OH + ISOK \rightarrow ISOR2$
$OH + CH_3COCH_2CH_3 \rightarrow CH_3COCH(O_2)CH_3$
$OH + HCOHCO \rightarrow fa_{45}\ (CHO + CO)$
$\rightarrow fb_{45}\ (CH_3CO)$
$\rightarrow fc_{45}\ (2CO + HO_2)$
$OH + RCOHCO \rightarrow CH_3CO + CO$
$NO + CH_3O_2 \rightarrow fa_{48}\ (NO_2 + CH_3O)$
$NO + C_2H_5O_2 \rightarrow fa_{49}\ (NO_2 + (1\text{-}fb_{49})(CH_2O + CH_3)$
$+ fb_{49}\ (HO_2 + CH_3CHO))$
$NO + C_3H_7O_2 \rightarrow fa_{50}(NO_2$
$+ (1\text{-}fb_{50}(CH_3CHO + CH_3O_2)$
$+ fb_{50}(HO_2 + CH_3COCH_3))$
$NO + C_4H_9O_2 \rightarrow$
$fa_{51}\ (NO_2 + (1 - fb_{51}\ (CH_3CHO + C_2H_5O_2)$
$+ fb_{51}\ (HO_2 + CH_3COCH_2CH_3)\ )$
$NO + C_6H_{13}O_2 \rightarrow fa_{52}\ (NO_2 + C_4H_9O_2 + CH_3CHO)$
$NO + AR1 \rightarrow NO_2 + HO_2 + AR2 + RCOHCO$
$NO + AR3 \rightarrow NO_2 + HO_2 + HCOHCO + RCOHCO$
$NO + ISOR1 \rightarrow fa_{55}\ (NO_2 + HO_2 + ISOK + CH_2O)$
$1.5\ NO + ISOR2 \rightarrow$
$1.5NO_2 + 0.67HO_2 + 0.43CH_2O$
$+ 0.67RCOHCO + 0.33CH_3CO + 0.33CH_3CHO$
$NO + CH3COCH(O_2)CH_3 \rightarrow$
$fa_{57}\ (NO_2 + HO_2 + CH_3COCOCH_3)$
$NO + CH_3COCH_2(O_2) \rightarrow NO_2 + HO_2 + CH_3COCHO$
$NO + CH_3CH(O_2)CH_2OH \rightarrow$

$NO_2 + CH_2O + CH_3CHO + HO_2$
$OH + CH_3CHO \rightarrow CH_3CO + H_2O$
$NO_3 + CH_3CHO \rightarrow HNO_3 + CH_3CO$
$CH_3CO + O_2 \rightarrow CH_3COO_2$
$CH_3COO_2 + NO \rightarrow CH_3 + NO_2 + CO_2$
$CH_3COO_2 + NO_2 + M \rightarrow PAN + M$
$PAN + M \rightarrow CH_3COO_2 + NO_2 + M$
$OH + PAN \rightarrow CH_2O + NO_2 + CO_2 + H_2O$
$CH_3COO_2 + CH_3O_2 \rightarrow CH_3O + CH_3 + CO_2 + O_2$
$CH_3COO_2 + CH_3O_2 \rightarrow CH_2O + CH_3COOH + O_2$
$CH_3O_2 + C_2H_5O_2 \rightarrow 0.5(CH_3O +$
$(1\text{-}fb_{68})(CH_2O + CH_3) + fb_{68}\ (HO_2 + CH_3CHO))$
$+ 0.25(CH_2O + CH_3CHO)$
$CH_3O_2 + C_3H_7O_2 \rightarrow 0.5(CH_3O + (1\text{-}fb_{69})$
$(CH_3CHO + CH_3O_2) + fb_{69}(HO_2 + CH_3COCH_3))$
$+ 0.25(CH_2O + CH_3COCH_3)$
$CH_3O_2 + C_4H_9O_2 \rightarrow 0.5(CH_3O +$
$(1\text{-}fb_{70})(CH_3CHO + C_2H_5O_2) + fb_{70}\ (HO_2$
$+ CH_3COCH_2CH_3)) + 0.25(CH_2O + CH_3COCH_2CH_3)$
$CH_3O_2 + C_6H_{13}O_2 \rightarrow CH_3O + CH_3CHO + C_4H_9O_2$
$CH_3O_2 + CH_3COCH_2(O_2) \rightarrow$
$CH_3O + CH_3COCHO + CH_2O + HO_2$
$CH_3O_2 + CH_3CH(O_2)CH_2OH \rightarrow$
$CH_3O + CH_3CHO + CH_2O + HO_2$
$CH_3O_2 + CH_3COCH(O_2)CH_3 \rightarrow$
$CH_3O + HO_2 + CH_3COCOCH_3$
$CH_3O_2 + ISOR1 \rightarrow CH_2O + CH_3O + HO_2 + ISOK$
$CH_3O_2 + ISOR2 \rightarrow RCOHCO + CH_3O + HO_2$
$HO_2 + C_2H_5O_2 \rightarrow CH_3O_2H$
$HO_2 + C_4H_7O_2 \rightarrow CH_3O_2H$
$HO_2 + C_4H_9O_2 \rightarrow CH_3O_2H$
$HO_2 + C_6H_{13}O_2 \rightarrow CH_3O_2H$
$HO_2 + CH_3COCH_2(O_2) \rightarrow CH_3O_2H$
$HO_2 + CH_3CH(O_2)CH_2OH \rightarrow CH_3O_2H$
$HO_2 + CH_3COCH(O_2)CH_3 \rightarrow CH_3O_2H$
$HO_2 + ISOR1 \rightarrow CH_3O_2H$
$HO_2 + ISOR2 \rightarrow CH_3O_2H$

Chemical reactions in the stratospheric module

Ox Reactions
$\mathbf{O(3P) + O_2 + M \rightarrow O_3 + M}$
$O(3P) + O_3 \rightarrow O_2 + O_2$

O(1D) Reactions
$O(1D) + N_2O \rightarrow N_2 + O_2$
$O(1D) + N_2O \rightarrow NO + NO$
$\mathbf{O(1D) + H_2O \rightarrow OH + OH}$
$O(1D) + CH_4 \rightarrow OH + CH_3$
$O(1D) + CH_4 \rightarrow CH_2O + H_2$
$O(1D) + H_2 \rightarrow OH + H$
$\mathbf{O(1D) + N_2 \rightarrow O(3P) + N_2}$
$\mathbf{O(1D) + O_2 \rightarrow O(3P) + O_2}$
$O(1D) + HCl \rightarrow Cl + OH$

$O(1D) + CFCl_3 \rightarrow Clx$
$O(1D) + CF_2Cl_2 \rightarrow Clx$
$O(1D) + CHCl_2CF_3 \rightarrow Clx$
$O(1D) + CH_3CCl_2F \rightarrow Clx$
$O(1D) + CH_3CClF_2 \rightarrow Clx$

HOx Reactions
$H + O_2 + M \rightarrow HO_2 + M$
$H + O_3 \rightarrow OH + O_2$
$O(3P) + OH \rightarrow O_2 + H$
$O(3P) + HO_2 \rightarrow OH + O_2$
$\mathbf{OH + HO_2 \rightarrow H_2O + O_2}$
$\mathbf{OH + O_3 \rightarrow HO_2 + O_2}$
$OH + OH \rightarrow H_2O + O(3P)$
$OH + H_2O_2 \rightarrow H_2O + HO_2$
$OH + H_2 \rightarrow H_2O + H$
$\mathbf{HO_2 + HO_2 \rightarrow H_2O_2 + O_2}$
$\mathbf{HO_2 + HO_2 + M \rightarrow H_2O_2 + O_2 + M}$
$\mathbf{HO_2 + O_3 \rightarrow OH + 2O_2}$

NOx Reactions
$N + O_2 \rightarrow NO + O(3P)$
$N + NO \rightarrow N_2 + O(3P)$
$\mathbf{O(3P) + NO_2 \rightarrow NO + O_2}$
$O(3P) + NO_2 + M \rightarrow NO_3 + M$
$\mathbf{O_3 + NO \rightarrow NO_2 + O_2}$
$\mathbf{NO + HO_2 \rightarrow NO_2 + OH}$
$\mathbf{NO + NO_3 \rightarrow 2NO_2}$
$\mathbf{OH + NO_2 + M \rightarrow HNO_3 + M}$
$\mathbf{OH + HNO_3 \rightarrow H_2O + NO_3}$
$\mathbf{OH + HO_2NO_2 \rightarrow O_2 + H_2O + NO_2}$
$\mathbf{NO_2 + HO_2 + M \rightarrow HO_2NO_2 + M}$
$\mathbf{O_3 + NO_2 \rightarrow NO_3 + O_2}$
$\mathbf{NO_2 + NO_3 + M \rightarrow N_2O_5 + M}$
$\mathbf{NO_2 + NO_3 \rightarrow NO + NO_2 + O_2}$

Hydrocarbon Reactions
$\mathbf{OH + CO \rightarrow CO_2 + H}$
$\mathbf{OH + CH_4 \rightarrow CH_3 + H_2O}$
$\mathbf{OH + CH_2O \rightarrow H_2O + HCO}$
$\mathbf{OH + CH_3O_2H \rightarrow CH_3O_2 + H_2O}$
$O(3P) + CH_2O \rightarrow HCO + OH$
$\mathbf{CH_3O_2 + NO \rightarrow CH_3O + NO_2}$
$\mathbf{HO_2 + CH_3O_2 \rightarrow CH_3OOH + O_2}$
ClOx Reactions
$Cl + O_3 \rightarrow ClO + O_2$
$Cl + H_2 \rightarrow HCl + H$
$Cl + CH_4 \rightarrow HCl + CH_3$
$Cl + CH_2O \rightarrow HCl + HCO$
$Cl + H_2O_2 \rightarrow HCl + HO_2$
$Cl + HO_2 \rightarrow HCl + O_2$
$Cl + HO_2 \rightarrow OH + ClO$
$Cl + ClONO_2 \rightarrow 2\ Cl + NO_3$
$Cl + O_2 + M \rightarrow ClOO + M$
$ClO + O(3P) \rightarrow Cl + O_2$

$ClO + NO \rightarrow NO_2 + Cl$
$ClO + NO_2 + M \rightarrow ClONO_2 + M$
$ClO + HO_2 \rightarrow OHCl + O_2$
$ClO + OH \rightarrow HO_2 + Cl$
$ClO + CO \rightarrow Cl + CO_2$
$ClO + ClO + M \rightarrow Cl_2O_2 + M$
$OH + HCl \rightarrow H_2O + Cl$
$OH + OHCl \rightarrow H_2O + ClO$
$OH + CH_3Cl \rightarrow Clx$
$OH + CF_2HCl \rightarrow Clx$
$OH + CH_3CCl_3 \rightarrow Clx$
$OH + CHCl_2CF_3 \rightarrow Clx$
$OH + CH_3CCl_2F \rightarrow Clx$
$OH + CH_3CClF_2 \rightarrow Clx$
$OH + ClONO_2 \rightarrow OHCl + NO_3$
$O(3P) + HCl \rightarrow OH + Cl$
$O(3P) + ClONO_2 \rightarrow NO_3 + ClO$
$OClO + O(3P) \rightarrow ClO + O_2$
$OClO + NO \rightarrow NO_2 + ClO$

BrOx Reactions
$Br + O_3 \rightarrow BrO + O_2$
$Br + H_2O_2 \rightarrow HBr + HO_2$
$Br + CH_2O \rightarrow HBr + CHO$
$Br + HO_2 \rightarrow HBr + O_2$
$BrO + O(3P) \rightarrow Br + O_2$
$BrO + ClO \rightarrow Br + OClO$
$BrO + ClO \rightarrow Br + ClOO$
$BrO + ClO \rightarrow BrCl + O_2$
$BrO + NO \rightarrow NO_2 + Br$
$BrO + NO_2 + M \rightarrow BrONO_2 + M$
$BrO + BrO \rightarrow 2Br + O_2$
$BrO + BrO \rightarrow Br_2 + O_2$
$BrO + O_3 \rightarrow Br + 2O_2$
$BrO + HO_2 \rightarrow OHBr + O_2$
$BrO + OH \rightarrow Br + HO_2$
$OH + Br_2 \rightarrow OHBr + Br$
$OH + HBr \rightarrow H_2O + Br$
$OH + CH_3Br \rightarrow Bry$
$O(3P) + HBr \rightarrow OH + Br$

Instantaneous reactions
$CH_3 + O_2 \rightarrow CH_3O_2$
$HCO + O_2 \rightarrow CO + HO_2$
$CH_3O + O_2 \rightarrow CH_2O + HO_2$

Thermal decomposition reactions
$\mathbf{HO_2NO_2 \rightarrow HO_2 + NO_2}$
$\mathbf{N_2O_5 \rightarrow NO_2 + NO_3}$
$ClOO \rightarrow Cl + O_2$
$Cl_2O_2 \rightarrow ClO + ClO$

Heterogeneous reactions
$N_2O_5 + HCl(s) \rightarrow ClNO_2 + HNO_3(s)$

N_2O_5 + H_2O(s) → 2 HNO_3(s)
$ClONO_2$ + HCl(s) → Cl_2 + HNO_3(s)
$ClONO_2$ + H_2O(s) → HOCl + HNO_3(s)
HOCl + HCl(s) → Cl_2 + H_2O(s)
$BrONO_2$ + H_2O(s) → OHBr + HNO_3(s)
$BrONO_2$ + HCl (s) → BrCl + HNO_3(s)
OHBr + HCl(s) → BrCl + H_2O(s)

's' indicates species staying on the particle, and applies only for reactions on PSCs/STS.

Bibliography

Baugchum, S.L. and Henderson, S.C. (1998) *A*ircraft emissions scenarios projected in year 2015 for the NASA Technology Concept Aircraft (TCA) high speed civil transport. NASA Cotract. Rep, Vol. NASA-CR-1998-207635.

Berglen, T.F.; Berntsen, T.K. and Sundet, J.K. (2004) *A* global model of coupled sulfur/oxidant chemistry in the troposphere: The sulfur cycle. J. Geophys. Res., Vol. 109.

Berntsen, T. and Isaksen, I.S.A. (1997) *A* global 3-D chemical transport model for the troposphere: 1. Model description and CO and ozone results. J.Geophys. Res., Vol. 102(D17): p. 21 239–21 280.

Brasseur, G.P.; Orlando, J.J. and Tyndall, G.S. (1999) *A*tmospheric Chemistry and Global Change (Oxford University Press).

Brewer, A.W. (1949) *E*vidence for a world circulation provided by the measurements of helium and water distribution in the stratosphere. Quart. J. Roy. Meteor. Soc, Vol. 75: p. 351–363.

Butler et al. (1987) *E*OS Science Steering Commitee Report Volume II. From Pattern to Process: The Strategy of the Earth Observed System. Published by NASA, Washington DC, USA.

Clerbaux, C.; Cunnold, D.M.; Anderson, J.; Engel, A.; Fraser, P.J.; Mahieu, E.; Manning, A.; Miller, J.; Montzka, S.A.; Nasser, R.; Prinn, R.; Reismann, S.; Rinsland, C.P.; Simmons, P.; Verdonik, D.; Weiss, R.; Wubbles, D. and Yokouchi, Y. (2007) *L*ong-Lived Compounds, Chapter 1 in Scientific Assesment of Ozone Depletion: 2006 (Global Ozone Research and Monitoring Project-Report NO. 50, 572 pp., World Meteorological Organization, Geneva, Switzerland).

Denman, K.L.; Brasseur, G.; Chidthaisong, A.; Ciais, P.; Cox, P.M.; Dickinson, R.E.; Hauglustaine, D.; Heinze, C.; Holland, E.; Jacob, D.; U.Lohmann; Ramachandran, S; da Silva Dias, P.L.; Wofsy, S.C. and Zhang, X. (2007) *C*ouplings Between Changes in the Climate System and Biogeochemistry. In: Climate Change 2007: The Physical Science Basis. Contribution of Working Group I to the Fourth Assessment Report of the Intergovernmental Panel on Climate Change [Solomon, S., D. Qin, M. Manning, Z. Chen, M. Marquis, K.B. Averyt, M.Tignor and H.L. Miller (eds.)]. (Cambridge University Press, Cambridge, United Kingdom and New York, NY, USA.).

Endemann, M.; Garé, P.; Langden, J.; Nett, H. and Readings, C.J. (2000) *M*ipas - An Envisat Instrument for Atmospheric Chemistry and Climate Research. ESA bulletin 101 - february.

Fahey, D.W. (2007) *T*wenty questions and answers about the ozone layer: 2006 update, from Scientific Assesment of Ozone Depletion: 2006 (Global Ozone Research and Monitoring Project-Report NO. 50, 572 pp., World Meteorological Organization, Geneva, Switzerland).

Forster, P.; Ramaswamy, V.; Artaxo, P.; Berntsen, T.; Betts, R.; Fahey, D.W.; Haywood, J.; Lean, J.; Lowe, D.C.; Myhre, G.; Nganga, J.; Prinn, R.; Raga, G.; Schulz, M. and Dorland, R. Van (2007) *C*hanges in Atmospheric Constituents and in Radiative Forcing. In: Climate Change 2007: The Physical Science Basis. Contribution of Working Group I to the Fourth Assessment Report of the Intergovernmental Panel on Climate Change [Solomon, S., D. Qin, M. Manning, Z. Chen, M. Marquis, K.B. Averyt, M.Tignor and H.L. Miller (eds.)]. (Cambridge University Press, Cambridge, United Kingdom and New York, NY, USA.).

Funke, B.; López-Puertas, M.; Gil-López, S.; von Clarmann, T.; Stiller, G. P.; Fischer, H. and Kellmann, S. (2005a) *D*ownward transport of upper atmospheric NO_x into the polar stratosphere and lower mesosphere during the Antarctic 2003 and Arctic 2002/2003 winters. J. Geophys. Res., Vol. 110.

Funke, B.; López-Puertas, M.; von Clarmann, T.; Stiller, G. P.; Fischer, H.; Glatthor, N.; Grabowski, U.; Höpfner, M.; Kellmann, S.; Kiefer, M.; Linden, A.; Mengistu Tsidu, G.; Milz, M.; Steck, T. and Wang, D. Y. (2005b) *R*etrieval of stratospheric NO_x from 5.3 and 6.2 μm nonlocal thermodynamic equilibrium emissions measured by Michelson Interferometer for Passive Atmospheric Sounding (MIPAS) on Envisat. J. Geophys. Res., Vol. 110(D9).

Gauss, M. (2003) *I*mpact of aircraft emissions and ozone changes in the 21^{st} century: 3-D model studies. Ph.D.thesis, University of Oslo, Department of geoscience,MetOs section.

Gauss, M.; Isaksen, I.S.A.; Lee, D.S. and Søvde, O.A. (2006) *I*mpact of aircraft NOx emissions on the atmosphere - tradeoffs to reduce the impact. Atmos.Chem.Phys, Vol. 6: p. 1529–1548.

Glatthor, N.; von Clarmann, T.; Fischer, H.; Funke, B.; Gil-López, S.; Grabowski, U.; Höpfner, M.; Kellmann, S.; Linden, A.; López-Puertas, M.; Mengistu Tsidu, G.; Milz, M.; Steck, T.; Stiller, G. P. and Wang, D.-Y. (2006) *R*etrieval of stratospheric ozone profiles from MIPAS/ENVISAT limb emission spectra: a sensitivity study. Atmos. Chem. Phys., Vol. 6: p. 2767–2781.

Glatthor, N.; von Clarmann, T.; Fischer, H.; Funke, B.; Grabowski, U.; Höpfner, M.; Kellmann, S.; Kiefer, M.; Linden, A.; Milz, M.; Steck, T.; Stiller, G. P.; Mengistu Tsidu, G. and Wang, D. Y. (2005) *M*ixing processes during the Antarctic vortex split in September/October 2002 as inferred from source gas and ozone distributions from ENVISAT-MIPAS. J. Atmos. Sci., Vol. 62(3): p. 787–800.

Glatthor, N.; von Clarmann, T.; Fischer, H.; Grabowski, U.; Höpfner, M.; Kellmann, S.; Kiefer, M.; Linden, A.; Milz, M.; Steck, T.; Stiller, G. P.; Mengistu Tsidu, G.; Wang, D. Y. and Funke, B. (2004) *S*paceborne ClO observations by the Michelson Interferometer for Passive Atmospheric Sounding (MIPAS) before and during the Antarctic major warming in September/October 2002. J. Geophys. Res., Vol. 109.

Grini, A.; Myhre, G.; Sundet, J.K. and Isaksen, I.S.A. (2002) *M*odelling the annual cycle of sea salt in the global 3D model Oslo CTM2: Concentrations, fluxes and radiative impact. J.Climate 15 (13), p. 1717–1730.

Grini, A.; Myhre, G.; Zender, C.S. and Isaksen, I.S.A. (2005) *M*odel simulations of dust sources and transport in the global atmosphere: Effects of soil erodibility and wind speed variability. J.Geophys.Res., Vol. 110(D2): p. D02 205.

Hesstvedt, E.; Hov, Ø. and Isaksen, I.S.A. (1978) *Q*uasi steady-state approximation in air pollution modelling: Comparison of two numerical schemes for oxidant prediction. Int. J. Chem. Kinet., Vol. 10: p. 971–978.

Holton, J.; Haynes, P.; McIntyre, M.; Douglass, A.; Rood, R. and Pfister, L. (1995) *S*tratosphere-troposphere exchange. Rewievs of Geophysics, Vol. 33: p. 403–439.

Holtslag, A.A.M.; DeBruijn, E.I.F. and Pan, H.L. (1990) *A* high resolution air mass transformation model for short-range weather forecasting. Mon.Wea.Rev., Vol. 118: p. 1561–1575.

Höpfner, M.; von Clarmann, T.; Fischer, H.; Glatthor, N.; Grabowski, U.; Kellmann, S.; Kiefer, M.; Linden, A.; Mengistu Tsidu, G.; Milz, M.; Steck, T.; Stiller, G. P.; Wang, D.-Y. and Funke, B. (2004) *F*irst spaceborne observations of Antarctic stratospheric $ClONO_2$ recovery: Austral spring 2002. J. Geophys. Res., Vol. 109(D11).

Jackman, C.H. and McPeters, R.D. (2004) *T*he Effect of Solar Proton Events on Ozone and Other Constituents. Geophys. monogr., Vol. 141: p. 305–319.

Jackman, C.H. et al. (2005a) *T*he influence of several very large solar proton events in years 2000-2003 on the neutral middle atmosphere. Adv. Space Res., Vol. 35: p. 445–450.

Jackman, C.H. et al. (2005b) *N*eutral atmospheric influences of the solar proton events in October-November 2003. J.Geophys. Res., Vol. 110.

Jacob, Daniel J. (1999) *I*ntroduction to Atmospheric Chemistry (Princeton University Press).

Liou, K.N. (1989) *A*n Introduction to Atmospheric Radiation (International geophysics series).

López-Puertas, M.; Funke, B.; Gil-López, S.; von Clarmann, T.; Stiller, G. P.; Höpfner, M.; Kellmann, S.; Mengistu Tsidu, G.; Fischer, H. and Jackman, C. H. (2005) HNO_3, N_2O_5 and $ClONO_2$ Enhancements after the October–November 2003 Solar Proton Events. J. Geophys. Res., Vol. 110(A9).

Mengistu Tsidu, G.; Stiller, G. P.; von Clarmann, T.; Funke, B.; Höpfner, M.; Fischer, H.; Glatthor, N.; Grabowski, U.; Kellmann, S.; Kiefer, M.; Linden, A.; López-Puertas, M.; Milz, M.; Steck, T. and Wang, D. Y. (2005) NO_y from Michelson Interferometer for Passive Atmospheric Sounding on Environmental Satellite during the Southern Hemisphere polar vortex split in September/October 2002. J. Geophys. Res., Vol. 110(D11).

Mengistu Tsidu, G.; von Clarmann, T.; Stiller, G. P.; Höpfner, M.; Fischer, H.; Glatthor, N.; Grabowski, U.; Kellmann, S.; Kiefer, M.; Linden, A.; Milz, M.; Steck, T.; Wang, D.-Y. and Funke, B. (2004) *S*tratospheric N_2O_5 in the austral spring 2002 as retrieved from limb emission spectra recorded by the Michelson Interferometer for Passive Atmospheric Sounding (MIPAS). J. Geophys. Res., Vol. 109.

Myhre, G.; Grini, A. and Metzger, S. (2006) *M*odelling of nitrate and ammonium containing aerosols in presence of sea salt. Atmos.Chem.Phys, Vol. 6: p. 1–13.

Olivier, J.; Peters, J.; Pétron, C.; Müller, J.F. and Wallens, S. (2003) *P*resent and future surface emissions of atmospheric compounds. POET Report 2, EU Project EVK-1999-00011 2003.

Orsolini, Y.J.; Manney, G.L.; Santee, M.L. and Randall, C.E. (2005) *A*n upper stratospheric layer of enhanced HNO3 following exceptional solar storms. Geophys. Res. Let, Vol. 32.

Pickering, K.E.; Wang, Y.; Tao, W.K.; Price, C. and Müller, J.F. (1998) *V*ertical distributions of lightning Nox for use in regional and global chemical transport models. J.Geophys.Res, Vol. 103: p. 31 203–31 216.

Prather, M.J. (1986) *N*umerical advection by conservation of 2nd order moments. J.Geophys.Res., Vol. 91(D6): p. 6671–6681.

Price, C.; Penner, J. and Prather, M. (1997a) *N*Ox from lightning: 1. Global distribution based on lightning physics. J.Geophys.Res, Vol. 102: p. 5929–5941.

Price, C.; Penner, J. and Prather, M. (1997b) *N*Ox from lightning: 2. Constraints from the global atmospheric electric circuit. J.Geophys.Res, Vol. 102: p. 5942–5951.

Rodhe, H. and Isaksen, I.S.A. (1980) *G*lobal distributions of sulfur compounds in the troposphere estimated in a height latitude transport model. J.Geophys.Res., Vol. 85(NC12): p. 7401–7409.

Schultz, M.G.; Pulles, T.; Brand, R.; van het Bolscher, M. and Dalsøren, S.B. (2006) *A* global dataset of anthropogenic CO, NOx and NMVOC emissions for 1960-2000. paper in preparation.

Stiller, G. P. (editor) (2000) *T*he Karlsruhe Optimized and Precise Radiative Transfer Algorithm (KOPRA), Vol. FZKA 6487 of *W*issenschaftliche Berichte (Forschungszentrum Karlsruhe).

Stiller, G. P.; von Clarmann, T.; Brühl, C.; Fischer, H.; Funke, B.; Glatthor, N.; Grabowski, U.; Höpfner, M.; Jöckel, P.; Kellmann, S.; Kiefer, M.; Linden, A.; Lòpez-Puertas, M.; Mengistu Tsidu, G.; Milz, M.; Steck, T. and Steil, B. (2007) *G*lobal distributions of HO_2NO_2 as observed by the Michelson Interferometer for Passive Atmospheric Sounding (MIPAS). J. Geophys. Res. Accepted for publication.

Stordal, F.; Isaksen, I.S.A. and Horntvedt, K. (1985) *A* diabatic circulation two-dimensional model with photochemistry: Simulations of ozone and long-lived tracers with surface sources. J.Geophys.Res, Vol. 90: p. 5757–5776.

Sundet, J.K. (1997) *M*odel studies with a 3-d global CTM using ECMWF data. Ph.D.thesis, University of Oslo, Department of geoscience,MetOs section.

Søvde, O.A. (2007) *C*hemistry in the Upper Troposphere and Lower Stratosphere: A model Study of Processes Important for Ozone. Ph.D.thesis, University of Oslo, Department of geoscience,MetOs section.

Søvde, O.A. and Isaksen, I.S.A (2006) *T*he use of ERA-40 and ECMWF IFS 60-layer meteorological data in the Oslo CTM2. Institute Report Series NO. 131, Department of Geosciences, University of Oslo.

UNEP (1985) *A*tmospheric Ozone 1985. Global Ozone Research and Monitoring Project, Report No.16 (World Meteorological Organization, Geneva. 1090s).

van Noije, T.P.C; H.J.Eskes; van Weele, M. and van Velthoven, P.F.J. (2004) *I*mplications of the enhanced Brewer-Dobson circulation in European Centre for Medium-Range Weather Forecast reanalysis ERA-40 for the stratospheric-tropospheric exchange of ozone in global chemistry transport models. J.Geophys.Res, Vol. 109(D19308).

von Clarmann, T.; Chidiezie Chineke, T.; Fischer, H.; Funke, B.; García-Comas, M.; Gil-López, S.; Glatthor, N.; Grabowski, U.; Höpfner, M.; Kellmann, S.; Kiefer, M.; Linden, A.; López-Puertas, M.; López-Valverde, M. Á.; Mengistu Tsidu, G.; Milz, M.; Steck, T. and Stiller, G. P. (2003a) *R*emote Sensing of the Middle Atmosphere with MIPAS. Proc. SPIE, Vol. 4882: p. 172–183.

von Clarmann, T.; Glatthor, N.; Grabowski, U.; Höpfner, M.; Kellmann, S.; Kiefer, M.; Linden, A.; Mengistu Tsidu, G.; Milz, M.; Steck, T.; Stiller, G. P.; Wang, D. Y.; Fischer, H.; Funke, B.; Gil-López, S. and López-Puertas, M. (2003b) *R*etrieval of temperature and tangent altitude pointing from limb emission spectra recorded from space by the Michelson Interferometer for Passive Atmospheric Sounding (MIPAS). J. Geophys. Res., Vol. 108(D23).

Wallace, J.M. and Hobbs, P.V. (1977) *A*tmospheric science; An Introductory Survey (Academic Press).